Title
Cooper-Pair Injection into Topological Insulators and Helical Wires

Author
Sato, Koji

Publication Date
2013

Peer reviewed|Thesis/dissertation

University of California
Los Angeles

Cooper-Pair Injection into Topological Insulators and Helical Wires

A dissertation submitted in partial satisfaction
of the requirements for the degree
Doctor of Philosophy in Physics

by

Koji Sato

2013

Abstract of the Dissertation

Cooper-Pair Injection into Topological Insulators and Helical Wires

by

Koji Sato

Doctor of Philosophy in Physics

University of California, Los Angeles, 2013

Professor Yaroslav Tserkovnyak, Chair

A Cooper-pair (CP) splitter is a device capable of spatially separating a pair of entangled electrons by sending a weak current from a superconductor (SC) to a pair of quantum dots or quantum wires. In this thesis, CP splitters based on quantum spin Hall insulators (QSHI), also known as two-dimensional topological insulator, and quantum wires are theoretically studied. Spin-entangled electrons can be extracted from the CP's in the SC, and transmitted by the helical electronic states hosted by these quantum heterostructures. In the introduction, the background information on the integer quantum Hall effect, QSHI, and CP splitters is provided.

In Chapter 2, CP spitter based on QSHI is considered. Due to electron interaction, spin-entangled CP splits into opposite edges of QSHI, which support gapless electronic helical modes. The momentum of electrons and spin are tightly locked in a helical state. Accordingly, the spin orientation determines charge curret, and the measurable current-current correlations can thus convey information on the initial spin entanglement of CP's, even after they are spatially separated.

In Chapter 3, conventional quantum wires with strong spin-orbit interactions, such as InAs, under magnetic field are shown to mimic the behavior of the helical QSHI edge states. These wires can thus provide a more direct and engineerable route toward spatial separation

of entangled electrons.

In Chapter 4, QSHI based CP splitter equipped with beam splitters at each edge is considered. The current-current correlations in such system can be used to experimentally test a Bell inequality. A violation of a Bell inequality indicates nonlocal quantum entanglement, which cannot be described by classical physics. The intrinsic dephasing mechanism in our system, which hinderes a Bell test, caused by Luttinger-liquid interactions at finite temperatures We study this chapter and show that it is generally still possible to obtain a violation of classical correlations.

The dissertation of Koji Sato is approved.

Louis Bouchard

Alex J. Levine

Sudip Chakravarty

Yaroslav Tserkovnyak, Committee Chair

University of California, Los Angeles

2013

Table of Contents

List of Figures

Acknowledgments

I would like to extend my gratitude to Professor Yaroslav Tserkovnyak for his deep insight and dedicated, patient advisory. My formative years here have been the most exciting and stimulating yet of my personal and professional life. I also would like to express my thanks to my fellow group members Mircea Trif, Silas Hoffman, and Scott Bender for sharing the whole experience together. The discussions I had with many of my colleagues also encouraged and inspired me throughout the time in graduate school, which I am very thankful for. Finally, my family members have been greatly supportive of my academic pursuit and various other aspects of my life, and I would like to address my sincere thanking to them.

Vita

2006 B.S. (Physics), California State Polytechnic University, Pomona.

2008 M.A. (Physics), University of California, Los Angeles, California.

Publications

[1]Sato, Koji and Loss, Daniel and Tserkovnyak, Yaroslav
"Cooper-Pair Injection into Quantum Spin Hall Insulators"
Physical Review Letter 105, 226401 (2010)

[2]Sato, Koji and Loss, Daniel and Tserkovnyak, Yaroslav
"Crossed Andreev reflection in quantum wires with strong spin-orbit interaction"
Physical Review B 85, 235433 (2012)

CHAPTER 1

Introduction

1.1 Integer Quantum Hall Effect

1.1.1 Introduction to classical and quantum Hall effect

A two-dimensional electron gas (2DEG) under a magnetic field perpendicular to the plane exhibits a Hall effect, where a voltage difference is induced in the transverse direction the current. This voltage difference comes from the charge accumulation on one side of the system caused by deflection of charge carriers due to Lorentz force. A classical treatment for this problem is to see the equation of motion of a single electron $m\dot{\mathbf{v}} = -e\mathbf{E} - e\mathbf{v}\times\mathbf{B} - m\tau^{-1}\mathbf{v}$, where $-e < 0$ is the electronic charge, and τ is the relaxation time. Note the electric field $\mathbf{E}$ contains the field induced by the charge accumulation as well an applied electric field. Given the current density $\mathbf{j} = -en_e\mathbf{v}$ (n_e is the electron density), the equation of motion above in the DC limit ($\dot{\mathbf{v}} = 0$) leads to

$$\begin{pmatrix} E_x \\ E_y \end{pmatrix} = \begin{pmatrix} \rho_{xx} & \rho_{xy} \\ \rho_{yx} & \rho_{yy} \end{pmatrix} \begin{pmatrix} j_x \\ j_y \end{pmatrix} , \tag{1.1}$$

where $\rho_{xx} = \rho_{yy} = m/e^2 n_e \tau$ and $\rho_{xy} = -\rho_{yx} = B/en_e$. ρ_{xy} is the Hall resistivity, and it linearly increases with B and is independent of the relaxation time τ. Due to the Hall resistivity, even when $j_y = 0$, the electric field E_x perpendicular to the current j_x can be induced. Inverting the resistivity tensor,

$$\begin{pmatrix} j_x \\ j_y \end{pmatrix} = \begin{pmatrix} \sigma_{xx} & \sigma_{xy} \\ \sigma_{yx} & \sigma_{yy} \end{pmatrix} \begin{pmatrix} E_x \\ E_y \end{pmatrix} , \tag{1.2}$$

we can find the conductivity tensor σ. Denoting the Drude conductivity $\sigma_0 = ne^2\tau/m$ and the cyclotron frequency $\omega_c = eB/m$, the longitudinal conductivity is $\sigma_{ii} = \sigma_0/(1+\omega_c^2\tau^2)$ $(i = x, y)$, and the Hall (transverse) conductivity is $\sigma_{xy} = -\sigma_{yx} = -\sigma_0\omega_c\tau/(1+\omega_c^2\tau^2)$.

In a clean sample ($\tau \to \infty$) under a strong magnetic field ($B \to \infty$), we find both $\sigma_{ii} \to 0$ and $\rho_{ii} \to 0$, meanwhile $\rho_{xy} = B/en_e$ and $\sigma_{yx} \to ne/B$ stay constant. In an experimental setting, such clean samples can be made by semiconductor heterostructures such as AlGaAs/GaAs. On the contrary to the above limit of the Hall resistivity being proportional to B, when the temperature k_BT is sufficiently low in comparison to the energy scale $\hbar\omega_c$, it was discovered that the Hall resistivity is quantized [KDP80] (see Figure 1.1), and the precision of its quantization is astonishingly high (one part in 10^9). Since both ρ_{ii} and σ_{ii} vanish in this limit, the Hall resistivity is reciprocally related to the Hall conductivity, which is likewise quantized. This effect followed by quantized Hall conductivity is called the integer quantum Hall effect (IQHE), and the Hall conductivity is given by $\sigma_{yx} = \nu e^2/h$ with ν being an integer.

This high precision of the quantization suggests that the underlying mechanism must not be sensitive to perturbations to some extent. It turns out the quantization mechanism for IQHE has its root in topology. Since the topology of a system is stable against small perturbations, and a physical phenomena arising from such a topological reason in turn becomes robust. Here, the distinction between the integer quantum Hall phase and an ordinary insulator phase is made by the presence of a topological order, which can be related to the integer arising in the Hall conductivity. This way of recognizing phases of matter is different from the conventional view on phase transition explained by Landau-Ginzburg theory, where a phase transition occurs by breaking underlying continuous symmetry developing order parameters as we can see in the examples of a magnet and crystal. Unlike an order parameter that can change contiguously, a topological order is a quantity that cannot change continuously and usually pertains to the global property of a system, such as a genus of a manifold. The integer of the Hall conductivity stems from such a topological quantity, hence

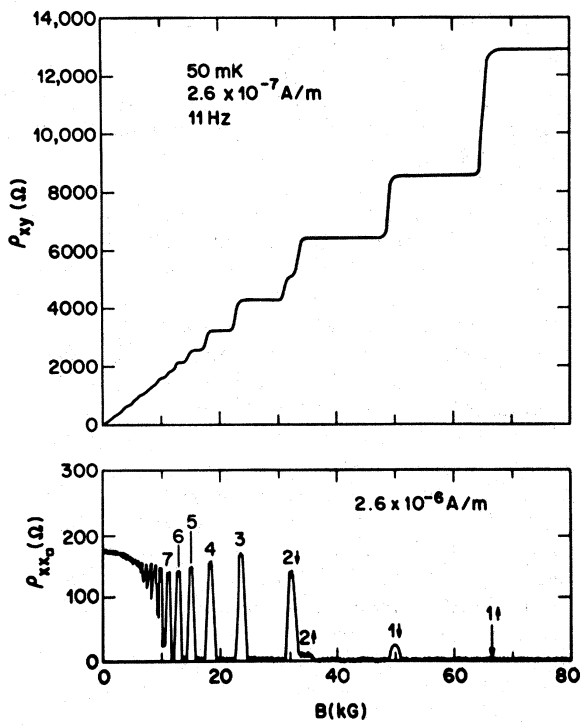

Figure 1.1: The longitudinal resistivity ρ_{xx} and transverse resistivity ρ_{xy} as a function of magnetic field B [PTG82]. Where ρ_{xy} plateaus, ρ_{xx} goes to zero.

it can be a very robust effect.

It turns out that a single-particle picture suffices to explain IQHE. However, in even cleaner sample and under higher magnetic field, the effect of the Coulomb interactions between electrons become important. In this limit, the filling factor ν in the Hall conductivity can take fractional values, hence this effect is called fractional quantum Hall effect (FQHE). $\nu = 1/3$ plateau was first discovered [TSG82], and further fine measurements revealed many more plateaus at fractional values of ν as seen in Figure 1.2. The specific case of $\nu = 1/q$ with q being odd integers was explained in a many-body state picture, where the ground state of this system is an incompressible quantum fluid with fractionally charged quasielectrons and quasiholes [Lau83]. Other plateaus at $\nu = p/(2sp + 1)$ with the integers p and s can be explained by the composite-fermion theory [Jai89b, Jai89a]. Furthermore, even denominator filling factor was observed [WES87], and it was showed that the ground state wave function of such even-denominator FQHE is described by Moore-Read Pfaffian wave

function [MR91, GWW91]. Its quasiparticle excitations are called anyons [Wil82], which exhibit non-Abelian statistics. Such particles with non-Abelian statistics can be utilized to perform topological quantum computation [NSS08].

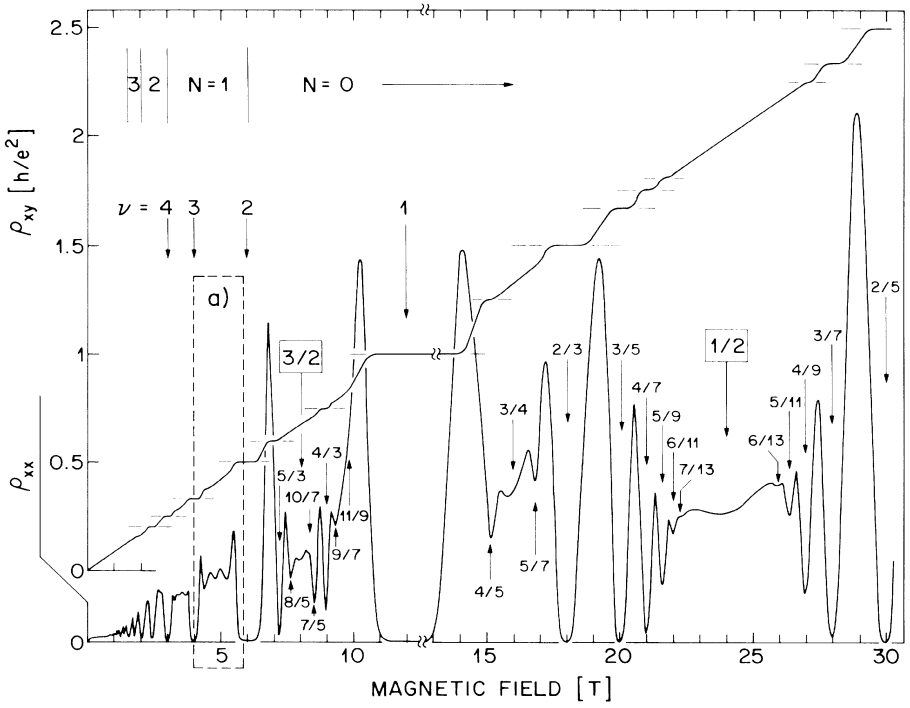

Figure 1.2: The longitudinal resistivity ρ_{xx} and the Hall resistivity ρ_{xy} in the unit of h/e^2 as a function of the applied field B [WES87]. The plateaus of ρ_{xy} occur not only at the integer values but also at fractional values. At the plateaus of ρ_{xy}, ρ_{xx} vanishes. .

Quantum Hall effect leads to a rich ground to study topology and strongly correlated electron systems. In the following sections, the aspect of topology appearing in IQHE is presented. The reviews on various other topics on quantum Hall effect can be found in Refs. [Yos10, Eza00, DP08, Goe09, Gir99].

1.1.2 Landau Levels: Two-Dimensional Electron Gas under a Magnetic Field

The simplest model toward grasping IQHE is the single-particle Hamiltonian for a two-dimensional electron gas in xy plane under the magnetic field B applied perpendicularly to

the plane, namely

$$H = \frac{1}{2m}\left(\mathbf{p} + e\mathbf{A}\right)^2 , \tag{1.3}$$

where $-e < 0$ is the electronic charge, and $\mathbf{A}$ is the vector potential with $\mathbf{B} = \nabla \times \mathbf{A}$. The 2D geometry here is in a strip form, where the length L_y in y direction is long enough so that the momentum in y direction is a good quantum number, but the width L_x in x direction is finite. It is natural to choose Landau gauge $\mathbf{A} = (0, Bx, 0)$ for this geometry, and an eigenstate is given by

$$\psi_k(x, y) = \frac{1}{\sqrt{L_y}} e^{iky} \phi_k(x) , \tag{1.4}$$

where $k = k_s = 2\pi s/L_y$ ($s \in \mathbb{Z}$) from the periodic boundary condition in y direction. The Hamiltonian in Eq. (1.3) then leads to

$$\left[\frac{p_x^2}{2m} + \frac{1}{2m}\left(\hbar k + eBx\right)^2\right] \phi_k(x) = E\phi_k(x) . \tag{1.5}$$

The left hand side of Eq. (1.5) can be rewritten in a more suggestive form

$$\frac{p_x^2}{2m} + \frac{1}{2}m\left(\frac{eB}{m}\right)^2 \left[x + \frac{\hbar k}{eB}\right]^2 = \frac{p_x^2}{2m} + \frac{1}{2}m\omega_c^2 \left(x - x_k\right)^2 , \tag{1.6}$$

where $\omega_c = eB/m$ is the cyclotron frequency, and $x_k = -l_B^2 k$ corresponds to a shift of the center of ψ_k state in x direction. Here, $l_B^2 = \hbar/eB$ is the magnetic length. The Hamiltonian in Eq. (1.6) is in the form of a simple harmonic oscillator $H_{SHO} = p^2/2m + m\omega_c^2 x^2/2$ with a shift in the x direction by x_k, so the solution is given by

$$\psi_{n,k}(x, y) = \frac{1}{\sqrt{L_y}} e^{iky} \phi_n(x - x_k) . \tag{1.7}$$

Here,

$$\phi_n(x) = \left(\frac{1}{2^n n! \sqrt{\pi} l_B}\right)^{1/2} \exp\left(-\frac{x^2}{2l_B^2}\right) H_n(x/l_B) , \tag{1.8}$$

with the Hermite polynomial $H_n(z)$. Its energy is given by the simple harmonic oscillator form $E_n = \hbar\omega_c(n + 1/2)$ with $n =\in \mathbb{Z}$. These energy levels are called Landau levels. Each Landau level is degenerate, since the states $\psi_{n,k}(x, y)$ for all k have the same energy E_n.

As indicated in Eq. (1.7), the center of an eigenstate is shifted by x_k which depends on the value of k, thus all the degenerate states in a given Landau level are juxtaposed with

the separation $\Delta x_k = x_{s+1} - x_s = 2\pi l_B^2/L_y$ in a strip form (of width l_B in x direction and extending in y direction). The number of such states that can be fitted in the width L_x is directly related to the number of degeneracy N_d in each Landau level; therefor $N_d = L_x/\Delta x_k = A/2\pi l_B^2$ (letting $\phi_0 = h/e$ be the flux quanta, N_d is also the number of flux quanta that can be fitted in the total flux, namely $N_d = AB/\phi_0$), where $A = L_x L_y$ is the area of the two-dimensional system. If the number of electrons in the system is N, the filling factor ν is defined by

$$\nu = \frac{N}{N_d} = \frac{N}{A} 2\pi l_B^2 = \frac{N}{A}\frac{h}{eB}\,, \tag{1.9}$$

which indicates how many of Landau levels are filled by the electrons.

In summary, non-interacting electrons in a two-dimensional system under a magnetic field forms highly degenerate Landau levels. Although we chose a specific gauge for this problem, the features of the physical quantities such as energy are independent of a choice of a gauge (we could have obtained Landau levels from the symmetric gauge for instance).

1.1.3 The Conductivity of 2DEG under a Magnetic Field

Now we see the transport property of such a 2DEG under a magnetic field. If an electric field is applied along x direction, the Hamiltonian for a given k state is

$$\begin{aligned} H_k &= \frac{1}{2m}\left[p_x^2 + (\hbar k + eBx)^2\right] + eEx \\ &= \frac{p_x^2}{2m} + \frac{1}{2}m\omega_c^2[x - x'_k]^2 + eEx'_k + \frac{1}{2}m\left(\frac{E}{B}\right)^2\,, \end{aligned} \tag{1.10}$$

where

$$x'_k = -l_B^2\left[k + \frac{mE}{\hbar B}\right]\,. \tag{1.11}$$

In Eq. (1.10), E/B is the drift velocity, and eEx'_k term corresponds to the electric potential energy at x'_k. The total energy is given by the sum of the Landau level energy, the potential energy due to the applied electric field, and the kinetic energy associated with the drift velocity.

By identifying the velocity operators

$$\begin{aligned} v_x &= \dot{x} = \frac{1}{i\hbar}[x, H] = \frac{1}{i\hbar}[x, p_x^2/2m] = \frac{p_x}{m}\,, \\ v_y &= \dot{y} = \frac{1}{i\hbar}[y, H] = \frac{1}{i\hbar}[y, (p_y + eBx)^2/2m] = \frac{p_y + eBx}{m}\,, \end{aligned} \tag{1.12}$$

the classical motion of the electron can be found from the expectation values of the velocities using the Heisenberg's equation of motion. Denoting $\psi_{n,k}(x,y) \to |n,k\rangle$, the expectation value of y momentum is $\langle k,n|p_y|k,n\rangle = \hbar k = -\hbar x'_k/l_B^2 - mE/B$, because $x'_k = \langle k,n|x|k,n\rangle = -l_B^2(k + mE/\hbar B)$. Then, the expectation values of the velocities are

$$\begin{aligned} \langle n,k|v_x|n,k\rangle &= \left\langle n,k\left|\frac{p_x}{m}\right|n,k\right\rangle = 0\,, \\ \langle n,k|v_y|n,k\rangle &= \left\langle n,k\left|\frac{p_y + eBx}{m}\right|n,k\right\rangle \\ &= -\frac{\hbar x'_k}{m l_B^2} - \frac{E}{B} + \frac{eB}{m}x'_x = -\frac{E}{B}\,. \end{aligned} \tag{1.13}$$

The electric field in x direction induces the drift velocity E/B in y direction, which is independent of k.

Given the above results, the current contributed from all the filled states are found by

$$\begin{aligned} I_y &= -e\langle v_y\rangle n_e L_x \\ &= -en_e\frac{E_x L_x}{B} = \frac{en_e}{B}V_x\,. \end{aligned} \tag{1.14}$$

Therefore, the Hall resistance is $R_H = -B/en$. This explains the classical Hall effect, but the quantization of the Hall conductivity doesn't come out of this formulation, and we need to extend the analysis furthermore.

It turns out the quantization of the Hall conductivity requires the presence of impurities. Supposing the strength of the impurity is much smaller than the Landau level energy spacing $\hbar\omega_c$ so that different Landau levels don't mix, and the variation of the impurity potential is smooth in comparison to the magnetic length. In this limit, the electric field due to impurities appear constant within the magnetic length scale, and we can adapt the picture that an electronic state is extended around a constant potential contour.

According to the scaling argument of Anderson localization [AAL79], no extended state can survive the presence of any amount of impurity in two-dimension, and all the states become localized. However, a magnetic field disrupts the quantum coherence needed for the localization, and the scaling argument breaks down. In a strong magnetic field in 2D, it is possible to have extended states in a disordered system [AA81, Pra81], indicated by the divergence of the localization length as the energy of a state approaches the original Landau levels [Tru83]. It turns out that each Landau level can host one current-carrying state, at the corresponding unperturbed Landau level energy, which can percolate one side of the sample to the other. In Figure 1.3, (a) and (b) show raising the Fermi energy populate only localized states; on the other hand, (c) shows that the Fermi energy hits the extended state which percolates from one side to the other. In fact, most of the equipotential contours in the bulk are closed around some impurities, leading to the localization of the electronic states following these closed contours. In turn, the degeneracy of each Landau level is lifted, and the density of state at each Landau level is broadened (see Figure 1.3). However, there exists one equipotential contour, per one Landau level, that percolates through the entire sample.

Under a careful analysis on 2DEG under a strong magnetic field with the presence of impurities, each Landau level contributes to one conduction channel (the state percolating through the sample). When only the lowest Landau level is completely filled, the corresponding current is calculated by

$$\begin{aligned} I_y &= -e\frac{E_x}{B}\frac{N_d}{A}L_x \\ &= -\frac{e}{BA}\frac{BA}{h/e}V_x = \frac{e^2}{h}V_x\,. \end{aligned} \tag{1.15}$$

Since there is only one channel that can contribute to the conduction, the above result implies this single conduction channel contributes $G_0 = e^2/h$ to the conductance (which is the same as conductivity in 2D). Since each of these conduction channel contributes e^2/h to

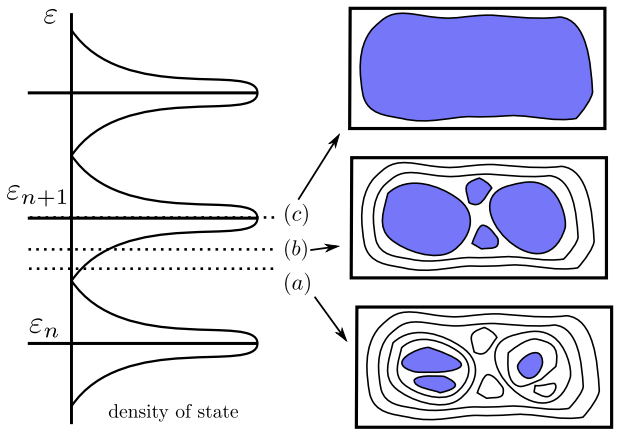

Figure 1.3: The left figure shows the energy v.s. the density of states. The the density of states around each Landau level ε_n are broadened due to the impurities. The figures on the right show the equipotential contours. In (a), the Fermi level is at the tail of the density of states from ε_{n+1}, which populates the states localized around lower energy potential contours. In (b), the Fermi level is raised, and higher energy contours are populated. In (c), as the Fermi level hits ε_{n+1}, the largest contour is populated, which percolates from one side of the sample to the other.

the Hall conductivity, the total Hall conductivity is given by

$$\sigma_{xy} = -\sigma_{yx} = -n\frac{e^2}{h}\,, \tag{1.16}$$

where n is the largest integer below the filling factor $\nu = N/N_d$. Note that n is the number of the populated conduction channels. As the Fermi energy is shifted in between two adjacent Landau levels, all the available states are localized, so the transverse conductivity doesn't change, which makes the Hall conductivity flat over some range of the chemical potential. Furthermore, this lack of conducting states at the plateaus of the Hall conductivity means that the resistivity ρ_{ii} vanishes. Raising the Fermi energy furthermore eventually populates a conduction channel in the next Landau level, and the Hall conductance jumps up by e^2/h, which explains the quantization of the Hall conductance.

1.1.4 Edge States

A semi-classical picture of an extended states can be understood as a skipping orbit at the edges of the sample as seen in Figure 1.4. Due to an external magnetic field, the trajectory of an electron is bent by the Lorentz force. When a state comes close to one of the edges of the system, it can bounce from the edge and bent by the Lorentz force to come back to the same edge. This bouncing motion can be repeated, and it can meanwhile move forward along the edge to carry current.

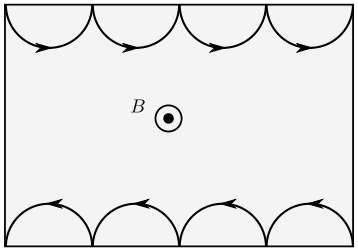

Figure 1.4: The states in the bulk are localized at the sites of impurities. In a semi-classical picture, the extended states near the edges can propagate along the edges by bouncing being subject to the Lorentz force from the magnetic field B.

Introducing a confinement potential that keeps electrons inside the system provides a way to formally treat such skipping orbits, which gives rise to the idea of an edge state that transports current [Hal82]. Suppose such a confinement potential in x direction is given by $U(x)$, then the Hamiltonian reads

$$H = \frac{1}{2m}\left[p_x^2 + \left(p_y^2 + eBx\right)^2\right] + U(x)\,. \tag{1.17}$$

The potential $U(x)$ goes up near the edges so that the electrons feel the forces inward to the system. Letting one edge be located at $x = 0$ and the other one at $x = L_x$, if the potential changes slowly relative to the magnetic length l_B, a linear approximation of the potential around the edges can be justified. If the potential is linear, the associated electric field is constant, which is the same problem as Eq. (1.10). The energy for a given k and n

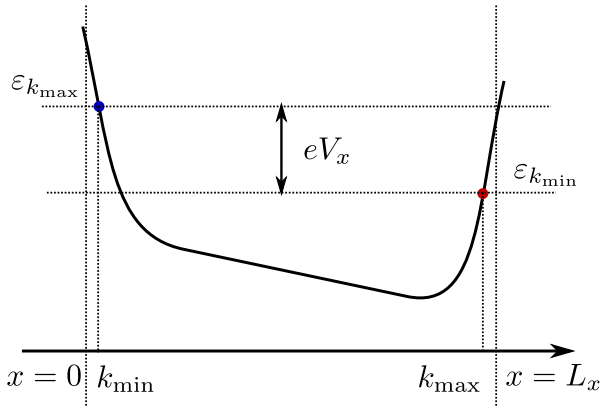

Figure 1.5: A constant energy Landau level picks up spatial dependence due to the confinement potential $U(x)$. The effect of a bias is also present, which makes the dispersion asymmetric. $x = 0, L_x$ are the edges of the sample. These two edges have different chemical potentials due to an applied bias. The blue (red) dot indicates the point on the dispersion that crosses with the chemical potential at $x = 0$ ($x = L_x$) edge. The corresponding momentum are given by $k_{\min}$ and $k_{\max}$ respectively as indicated in the figure.

state is

$$\varepsilon_{n,k} = \hbar\omega_c(n + 1/2) - eE(x)l_B^2\left[k + \frac{mE(x)}{\hbar B}\right] + \frac{1}{2}m\left[\frac{E(x)}{B}\right]^2 . \tag{1.18}$$

The velocity for this state is

$$v_{n,k} = \frac{1}{\hbar}\frac{\partial\varepsilon_{n,k}}{\partial k} , \tag{1.19}$$

thus the current is given by counting all the filled states.

$$\begin{aligned} I_y &= -e\sum_{n=1}^{N_{max}}\frac{1}{L_y}\sum_k v_{n,k} = -e\sum_{n=1}^{N_{max}}\int_{k_{min}}^{k_{max}}\frac{dk}{2\pi}\frac{1}{\hbar}\frac{\partial\varepsilon_{n,k}}{\partial k} \\ &= -\frac{e}{h}\sum_{n=1}^{N_{max}}(\varepsilon_{n,k_{max}} - \varepsilon_{n,k_{min}}) = \frac{e^2}{h}\sum_{n=1}^{N_{max}}V_x = N_{\max}\frac{e^2}{h}V_x , \end{aligned} \tag{1.20}$$

where $-eV_x = \varepsilon_{n,k_{max}} - \varepsilon_{n,k_{min}}$ is the potential energy difference between the two edges as indicated in Figure 1.5. Therefore, the Hall conductivity is

$$\sigma_{xy} = -\sigma_{yx} = -\frac{I_y}{V_x} = -\frac{e^2}{h}N_{\max} . \tag{1.21}$$

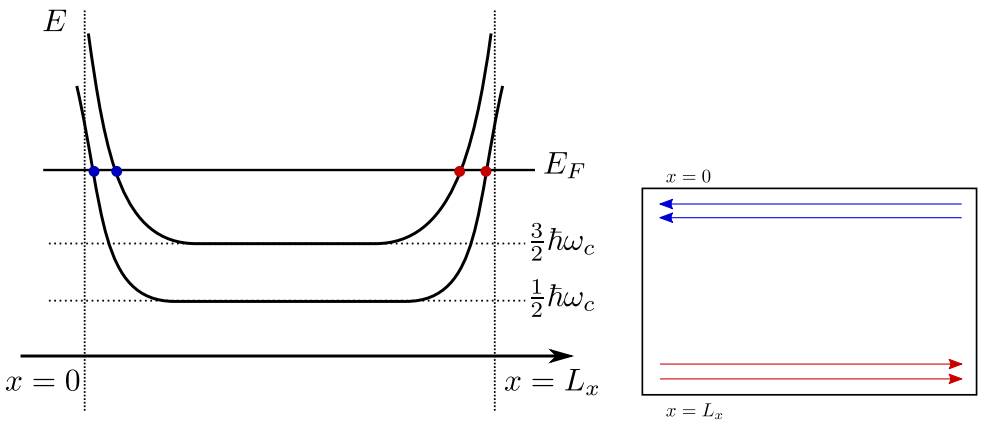

Figure 1.6: The left figure shows the energy profiles of $n = 0$ and $n = 1$ Landau levels without bias. Due to the confinement potential, the energy rises near the edges of the system at $x = 0, L_x$. The Fermi energy E_F crosses two states in a given edge, and these states at the E_F are the edge states. Note that the slopes of the dispersions of the edge states in a given edge is opposite from the ones on the other edge, indicating that the edge states at one edge propagate in the opposite direction from the ones on the other. The right figure shows the propagation of the corresponding edge states on a quantum Hall bar. The blue (red) dots on the right figure correspond to the top (bottom) edge states on the left figure.

The integer giving rise to the Hall conductivity is directly related to the number of the edge states on a given edge. Figure 1.6 shows the energy profile of the lowest two Landau levels and the corresponding edge states on the quantum Hall bar.

An edge state can be perceived as an one-dimensional ballistic channel with the unity transmission ($T = 1$). Connecting two reservoirs with chemical potential $\mu_1 = eV_1$ and $\mu_2 = eV_2$ respectively, the current through such channel is given by $I = (e/h)T(\mu_1 - \mu_2) = (e^2/h)V_H$ [BIL85, B88, B92], where $V_H = V_1 - V_2$.

If the effect of the impurities are taken into account, the Landau level energy is smeared as shown in Figure 1.7. Nonetheless, the dispersion crosses with the Fermi level near the edges, ensuring the existence of the edge states regardless of the perturbations from the

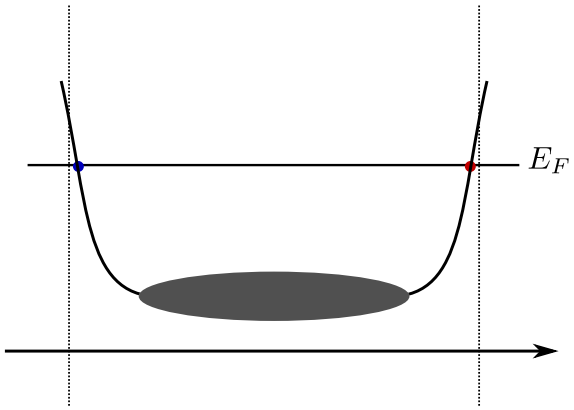

Figure 1.7: Due to the impurities, the Landau level in the bulk is smeared, indicated by the shaded area in the figure. However, the edge states are still present.

impurities [Hal82]. This robustness for the existence of the edge states explains the stability of the quantization of the transverse conductance. In the next section, the number of the edge state is related to a topological quantity.

1.1.5 Topological Interpretation of the quantization of σ_{xy}

Since IQHE is a very robust effect, it is natural to suspect that there is some underlying mechanism which depends only on its global property. Such global argument often pertains to the idea of topology, which turns out to explain the quantization in IQHE. Here, we introduce the Laughlin's gedanken experiment that relates such topological quantity to the integer in the Hall conductance.

The exactness of the quantization can be explained from the gauge invariance and existence of a energy gap [Lau81, Hal82]. Consider a thin strip of two-dimensional electron system wrapped around in a cylindrical form as shown in Figure 1.8, where the circumference direction is define as y and the axis direction is x. An external magnetic field B is applied in the perpendicular direction to the cylindrical surface, and there is an extra flux Φ threading along the axis of the cylinder. The potential difference V_x is also applied in x direction. The

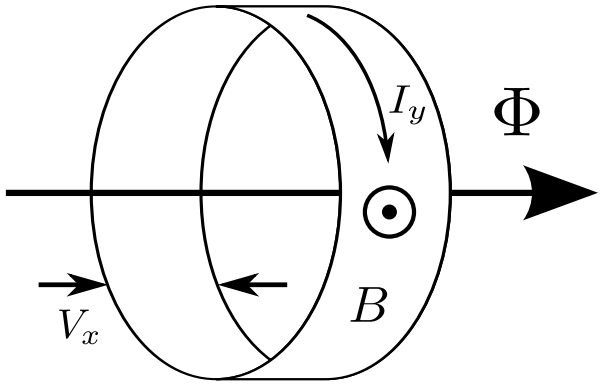

Figure 1.8: A quantum Hall bar is wrapped around in a cylindrical form. A magnetic field is applied in the radial direction, and there is an extra flux penetrating at the axis of the cylinder. The Hall voltage V_x is induced along the height of the cylinder, and the current I_y runs around the circumference correspondingly.

vector potential due to this extra flux is given by

$$\mathbf{A}' = (0, \Phi/L_y)\,, \tag{1.22}$$

where L_y is the length of the circumference, then the total Hamiltonian in Landau gauge is given by

$$H = \frac{p_x^2}{2m} + \frac{1}{2m}\left(p_y + eBx + \frac{e\Phi}{L_y}\right)^2 + eV_x x\,. \tag{1.23}$$

By comparison to Eq. (1.10), we can simply see that x_k is replaced by

$$x_k \to -l_B^2\left(k + l_B^2\frac{mE}{\hbar B}\right) - \frac{\Phi}{BL_y\phi_0}\,. \tag{1.24}$$

The extended states, whose center is initially located at x_k, is shifted by $-\Phi/BL_y\phi_0$ as the extra flux is changed.

The change of the extra flux is equivalent to a gauge transformation, and the wave function correspondingly picks up a phase $\exp(ieA'y/\hbar)$. If a state is localized at an impurity site, such a gauge transformation multiplies a trivial phase factor to the wave function since this localized state doesn't enclose the extra flux. On the other hand, an extended state that

extends around the circumference of the cylinder has to necessarily encloses the flux, thus the single valuedness condition on the wave function around the circumference imposes non-trivial condition $\exp(ieA'L_y/\hbar) = 1$. Only allowed value of the gauge field is $A' = n\phi_0/L_y$, where n is an integer. Then, the only allowed shift in x direction due to the flux insertion is $n\phi_0/BL_y = 2\pi l_B^2/L_y$. Hence, as one flux quanta ϕ_0 is inserted, all the extended states moves by ϕ_0/BL_y. This entire movement can be viewed as transporting one electron per Landau level from one edge to the other, thus N number of electrons can be transported if N Landau levels are filled. Since there is a potential difference V_x between the edges of the cylinder, transporting electrons from one edge to the other changes the energy of the system.

Such a change in energy due to varying the flux can be associated with the current around the circumference by $j_y = \partial E/L_x\partial\phi$. This derivative is non-zero only if the wave function is phase coherent around the loop. The the states localized somewhere in the cylinder only acquires trivial phases as the flux is changed, thus the energy of such states cannot change due to this flux change.

Here, we recall that there are energy gaps between Landau levels. Due to the gap, the adiabatic change of the flux cannot excite electrons from one Landau level to another, which means that the only energy change due to the flux change comes from transporting electrons from one edge to the other. Therefore, the current contribution comes only from the states extended around the circumference. If N Landau levels are filled, N electrons are transported across the potential differen $V_x = L_xE_x$, so the energy gain of the system is NeV_x. The quantization of the Hall conductivity comes from the existence of the extended states around the loop, and the integer associated with the quantization is explained by the single valuedness condition for such a state under this gauge transformation coming from the flux insertion:

$$j_y = \frac{1}{L_x}\frac{\Delta E}{\Delta\phi} = N\frac{eV_x}{L_x\phi_0} = N\frac{e^2}{h}E_x\,. \tag{1.25}$$

Therefore, the existence of the energy gap and gauge transformation can explain the quantization of the Hall conductivity.

1.1.6 TKNN Invariant

The integer appearing in the Hall conductivity can be explained in terms of a topological number called TKNN invariant [TKN82, Koh85], which is also called Chern number in the context of geometry.

Consider two-dimensional non-interacting electron system with perpendicular magnetic field with a periodic potential $U(x, y)$, then the Schrödinger equation is

$$H\Psi = \left[\frac{1}{2m}\left(\mathbf{p} + e\mathbf{A}\right)^2 + U(x, y)\right]\Psi = E\Psi\,. \tag{1.26}$$

The period of the potential is characterized by $U(x+a, y) = U(x, y+b) = U(x, y)$. By Bloch theorem, the solution under a periodic potential is given by

$$\psi^n_{\mathbf{k}}(x, y) = e^{i\mathbf{k}\cdot\mathbf{r}} u^n_{\mathbf{k}}(x, y)\,, \tag{1.27}$$

where $\mathbf{k} = (k_1, k_2)$ and $\mathbf{r} = (x, y)$, n is a band index, and the periodic conditions for the Bloch wave functions are $u^n_{\mathbf{k}}(x + qa, y) = e^{-i\pi py/b} u^n_{\mathbf{k}}(x, y)$ and $u^n_{\mathbf{k}}(x, y + b) = e^{i\pi px/qa} u^n_{\mathbf{k}}(x, y)$ when the flux through the system $\phi = eB/h$ is a rational number $\phi = p/q$. Under a gauge transformation $\mathbf{A}' = \mathbf{A} + \nabla\chi$, then the wave function picks up phase by $\psi' = e^{-ie\chi/\hbar}\psi$.

From Eq. (1.26), with $p_i = -i\hbar\partial_{x_i}$, the Schrödinger equation can be further written as

$$H(\mathbf{k})u^n_{\mathbf{k}}(x, y) \;=\; \left[\frac{1}{2m}\left(-i\hbar\nabla + \hbar\mathbf{k} + e\mathbf{A}\right)^2 + U(x, y)\right] u^n_{\mathbf{k}}(x, y) = E^n(\mathbf{k})u^n_{\mathbf{k}}(x, y) \tag{1.28}$$

When a small electric field is applied, a current flows as a linear response. The response function, which is the transverse conductivity in the context of quantum Hall effect, is given by Kubo formula as follows;

$$\sigma_{xy} = -ie^2\hbar \sum_{E^\alpha < E_F < E^\beta} \frac{(v_y)_{nm}(v_x)_{mn} - (v_x)_{nm}(v_y)_{mn}}{(E^n - E^m)^2}\,. \tag{1.29}$$

The velocity operator is $\mathbf{v} = (-i\hbar\nabla + e\mathbf{A})/m$, and the matrix element of the velocity operator above is

$$(\mathbf{v})_{nm} = \delta_{k_1,k_1'}\delta_{k_2,k_2'} \int_0^{qa} dx \int_0^b dy (u^n_{\mathbf{k}})^* \mathbf{v} u^m_{\mathbf{k}}(x, y)\,. \tag{1.30}$$

Note this matrix element is between two states with the same $\mathbf{k}$ belonging to the nth and mth bands respectively. Since we can also express the velocity operator in terms of the k derivative of the Hamiltonian, we can denote the velocity operators as

$$\begin{aligned}(v_i)_{nm} &= \frac{1}{\hbar}\left\langle u^n_{\mathbf{k}}\left|\frac{\partial H}{\partial k_i}\right|u^m_{\mathbf{k}}\right\rangle . \\ &= (E^m - E^n)\left\langle u^n_{\mathbf{k}}|\partial_{k_i}u^m_{\mathbf{k}}\right\rangle = -(E^m-E^n)\left\langle \partial_{k_i}u^n_{\mathbf{k}}|u^m_{\mathbf{k}}\right\rangle . \end{aligned} \tag{1.31}$$

Therefore the transverse conductance can be written in the sum of the contributions coming from each band;

$$\begin{aligned}\sigma_{xy} &= -i\frac{e^2}{\hbar}\sum_{E^n<E_F<E^m}\left[\langle\partial_{k_2}u^n|u^m\rangle\langle u^n|\partial_{k_2}u^m\rangle - \langle\partial_{k_1}u^n|u^m\rangle\langle u^n|\partial_{k_1}u^m\rangle\right] \\ &= -i\frac{e^2}{h2\pi}\sum_n\int d^2k\int d^2r\left[\partial_{k_2}(u^n_{\mathbf{k}})^*\partial_{k_1}u^n_{\mathbf{k}} - \partial_{k_1}(u^n_{\mathbf{k}})^*\partial_{k_2}u^n_{\mathbf{k}}\right] \\ &= -i\frac{e^2}{h2\pi}\sum_n\int d^2k\left[\partial_{k_2}\langle u^n_{\mathbf{k}}|\partial_{k_1}u^n_{\mathbf{k}}\rangle - \partial_{k_1}\langle u^n_{\mathbf{k}}|\partial_{k_2}u^n_{\mathbf{k}}\rangle\right] = \sum_n\sigma^n_{xy}\,. \end{aligned} \tag{1.32}$$

The Berry's connection can be defined to write the above expression in an elegant form,

$$\mathbf{A}^n_B(\mathbf{k}) = -i\int d^2r u^{n*}_{\mathbf{k}}\nabla_k u^n_{\mathbf{k}} = -i\left\langle u^n_{\mathbf{k}}|\nabla_k|u^n_{\mathbf{k}}\right\rangle , \tag{1.33}$$

which is not to be confused with the gauge field $\mathbf{A}$ introduced earlier. This leads to

$$\begin{aligned}\sigma^n_{xy} &= \frac{e^2}{h2\pi}\sum_n\int d^2k\left[\partial_{k_2}A^n_{B,1} - \partial_{k_1}A^n_{B,2}\right] \\ &= \frac{e^2}{h}\frac{1}{2\pi}\int d^2k[\nabla_{\mathbf{k}}\times\mathbf{A}^n_B(\mathbf{k})]_3\,, \end{aligned} \tag{1.34}$$

where 3 refers to the component perpendicular to $k_{1,2}$ plane. With this gauge field, a gauge transformation can be performed by

$$\mathbf{A}'^n_B = \mathbf{A}^n_B + \nabla_{\mathbf{k}}\chi^n\,. \tag{1.35}$$

Going back to Eq. (1.28), we find the appropriate transformation of the Bloch wave function under such a gauge transformation of the Berry's connection is $u'^n_{\mathbf{k}} = e^{i\chi^n}u^n_{\mathbf{k}}$.

Due to the periodicity in the potential, k space forms a Brillouin zone. Identifying the edges along k_1, and the other edges along with k_2, the first Brillouin zone forms a torus. In

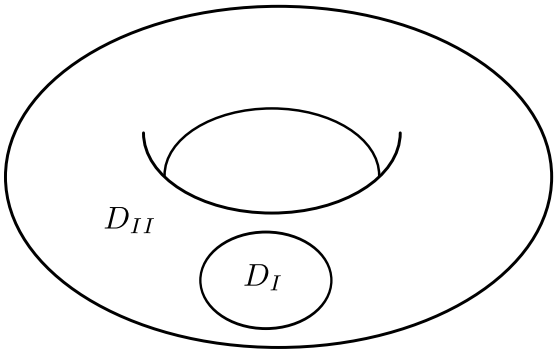

Figure 1.9: The first Brillouin zone is identified as a torus. As σ_{xy} is calculated from the Berry's connection in Eq. (1.34), the torus is divided into two regions D_I and D_{II}. The Berry's connection in D_I is related to the one in D_{II} by a gauge transformation.

order to calculate the Hall conductivity in Eq. (1.34), the Berry's connection has to be well defined in the entire base manifold. However, the Berry's connection becomes ill defined if the modulus of a Block wavefunction is zero for some $\mathbf{k}$. When this happens, one function for the Berry's connection cannot cover the entire manifold. This can be reconciled by dividing the torus into two regions; one is surrounded by a loop formed by the boundary of region D_I, and another is the complement of this region in the torus is region D_{II} as in Figure (1.9), and assign well defined Berry's connections $\mathbf{A}^n_I$ to D_I and $\mathbf{A}^n_{II}$ to D_{II}. Impossibility of writing down a Berry's connection that can cover the entire base manifold is associated with topological non-triviality of the system. These two connections are related by the gauge transformation,

$$\mathbf{A}^n_{B,II} = \mathbf{A}^n_{B,I} + \nabla_{\mathbf{k}}\chi^n \,. \tag{1.36}$$

Finally, the transverse conductance is

$$\begin{aligned}
\sigma^n_{xy} &= \frac{e^2}{h}\frac{1}{2\pi}\left\{\int_{D_I}\left[\nabla_k \times \mathbf{A}^n_{B,I}(\mathbf{k})\right]_3 + \int_{D_{II}}\left[\nabla_k \times \mathbf{A}^n_{B,II}(\mathbf{k})\right]_3\right\} \\
&= \frac{e^2}{h}\frac{1}{2\pi}\int_{\partial D_{II}} d\mathbf{k}\cdot\left[\mathbf{A}^n_{B,II}(\mathbf{k}) - \mathbf{A}^n_{B,I}(\mathbf{k})\right] \\
&= \frac{e^2}{h}\frac{1}{2\pi}\int_{\partial D_{II}} d\mathbf{k}\cdot\nabla\chi^n(\mathbf{k}) = \frac{e^2}{h}\frac{1}{2\pi}\left[\chi^n(\theta=2\pi) - \chi^n(\theta=0)\right] \,,
\end{aligned} \tag{1.37}$$

where θ here parameterizes the loop $\partial D_{II} = -\partial D_I$. Because of the phase picked up by the wave function under gauge transformation, we need to impose single valuedness condition to the Bloch wave function $u'_k = e^{i\chi} u_k$ under the gauge transformation, $\chi^n(\theta = 2\pi) - \chi^n(\theta = 0) = 2\pi N_n$ with $N_n \in \mathbb{Z}$, which means the above integer

$$N_n = \frac{1}{2\pi} \int_{\partial D_{II}} d\mathbf{k} \cdot \nabla \chi^n(\mathbf{k}) \tag{1.38}$$

gives an integer N_n. Therefore, the total conductance is also integral multiple of e^2/h.

The integer appearing in Eq. (1.38), called a winding number, is a topological quantity that is robust against small perturbations on the system. Introducing perturbations via impurities may modify the bands, but this topological quantity cannot change as long as the gap doesn't close due to the perturbations. The winding number that captures the degree of "twist" in the system giving rise to non-trivial topology.

In abstraction, the gauge potential given above can be thought as mathematical object called connection, which can be related to the curvature F in the following way. Given an 1-form connection $A = A_i dk^i$ over a base manifold M, the 2-form curvature is found by

$$F = dA = \partial_{k_i} A_j dk^i \wedge dk^j \,. \tag{1.39}$$

Integration of this curvature over the base manifold is a topologically invariant quantity called the first Chern number c_1,

$$\begin{aligned} c_1 &= \frac{1}{2\pi} \int_M F = \frac{1}{2\pi} \int_M \partial_{k_i} A_j dk^i \wedge dk^j = \frac{1}{2\pi} \int_M \left(\partial_{k_1} A_2 - \partial_{k_2} A_1\right) dk^1 dk^2 \\ &= \frac{1}{2\pi} \int_M dA = \frac{1}{2\pi} \int_{\partial M} A \,. \end{aligned} \tag{1.40}$$

In the second line, Stoke's theorem was used. This result corresponds to the integral in Eq. (1.37). The Chern number c_1 above is always an integer. The topology of the map from the first Brillouin zone (torus) to the Bloch wave function, $(k_1, k_2) \to u^n_{k_1,k_2}$, is characterized by the Chern number.

Now we have a coherent understanding of how integer quantum Hall effect comes about. The quantization of the Hall conductivity is a robust effect because it is a manifestation of a

topological number that cannot be changed by small perturbations. When the Fermi energy lies in energy gap of quantum Hall system, the Kubo formula for the Hall conductance is identified to be proportional to the Chern number, which is always integer. From Laughlin's gadanken experiment, this integer from the Chern number is related to the number of Landau levels under the Fermi energy.

1.2 Topological Insulator

1.2.1 Hall Effect without an External Magnetic Field

1.2.1.1 Anomalous Hall Effect and Spin Hall Effect

The quantization of the Hall conductivity in the integer quantum Hall effect has its origin in the topological order, which explains the robustness of the effect. The Chern number derived from its topological property is directly related to the number of the edge states. Charges can be transported ballistically through the edge states, hence dissipationless charge current can flow, as indicated by the vanishing of the longitudinal resistivity at the plateaus of the Hall resistivity.

In ferromagnetic conductors, the anomalous Hall effect (AHE) occurs, where the spin dependent transverse conductivity is acquired by the anomalous velocity. Since there is an imbalance between the majority and minority spin carriers in ferromagnetic conductors, the effect of their anomalous velocities don't cancel, which leads to non-zero contributions to the transverse conductivity. The anomalous velocity mainly comes from three effects; the intrinsic deflection originated from the Berry curvature of the bands, the side jump coming from the spin dependent force due to the interaction between the electron and the electric field from the impurity, and the skew scattering due to the effective spin-orbit coupling of the electron or the impurity [ERH06, NSO10]. Hence, the AHE exhibits non-zero transverse conductivity without an external magnetic field.

Since spin up and down electrons are deflected in the opposite directions due to the

AHE, the spin Hall effect, where an external electric field induces a spin current, can be expected [Hir99]. For an ordinary Hall effect, an external electric field in the plane of the system induces an in-plane charge current perpendicular to the field because electrons of both spin up and down are deflected in the same direction due to Lorentz force. For the spin Hall effect [IO05], spin up and down electrons are deflected in the opposite directions (yet perpendicular to the electric field), hence a spin current flows in the perpendicular direction to the field (see Figure 1.10). Due to the spin current, a spin accumulation can be induced by an external electric field, which have been also verified by some experiments [KMG04, WKS05].

The classical Hall effect lead to the discovery of the integer Hall effect, which exhibits dissipationless charge current due to the topological protected edge states. This feature of IQHE and the idea of the spin Hall effect lead to the possibility to generate a dissipationless spin current. Theoretical proposals for a dissipationless spin current were pursued in hole-doped semiconductors [MNZ03], and zero gap and narrow gap semiconductors [MNZ04] where the spin Hall conductivity comes from the Berry curvature; and high-mobility 2DEG with a strong Rashba interaction [SCN04]. Seeking a dissipationless spin current eventually resulted in the idea of topological insulator.

1.2.1.2 Haldane Model

One of the seminal works that lead to the discovery of the topological insulator showed the possibility of a quantum Hall effect without any external magnetic field for spinless electron system in graphene [Hal88]. Graphene has a honeycomb lattice structure, where its unit cell is a hexagonal lattice consisting of two triangular sublattices, and correspondingly the Brillouin zone is also hexagonal. The band structure of a graphene, which is derived from the nearest neighbor hopping tight binding model, is semi-metallic, where the conduction band touches the valence band at two points in the first Brillouin zone (K and K' points) [CGP09, Goe11]. Furthermore, the second nearest neighbor hopping (which breaks particle-hole symmetry)

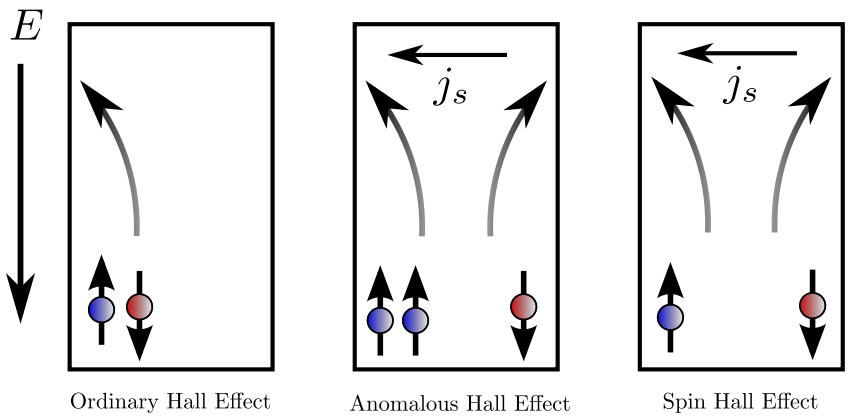

Figure 1.10: In each figure, an in-plane external electric field is applied in the vertical direction to induce electric current. The left figure shows the ordinary Hall effect, where both spin up and down electrons are deflected in the same direction to cause a charge accumulation on one edge leading to the Hall voltage. The middle picture shows the anomalous Hall effect (AHE) in a ferromagnetic conductor. Here, spin up and down electrons are deflected in the opposite direction. Since there is an imbalance between the spin up and down electrons in a ferromagnetic conductor, it induces a charge accumulation on one edge leading to the Hall voltage. Furthermore, a spin current flows in the perpendicular direction to the electric current. The right figure shows the spin Hall effect. As in the AHE, spin up and down electrons are deflected in the opposite directions, however the Hall voltage is not induced because there is no imbalance between the up and down spin electrons. A spin current also flows perpendicularly to the field in this case.

and a local flux which sums up to zero in a unit cell (which breaks the time reversal symmetry) are considered. The graphene under this condition is known as Haldane model.

Expanding such tight binding Hamiltonian around K and K', two Dirac Hamiltonian corresponding to K and K' points can be derived. The mass terms at K and K' of these Dirac Hamiltonian depend differently on the second nearest neighbor hopping strength and the internal flux, and the signs of the mass terms at K and K' are either the same or opposite depending on the relative contributions of those two parameters. It is shown that when the sign of the mass terms switches from K to K' points, an integer quantum Hall effect with

$\nu = \pm 1$ occurs. If the sign is the same, the states can be adiabatically connected to the massless case, which is time reversal symmetric; hence the transverse conductance is zero (an ordinary insulator phase).

Exhibiting a quantum Hall effect, the Haldane model must be associated with edge states. In fact, the band calculation of semi-infinite graphene shows that there is a state that traverses the gap, and this state corresponds to the edge state that gives rise to the integer quantum Hall effect. The Haldane model can be understood as the existence of two topologically distinct states with or without the presence of quantum Hall effect, which is signaled by the sign of the time reversal symmetry breaking mass terms of the effective Dirac Hamiltonian at K and K' pints.

1.2.1.3 Quantum Spin Hall Effect on Kane-Mele Model of Graphene

The Haldane model was extended to the model of graphene with the mass term that is both time reversal and inversion symmetric, so called Kane-Mele model [KM05a, Kan07]. The effective Hamiltonian around K and K' points are the massless Dirac Hamiltonian:

$$H_0 = -i\hbar v_F \psi^\dagger (\sigma_x \tau_z \partial_x + \sigma_y \partial_y)\psi \,. \tag{1.41}$$

Here, $\boldsymbol{\sigma}$ refers to the pseudo spin pertaining to the sublattice A and B with $\sigma_z = \pm 1$ describing the state on A (B), and similarly $\boldsymbol{\tau}$ refers to K and K' points with $\tau_z = \pm 1$ describing the state on K (K'). The Hamiltonian in Eq. (1.41) gives the gapless states with the dispersion $E(\mathbf{q}) = \pm\hbar v_F |\mathbf{q}|$. There can be various mass terms that can be introduced to open a gap. The mass term proportional to σ_z corresponds to a staggered sublattice potential alternating its sign depending on A and B sublattices, is odd under parity. The mass term in the form $\sigma_z\tau_z$ is even under parity and odd under time reversal, and it corresponds to the type of term introduced in Haldane model for the zero-net-flux internal magnetic field. The term $\sigma_z\tau_z s_z$ is even under both parity and time reversal, and this term introduces a new topological phase.

$\sigma_z\tau_z s_z$ term introduces masses with opposite signs at K and K' points. Under such a

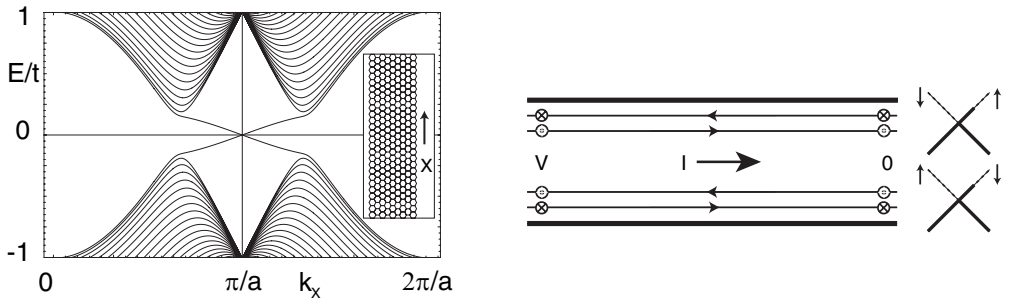

Figure 1.11: The left figure shows the energy bands in a given edge of a strip of graphene. There are two states traversing the gap have opposite spins, hence the edge is spin filtered. In the right figure, spin filtered edges are shown. Each edge has two counterpropagating states with the opposite spins. The figures are cited from [KM05a].

mass term, the energy of a state is rased on one of K and K' points and lowered on the other, and we can realize a state that traverses the energy gap. In fact, the band calculation with $\sigma_z\tau_z s_z$ mass term gives rise to two gapless states with opposite slopes on a given edge, which traverse the bulk gap, and they are localized at the edge of the graphene strip as shown in Figure 1.11. Since the slopes of these gapless states are opposite, they propagate in the opposite directions. The two states on a given edge are related by time reversal operation, and such a pair is call Kramers' pair. If s_z is a good quantum number (it is the case if there is no spin flipping interaction such as Rashba spin-orbit interaction), one state is associated with $s_z = \hbar/2$, and the other with $s_z = -\hbar/2$.

Thus, the edges of the graphene under the time reversal and inversion symmetric spin-orbit interaction of the form $\sigma_z\tau_z s_z$ are equipped with the spin filtered edge states, where a given edge has counter propagating states with opposite spins, known as helical edge states. Each edge state leads to quantized Hall conductance value $\sigma_{xy} = \pm e^2/h$ [Hal88], where the sign of the conductivity depends on the spin (or equivalently on the direction of propagation).

Due to the time reversal symmetry, the total transverse conductivity, which is the sum of spin up and down contributions, must be zero. However, the difference in the spin up and down currents do not vanish, and we find the spin current given by $J_s = \frac{\hbar}{2e}(J_\uparrow - J_\downarrow)$. This

gives a quantized spin Hall conductivity $\sigma^s_{xy} = (\hbar/2e)2\sigma_{xy} = e/2\pi$, which is also quantized. Since each quantum Hall edge channel can propagate ballistically, dissipationless spin current can be generated by applying an electric field. These edge states are also robust against weak perturbations that are time reversal symmetric, because the degeneracy where the crossing point of these two states in the bulk gap cannot be lifted by such a perturbation. This fact that these edge states are robust against time reversal perturbation is due to its topological origin, and it will be discussed in the next section. Although the quantization of the spin quantum Hall conductivity cannot persist under spin flipping perturbation such as Rashba spin-orbit interaction, the topological order still remains [KM05b].

1.2.2 Z_2 Topological Invariant

1.2.2.1 Charge Pumping and TKNN Invariant

The field of topological insulator [HK10, ZHX11, QZ11, Moo10, QZ10] grew rapidly. Although it turns out that the spin-orbit interaction in graphene, which leads to the quantum spin Hall effect, is too small to be observed experimentally, this example shed some light on the further development in the search of quantum spin Hall effect.

The key idea in the example of graphene is that a given edge is endowed by Kramers pair whose degeneracy is protected by the time reversal symmetry. When there is only one Kramers pair, this degeneracy cannot be lifted by any time reversal symmetric perturbation, hence these states form bands that necessarily traverse the gap. This state of matter is topologically distinct from an ordinary insulator because they cannot be connected by adiabatic transformation of the parameters in the Hamiltonian. However, if there are even number of Kramers pairs, the gap traversing states can be reconnected in the way that the resultant bands are topologically same as an ordinary insulator under some perturbation including time reversal symmetric one such as Rashba S.O. interaction [KM05b]. This seems to suggest the even or odd number of Kramers pairs at a given edge is related to the distinction between a topologically non-trivial state and an ordinary insulator.

Non-triviality of the integer quantum Hall system is characterized by Chern number, which pertains to the information of the topology of the system. This number is obtained by integrating the Berry curvature over the magnetic Brillouin zone as calculated in Eq. (1.34). Since this number is topological, it cannot change by small perturbations in the system. If the edge states appearing in the quantum spin Hall system are also topological, there should be such number associated with them. It was shown that the robustness of the edge states in quantum spin Hall system can be explained by Z_2 topological invariant [KM05b, FK06] (either 0 or 1 to distinguish non-trivial and trivial topological phases), where in the context of graphene example, it refers to even or odd number of Kramers pairs in a given edge.

Z_2 topological invariant is constructed in a similar way to Chern number in the integer quantum Hall system. In order to gain insight for obtaining Z_2 invariant, it is convenient to go over an alternative way of finding Chern number in relation to the charge polarization of the system.

In an one-dimensional ring of lattices with length L (there are $N = L/a$ lattice points, where a is the lattice spacing), we find the Bloch wave function

$$|\psi_{n,k}\rangle = \frac{1}{\sqrt{L}} e^{ikx} |u_{n,k}\rangle \,, \tag{1.42}$$

where k is the crystal momentum and n is the band index. Then, the Wannier function at a lattice point R is given by

$$|R, n\rangle = \int \frac{dk}{2\pi} e^{-ik(R-r)} |u_{n,k}\rangle \,, \tag{1.43}$$

which describes a localized orbital function around R. The charge polarization P_ρ is the expectation value of the center of the Wannier function at one of the lattices, say $R = 0$,

and it is

$$\begin{aligned} P_\rho &= \sum_n \langle 0,n|x|0,n\rangle = \sum_n \sum_{k',k} \frac{1}{L}\langle u_{n,k'}|e^{-ik'x}xe^{ikx}|u_{n,k}\rangle \\ &= \sum_n \sum_{k',k} \frac{1}{L}\langle u_{n,k'}|e^{-ik'x}\left(-i\partial_k e^{ikx}\right)|u_{n,k}\rangle = \sum_n \sum_{k',k} \frac{1}{L} e^{i(k-k')x}\langle u_{n,k'}|i\partial_k|u_{n,k}\rangle \\ &= \sum_n \sum_{k',k} \delta_{k,k'}\frac{1}{L}\langle u_{n,k}|i\partial_k|u_{n,k}\rangle = \sum_n \sum_k \frac{1}{L}\langle u_{n,k}|i\partial_k|u_{n,k}\rangle \\ &= \oint \frac{dk}{2\pi} A_k(k)\,. \end{aligned} \tag{1.44}$$

Note the Berry's connection appeared on the way, which are defined by

$$\begin{aligned} A_k(k) &= \sum_n i\langle u_{n,k}|\partial_k|u_{n,k}\rangle\,, \\ A_t(k) &= \sum_n i\langle u_{n,k}|\partial_t|u_{n,k}\rangle\,. \end{aligned} \tag{1.45}$$

In Eq. (1.44), only A_k came up, but A_t is also define here for later convenience.

Because the first Brillouin zone is periodic, $k = -\pi$ and $k = \pi$ are identical, which is why we have a closed loop integral in Eq. (1.44). We can see how this charge density evolves in time by takeing the difference in the charge polarizations at $t = 0$ and $t = T$,

$$\begin{aligned} P_\rho(T) - P_\rho(0) &= \oint_{c_T} \frac{dk}{2\pi} A_k(k,T) - \oint_{c_0} \frac{dk}{2\pi} A_k(k,0) \\ &= \int_{-\pi}^{\pi} \frac{dk}{2\pi} \int_0^T dt \partial_t A(k,t) \\ &= \int_{-\pi}^{\pi} \frac{dk}{2\pi} \int_0^T dt\left[\partial_t A(k,t) - \partial_k A_t(k,t)\right] \\ &= \frac{1}{2\pi}\int_S dt dk F(k,t)\,. \end{aligned} \tag{1.46}$$

$c_{0,T}$ are the paths for time $t = 0, T$ respectively. In the third line, the second term can be added for free because it is zero over a loop integral of k. $F(k,t)$ is the Berry curvature given by

$$\begin{aligned} F(k,t) &= i\sum_n \left[\langle \partial_t u_{n,k}|\partial_k u_{n,k}\rangle - \langle \partial_k u_{n,k}|\partial_t u_{n,k}\rangle\right] \\ &= \partial_t A_k(k,t) - \partial_k A_t(k,t) \end{aligned} \tag{1.47}$$

Furthermore, if the Hamiltonian has a cycle of T, namely $H(t) = H(t+T)$, the time points $t = 0$ and $t = T$ can be identified so that the base manifold is a torus in the space spanned by k and t. Then, we can write

$$P_\rho(T) - P_\rho(0) = \frac{1}{2\pi} \int_{T^2} dtdkF(k,t)\,. \tag{1.48}$$

This result is to be compared to the Chern number seen in Eq. (1.40), and it must give an integer associated with the topology of the system. Therefore the charge polarization over one period T of the Hamiltonian is an integer. If a system has a non-trivial topology, it can transport integer number of charges as a parameters of Hamiltonian is changed over a period, which is known as charge pumping.

The process of charge pumping can be related to Laughling's argument of the integer quantum Hall cylinder threaded by a magnetic flux. The pumping parameter t is identified as the flux in Laughlin's context, and further this flux can be directly related to the crystal momentum perpendicular to k in Eq. (1.48). Therefore, we can let $t \to k_1$ and $k \to k_2$ to recover the Chern number formula in Eq. (1.40). Hence, the topological invariance for the integer Hall system can be viewed as the charge polarization over one period of the charge pumping cycle.

1.2.2.2 Time Reversal Polarization as Z_2 Invariant

When there is no spin-orbit interaction that mixes spins, such as Rashba spin-orbit interaction, the z component of spin is conserved. Under this circumstance, we can simply assign up and down spins for a Kramers pair. Suppose we have a cylindrical geometry. One edge has a pair of counter propagating states with spin up and down, and the other edge has also a counter propagating pair but with opposite spin configuration due to time reversal symmetry. We can view such system as two copies of integer quantum Hall effect with counter propagating edge states endowed with opposite spins [BZ06, Kan07]. Note the transverse conductance coming from these two states are opposite in sign because they are moving in opposite directions. The total transverse conductance, hence, is zero, which can be also

concluded from time reversal symmetry of Kramers pair.

As in Laughlin's argument, the integer quantum Hall system in a cylindrical form transports an integer number of charges from one end to the other upon insertion of one flux quanta, which is related to the integer appearing in the Hall conductance. Due to this transport of the charges, the final state of the cylinder is charge polarized. By analogy, as one-half of a flux quanta threads the cylinder with a Kramers' pairs at a given edge of the cylinder, a half of spin up is transported from one side to the other, and a half of spin down is transported in the opposite direction. The net transport of spin $\hbar/2$ from one side to the other thus occurs, and the cylinder becomes spin polarized. This is one instance of so called "time reversal polarization". If s_z is not conserved, we cannot label the time reversal polarization by spin as we did here, but the time reversal polarization can still mean as the measure of switching of Kramers pairs from one ends to the other. Hence, the time reversal polarization is characterized by keeping track of the center of Wannier functions of the Kramers' pairs.

More explicit formulation of the time reversal polarization is shown as follows. The time reversal operator for a spin 1/2 particle is given by $\Theta = -i\sigma_y K$, where K is complex conjugation operator, and consequently $\Theta^2 = -1$. Suppose we have a Hamiltonian that has properties: $H[t+T] = H[t]$ and $H[-t] = \Theta H[t]\Theta^{-1}$. There are two special time points $t = 0, T/2$, where the Hamiltonian becomes time reversal invariant. Suppose there are $2N$ eigenstates, coming from N Kramers pairs formed at the time reversal invariant points. We denote such Kramers' pair by $|u^I_{k,\alpha}\rangle$ and $|u^{II}_{-k,\alpha}\rangle$, where $\alpha = 1, 2, \cdots, N$. The relation between each Kramers' pair is given by the time reversal operation as

$$\begin{aligned} |u^I_{-k,\alpha}\rangle &= e^{i\chi_\alpha(k)}\Theta|u^{II}_{k,\alpha}\rangle\,, \\ |u^{II}_{-k,\alpha}\rangle &= -e^{i\chi_\alpha(-k)}\Theta|u^I_{k,\alpha}\rangle\,. \end{aligned} \tag{1.49}$$

As in the charge polarization, we can define the Wannier center of state I and II by

$$\begin{aligned} P^s &= \int_{-\pi}^{\pi}\frac{dk}{2\pi}A^s(k) \\ &= \int_0^{\pi}\frac{dk}{2\pi}\left[A^s(k) + A^s(-k)\right]\,, \end{aligned} \tag{1.50}$$

where $s = I, II$, and the associated Berry's connection is defined by

$$A^s(k) = i \sum_\alpha \langle u^s_{k,\alpha} | \partial_k | u^s_{k,\alpha} \rangle \,. \tag{1.51}$$

The matrix element of an operator between time reversed states reads

$$\begin{aligned} \langle \Theta u^{II}_{k,\alpha} | i\partial_k | \Theta u^{II}_{k,\alpha} \rangle &= \langle u^{II}_{k,\alpha} | \Theta (i\partial_k)^\dagger \Theta^{-1} | u^{II}_{k,\alpha} \rangle \\ &= -\langle u^{II}_{k,\alpha,} | i\partial_k | u^{II}_{k,\alpha,} \rangle \end{aligned} \tag{1.52}$$

From Eq. (1.50), For P^I, the second term containing $A^I(-k)$ is expressed as

$$\begin{aligned} A^I(-k) &= \sum_\alpha \langle u^I_{-k,\alpha,} | i\partial_k | u^I_{-k,\alpha} \rangle = \sum_\alpha \langle \Theta u^{II}_{-k,\alpha} | e^{-i\chi_{k,\alpha}} i\partial_k e^{i\chi_{k,\alpha}} | \Theta u^{II}_{-k,\alpha} \rangle \\ &= \sum_\alpha \langle \Theta u^{II}_{-k,\alpha} | i\partial_k | \Theta u^{II}_{-k,\alpha} \rangle - \sum_\alpha \partial_k \chi_\alpha(k) = -\sum_\alpha \langle u^{II}_{-k,\alpha} | i\partial_k | u^{II}_{-k,\alpha} \rangle - \sum_\alpha \partial_k \chi_\alpha(k) \\ &= \sum_\alpha \langle u^{II}_{k,\alpha} | i\partial_k | u^{II}_{k,\alpha} \rangle - \sum_\alpha \partial_k \chi_\alpha(k) = A^{II}(k) - \sum_\alpha \partial_k \chi_\alpha(k) \,. \end{aligned} \tag{1.53}$$

Then, P^I is further expressed as

$$\int_0^\pi \frac{dk}{2\pi} \left[A^I(k) + A^{II}(k) \right] - \frac{1}{2\pi} \sum_\alpha \left[\chi_\alpha(\pi) - \chi_\alpha(0) \right] \,. \tag{1.54}$$

The second term can be expressed in terms of the matrix element of the time reversal operator:

$$w_{\alpha\beta}(k) = \langle u_{-k,\alpha} | \Theta | u_{k,\beta} \rangle \,. \tag{1.55}$$

This matrix element is non-zero only when $\alpha = \beta$, $w_{\alpha\alpha}$ is a 2×2 matrix of the form

$$\begin{aligned} w_{\alpha\alpha}(k) &= \begin{pmatrix} \langle u^I_{\alpha,-k} | \Theta | u^I_{k,\alpha} \rangle & \langle u^I_{-k,\alpha} | \Theta | u^{II}_{k,\alpha} \rangle \\ \langle u^{II}_{\alpha,-k} | \Theta | u^I_{k,\alpha} \rangle & \langle u^{II}_{-k,\alpha} | \Theta | u^{II}_{k,\alpha} \rangle \end{pmatrix} \\ &= \begin{pmatrix} 0 & e^{i\chi_\alpha(k)} \\ -e^{i\chi_\alpha(-k)} & 0 \end{pmatrix} , \end{aligned} \tag{1.56}$$

and $w_{\alpha\beta}$ is in the form of N blocks of such 2×2 matrixes on the diagonal. At the time reversal invariant momentum points $k = 0, \pi$, $\chi_\alpha(\pi) = \chi_\alpha(-\pi)$, and the matrix above is anti-symmetric. For an anti-symmetric matrix, Pffafian, whose square is equal to determinant, can be used to express the sum in the second term in Eq. (1.54) is given by

$$e^{i \sum_\alpha [\chi_\alpha(\pi) - \chi_\alpha(0)]} = \frac{\mathrm{Pf}[w(\pi)]}{\mathrm{Pf}[w(0)]} \,, \tag{1.57}$$

which can be written as

$$\sum_{\alpha} \left[\chi_\alpha(\pi) - \chi_\alpha(0)\right] = -i \log\left(\frac{\mathrm{Pf}[w(\pi)]}{\mathrm{Pf}[w(0)]}\right) . \tag{1.58}$$

Finally, the polarization of the first Wannier state is given by

$$P^I = \int_0^\pi \frac{dk}{2\pi}\left[A^I(k) + A^{II}(k)\right] + \frac{i}{2\pi}\log\left(\frac{\mathrm{Pf}[w(\pi)]}{\mathrm{Pf}[w(0)]}\right) . \tag{1.59}$$

In the similar way, we can also obtain P^{II}, then the time-reversal polarization is defined by the difference in the polarization of the Wannier centers of Kramers pairs:

$$\begin{aligned}
P_\theta &= P^I - P^{II} \\
&= \int_0^\pi \frac{dk}{2\pi}\left[A^I(k) + A^{II}(k)\right] - \int_{-\pi}^0 \frac{dk}{2\pi}\left[A^I(k) + A^{II}(k)\right] + \frac{i}{\pi}\log\left(\frac{\mathrm{Pf}[w(\pi)]}{\mathrm{Pf}[w(0)]}\right) \\
&= \int_0^\pi \frac{dk}{2\pi}\left[A^I(k) + A^{II}(k)\right] - \int_0^\pi \frac{dk}{2\pi}\left[A^I(-k) + A^{II}(-k)\right] + \frac{i}{\pi}\log\left(\frac{\mathrm{Pf}[w(\pi)]}{\mathrm{Pf}[w(0)]}\right) \\
&= \frac{1}{2\pi i}\left[\int_0^\pi \partial_k \log\det[w(k)] - 2\log\left(\frac{\mathrm{Pf}[w(\pi)]}{\mathrm{Pf}[w(0)]}\right)\right] \\
&= \frac{1}{\pi i}\log\left(\frac{\sqrt{\det[w(\pi)]}\mathrm{Pf}[w(0)]}{\sqrt{\det[w(0)]}\mathrm{Pf}[w(\pi)]}\right) .
\end{aligned} \tag{1.60}$$

Since $\det[w] = \mathrm{Pf}[w]^2$, $P_\theta = \log(\pm 1)/i\pi = \pm 1$, and we can also write down

$$(-1)^{P_\theta} = \frac{\sqrt{\det[w(0)]}}{\mathrm{Pf}[w(0)]}\frac{\sqrt{\det[w(\pi)]}}{\mathrm{Pf}[w(\pi)]} . \tag{1.61}$$

Following the charge polarization procedure for obtaining the topological invariant, we need to take the difference of this time-reversal polarization at different times. The change in the time-reversal polarization between $t = 0$ and $t = T/2$ is gauge invariant up to modulo 2, therefore we define Z_2 topological invariant ν as

$$\nu = \left[P_\theta(T/2) - P_\theta(0)\right] , \tag{1.62}$$

which can be also written as

$$(-1)^\nu = \prod_{i=1}^{4} \frac{\sqrt{\det[w(\Gamma_i)]}}{\mathrm{Pf}[w(\Gamma_i)]} , \tag{1.63}$$

where $\Gamma_{1,2,3,4} = (0,0), (0,\pi), (\pi,\pi), (\pi,0)$ are the time reversal invariant momentum points shown in Figure 1.12(b).

The time-reversal polarization can be visualized by keeping track of the evolution of the Wannier center of the Kramers' pairs. If a system is in a topologically non-trivial phase, Kramers' pairs at $t = 0$ will switch partners at $t = T/2$ by leaving stray states of different species at opposite ends as shown in Figure 1.12(a). On the other hand, in a topologically trivial phase, initial Kramers' pairs at $t = 0$ will come back to the same pairs at $t = T/2$, so there will be no stray states at the ends. This difference is captured by the Z_2 invariant ν defined in Eq. (1.62), and $\nu = 0, 1$ distinguishes trivial and non-trivial phases.

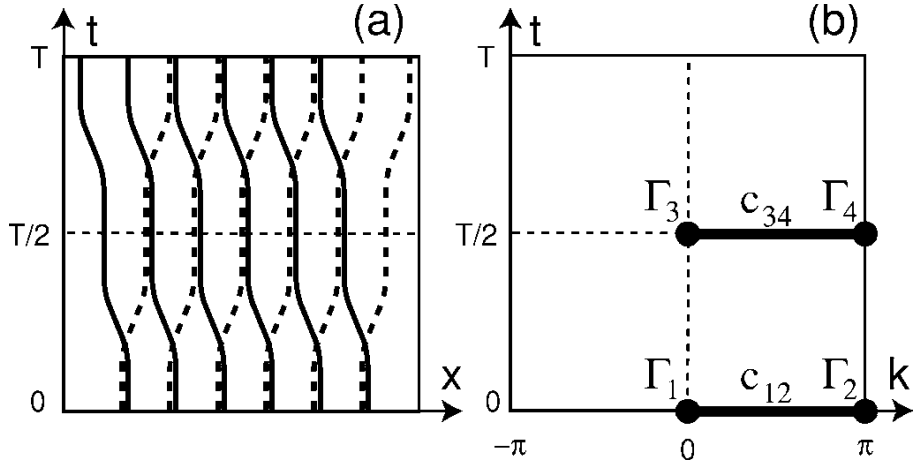

Figure 1.12: (a)The time evolution of the Kramers' pairs. Initially paired partners at $t = 0$ switches partners at $t = T/2$, and there are stray states at each ends. In some sense, the system is polarized because different species from the original Kramers pairs are present at opposite ends. (b)The time-reversal invariant points Γ_i, where $i = 1, 2, 3, 4$ in the torus Brillouin zone. The figures taken from [FK06].

1.2.2.3 HgTe/CdTe Quantum Well

One of the significant features of topological insulator is its unique helical edge states, where a given edge has Kramers' pairs. If s_z is conserved, we can think of a Kramers pair as

counter propagating states with opposite spins. Furthermore, if a system is in a topologically non-trivial phase, these edge states are protected against a time reversal symmetric perturbation, and they can propagate without backscattering [WBZ06, XM06]. Since states with opposite spins propagate in the opposite directions, in principle it is possible to have dissipationless spin current. Hence, experimental realizations of topological insulators would bring tremendous interest for not only theoretical but also various applications dealing with spin current.

The model of HgTe/CdTe quantum well was proposed to exhibit a non-trivial topological phase [BHZ06]. HgTe is a semiconductor in zinc blende crystalline structure, but the order of the bands are inverted from the usual order. The s-type Γ_6 band is usually above the p-type Γ_8 band, but the band order of HgTe is reversed because the strong spin-orbit interaction due to heavy Hg splits the Γ_8 band and places above Γ_6. On the other hand, CdTe has the normal band order, where Γ_6 band is above Γ_8 (Figure 1.13(A)). As a quantum well is formed by sandwiching HgTe by CdTe, the band order in the well can be controlled by the thickness of the HgTe. If HgTe is thicker than the critical thickness d_c, the band order is inverted. If it is less than d_c, the band order is the normal order because the band feature of CdTe becomes more dominant. It turns out that when the band order is inverted as in Figure 1.13(B), this system exhibits a quantum spin Hall effect, which is the signature of the non-trivial topological phase discussed in the previous section. In the case that the band order is normal, the system loses the feature of the quantum spin Hall effect.

This quantum well can be described by a four-band model with quantum well subbands $|E1, m_J = \pm 1/2\rangle$ consisting of $|\Gamma_6, m_J = \pm 1/2\rangle$ and $|\Gamma_8, m_J = \pm 1/2\rangle$, and other subbands $|H1, m_J = \pm 3/2\rangle$ consisting of $|\Gamma_8, m_J = \pm 3/2\rangle$, where m_J labels the z component of the total angular momentum. The Hamiltonian is given in the basis of $|E1, m_J = 1/2\rangle$, $|H1, m_J = 3/2\rangle$, $|E1, m_J = -1/2\rangle$, and $|H1, m_J = -3/2\rangle$ as

$$H(k_x, k_y) = \begin{pmatrix} h(k) & 0 \\ 0 & h^*(-k) \end{pmatrix}, \tag{1.64}$$

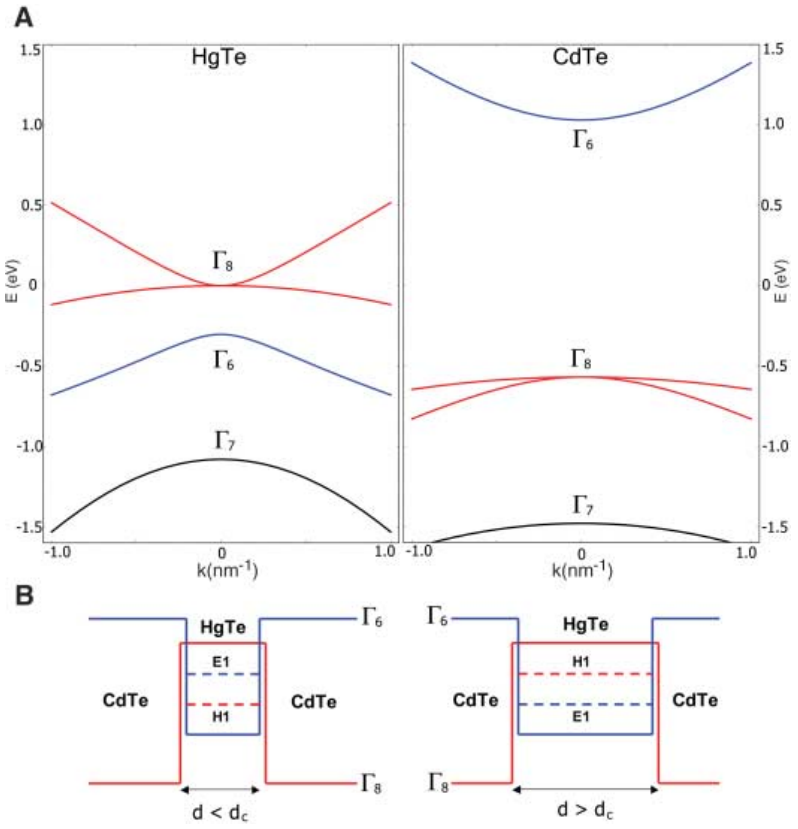

Figure 1.13: (A)The band structures of HgTe and CdTe are shown. For CdTe, Γ_6 band is above Γ_8 is normal order, however, the order of these bands is inverted with HgTe. (B)A quantum well is formed by sandwiching HgTe by CdTe. When the thickness of HgTe exceeds d_c, the system exhibits a quantum spin Hall phase. When the thickness is less than d_c, it is in a trivial phase. The left figure is topologically trivial phase ($d < d_c$), where the band order in HgTe is dominated by CdTe order. The right figure shows the topologically non-trivial phase, where the band order is inverted. The figure is taken from [BHZ06].

where $h(k) = \varepsilon(k) + \mathbf{d} \cdot \boldsymbol{\sigma}$. Although the crystalline structure breaks inversion symmetry due to its zinc blende structure, it is neglected for simplicity in this model. The the components of the $\mathbf{d}$ vector and $\varepsilon(k)$ in the 2×2 block Hamiltonian $h(k)$ are given by

$$\begin{aligned} d_1 &= Ak_x \,, \\ d_2 &= Ak_y \,, \\ d_3 &= M - B(k_x^2 + k_y^2) \,, \\ \varepsilon(k) &= C - 2D\left[2 - \cos k_x - \cos k_y\right] \,. \end{aligned} \tag{1.65}$$

Here, the lattice constants are set to unity. The gap parameter M is the energy difference between $E1$ and $H1$ bands, and $E1 > H1$ when $d < d_c$ and $E1 < H1$ when $d > d_c$, so M changes sign across the critical thickness d_c.

The Hall conductance for the type of Hamiltonian in Eq. (1.64) was studied in Ref. [QWZ06] in the context of a semiconductor exhibiting quantized anomalous Hall effect. The Hall conductance for each 2×2 block is given by

$$\sigma_{xy} = -\frac{e^2}{h} \frac{1}{8\pi} \int dk_x dk_y \hat{\mathbf{d}} \cdot \partial_{k_x} \hat{\mathbf{d}} \times \partial_{k_y} \hat{\mathbf{d}} \,, \tag{1.66}$$

where $\hat{\mathbf{d}} = \mathbf{d}/|\mathbf{d}|$ is the unit vector in the 2×2 block Hamiltonian $h(k)$. The expression under the integral is the Jacobian of the map $\hat{\mathbf{d}} : R^2 \to S^2$. $d_3/|\mathbf{d}| = \mathrm{sgn}(M)$ for $k = 0$, and $d_3/|\mathbf{d}| \to 0$ for $k \to \infty$. Since d_1 and d_2 parts always cover all the azimuthal direction, the direction of d_3 determines whether the northern or southern hemisphere of S^2 is covered as all k_x and k_y are swept. When $M > 0$ ($M < 0$), the northern (southern) hemisphere is covered. Therefore, depending on the sign of M, the Hall conductivity is $\sigma_{xy} = \pm e^2/2h$. This kind of half-integral Hall conductance is not allowed, and it is because the approximation of this particular theory fails to capture higher-energy spectrum (the fermion-doubling problem [NN81a, NN81b]). It turns out there is a missing contribution to either add another half-integral Hall conductance or cancel it. Although the present theory cannot capture this missing part, it can show that the Hall conductivity changes by $\Delta\sigma_{xy} = e^2/h$ as M changes its sign. Since the system has to change its Hall conductivity by e^2/h, either

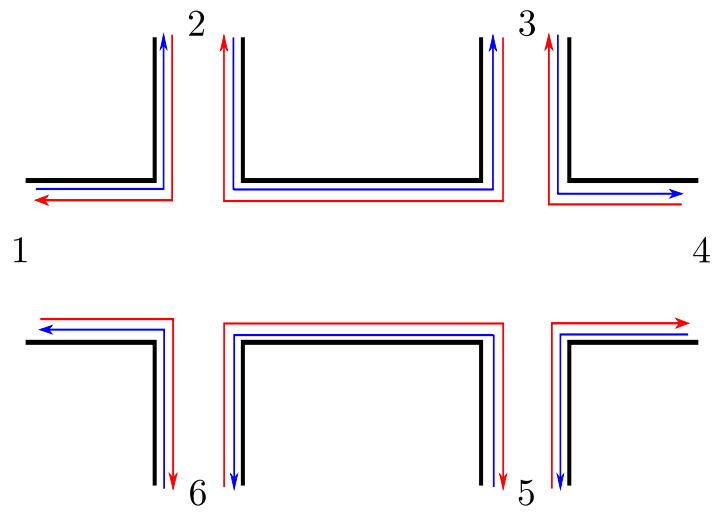

Figure 1.14: The figure shows the 6 terminal geometry for transport measurement. The blue indicate it is spin up, and the red is spin down. For a given edge, there are counter propagating states with opposite spins.

$M > 0$ or $M < 0$ has to be topologically non-trivial phase. From Ref.[KWB07], $M > 0$ for $d < d_c$ and $M < 0$ for $d > d_c$. Therefore, $M < 0$ with $d > d_c$, which is the inverted band order regime, exhibits quantized Hall conductance. The contribution to the Hall conductance from the lower 2×2 block $h^*(-k)$ is opposite in sign in comparison to the one from $h(k)$ block, which makes the total charge Hall conductance to vanish. However, the difference between these Hall conductances is non-zero, which means the spin Hall conductance is $\sigma_{xy}^{(s)} = e/\pi$.

The helical edge states result in a non-zero quantized spin Hall conductance, where each edge has counter propagating states with opposite spins as in Figure 1.14. The existence of such helical edge states were partially verified by transport measurements [KWB07, KBM08, RBB09]. The four terminal resistance measurement gives $R_{12,34} = I_{12}/V_{34} = h/2e^2$, if there are two ballistic channels. The experimental result for such four terminal resistance measurement with HgTe is shown in Figure 1.15. When the thickness of the well is smaller than the critical thickness ($d < d_c$), the system is in trivial state, and the resistance is high. When the thickness exceeds the critical thickness $d > d_c$, the system is in the quantum spin Hall

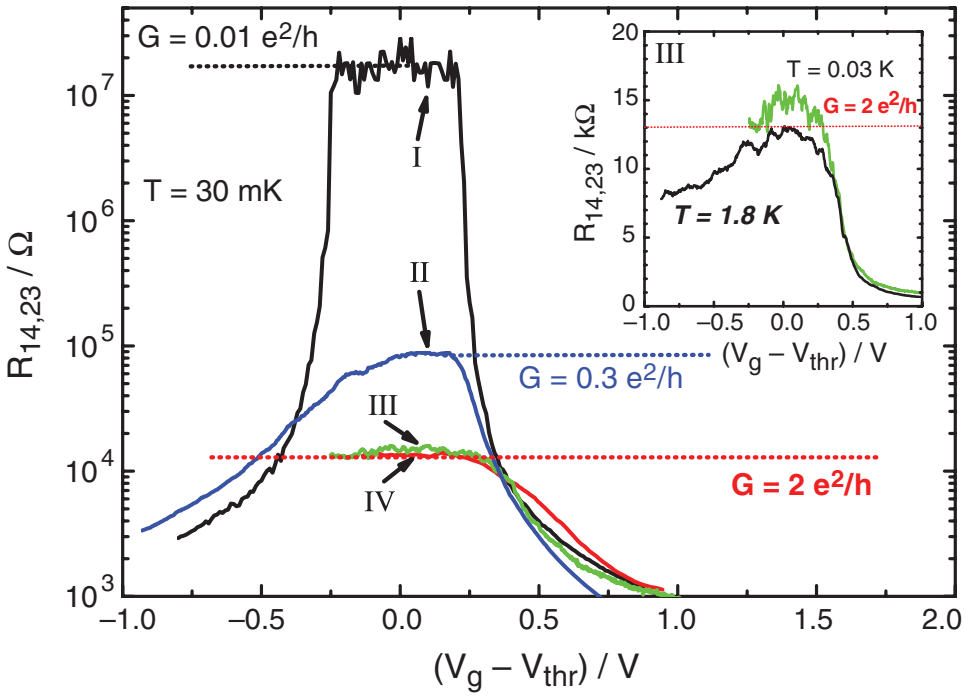

Figure 1.15: The longitudinal four terminal resistance measurement for different well thickness is shown. I is for $d = 5.5nm$ in the normal band order regime, and II, III, and IV are for $d = 7.3nm$ which is in the inverted band order regime. III and IV show that the length of the bar doesn't affect on the resistance, which indicates that the transport is channel is ballistic. The figure is taken from [KWB07].

phase, and there are two channels for spin up and down that can carry current ballistically. This means the conductance is $G = 2e^2/h$, which can be seen in the measurements as well. Note that the resistance in the non-trivial phase doesn't depend on the length of the well, indicating that the channel is ballistic.

Furthermore, various other terminal resistance measurement were performed [RBB09], and the results show the consistency with the interpretation of quantum spin Hall effect, which can be seen in Figure 1.16.

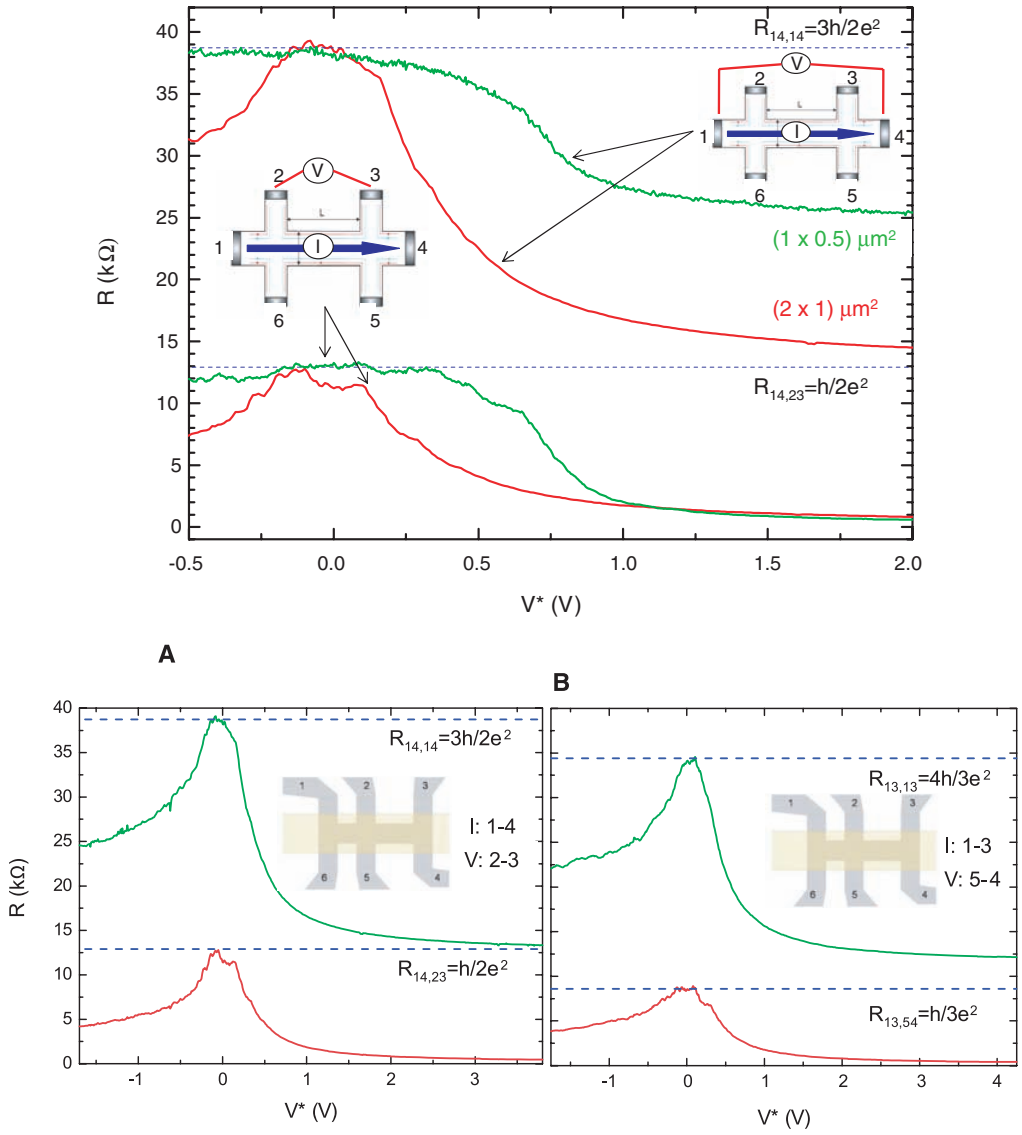

Figure 1.16: The top figure shows the resistance versus gate voltage of the Hall bar devices with different dimensions. Both two terminal and four terminal resistance measurements are shown. The bottom figure shows four and two-terminal resistance measured on the devices with the geometries shown in the insets. The figures are taken from [RBB09].

1.3 Cooper-Pair Splitter

1.3.1 Entanglement

One of the distinct features of quantum mechanics is the entanglement of multi particles. A state is entangled if it CANNOT be written as a tensor product form: $\Psi = \psi_1 \otimes \psi_2 \otimes \cdots \otimes \psi_N$ for a N-particle system with wave functions ψ_i for ith particle [Wer89]. The simplest example is a spin-singlet state, where a two-particle spin state is expressed in terms of antisymmetric combinations of two spins:

$$|S\rangle = \frac{1}{\sqrt{2}} \left(|\uparrow\rangle \otimes |\downarrow\rangle - |\downarrow\rangle \otimes |\uparrow\rangle \right) , \tag{1.67}$$

where the first and second ket state refer to the first and second particle respectively. Although this seems to be harmless, the completeness of quantum mechanics was question by Einstein-Podolsky-Rosen (EPR) based on the non-local feature of entangled states [EPR35, Per93].

Suppose a spin-singlet state decays and splits into two spin 1/2 particles, and these two particles are detected at two distant locations. Quantum mechanics permits the situation where the spins of those two particles are still in the state of superposition, and the actual value of the spin of each particle is not known until a measurement is performed. This indicates that if an observer on one side makes a measurement to identify the spin of one of the particles, the spin of the other particle on the other location is immediately determined. In the Copenhagen interpretation, if one particle's spin is measured, the wave function of the two-particle state instantly collapses into the measured state, and the other particle's spin is correspondingly determined. This seems to somewhat contradictory, because the information of the measurement on one side traveled to the other side faster than the speed of light, hence EPR questioned the completeness of quantum mechanics based on the locality principle. It was pointed out that perhaps the probabilistic interpretation of quantum mechanics is the consequence of failing to capture some variables in nature, so called hidden variable, and we might obtain complete description if we know all the hidden variables.

However, such a description based on hidden variables turns out to be wrong due to Bell's inequality [Bel66, CHS69]. The Bell's inequality is constructed in the way that if the correlations of initially entangled particles can be explained by hidden variables, the inequality is satisfied. Namely, the correlations can be explained by some classical physics. If we use quantum mechanical frame work, the inequality is violated, hence quantum mechanics is not compatible with the hidden variable frame work. There are a number of experiments with entangled photons, and the violation of the Bell's inequality was verified unambiguously [AGR81, AGR82, Fra89]. Therefore, the quantum mechanical entanglement cannot be described by any hidden variable theory.

This quantum entanglement is not merely academic, but it provides ample potential applications. Entanglement of multi particles is utilized in the field of quantum computation [NC00], quantum teleportation [BBC93], and quantum cryptography [BB84, Eke91, GRT02] etc. Many of these applications operate in solid-state environments, which tend to destroy the coherence of quantum systems due to the interactions happening in the systems. Reading out the information of entanglement and controlling spatial locations of entangled particles in a solid-state environment are important tasks necessary to achieve such application purposes. Here, we review a few of the ways to manipulate and read out entangled states via a solid state structure such as beam splitters and how to separate entangled particles using Cooper-pair splitters (a good review is found in [Bur07]).

1.3.2 Detection of the Spin Entanglement

Let us first go though the basics of the correlations that arise from the statistics of particles [BB00]. A beam splitter with two incoming (1 and 2) and two outgoing (3 and 4) ports as in Figure 1.17 is considered. Let the transmission be T and reflection be R through the beam splitter. There are three out comes: (a) two particles are detected at 3 with probability $P(2,0)$, (b) two particles are detected at 4 with probability $P(0,2)$, and (c) one particle is detected at 3 and another one at 4 with probability $P(1,1)$. Denoting $|J|$ as the overlap

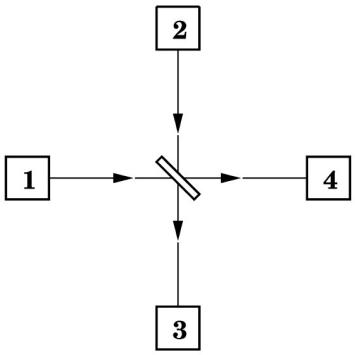

Figure 1.17: Particles come in from the port 1 and 2, and they come out on the port 3 and 4 through a half mirror place in the middle. Depending on whether the incoming particles are bosons or fermions, the outgoing amplitude is different due to the interference coming from the difference in their statistics.

integral between two incoming states, then the probabilities for the three outcomes above with the case of classical particles, bosons, and fermions are given as shown in the charge below.

Probability	Classical	Bosons	Fermions
$P(2,0)$	RT	$RT(1+\|J\|^2)$	$RT(1-\|J\|^2)$
$P(1,1)$	R^2+T^2	$R^2+T^2-2RT\|J\|^2$	$R^2+T^2+2RT\|J\|^2$
$P(0,2)$	RT	$RT(1+\|J\|^2)$	$RT(1-\|J\|^2)$

Due to the quantum statistics, the probabilities of each outcome is different depending on what kind of particle it is. One observation is that it is more probable for two incoming bososns to be detected in the same outgoing port, but two incoming fermions are more probable to be detected in the separate outgoing ports. If the overlap of the two incoming state at the beam splitter is perfect, namely $|J| = 1$, two bosons are always detected in one of the outgoing ports, but two fermions are always detected at two separate outgoing ports. This means that bosons tend to come together, while fermions repel each other due to Pauli's exclusion principle. We call the effect of bosons coming together as bunching, and fermions tending to separate as anti-bunching effect. Therefore, this type of beam

splitter setting can generate outcomes that are sensitive to the statistics of incoming particles. Related phenomenon are tested for light [HT56], for electrons [LOY98, OKL99, HOS99]. Interestingly, if the two incoming fermions are entangled, they exhibit bunching or anti-bunching depending on the initial spin states of two entangled fermions.

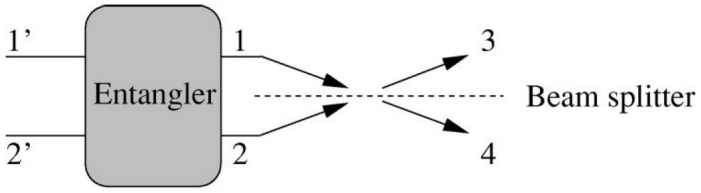

Figure 1.18: Two particles come in to $1'$ and $2'$, and they are entangled in the entangler region. The entangled particles come out in 1 and 2 separately and go through the beam splitter to reach the detection points 3 and 4. The figure is taken from [BEL00].

This idea of beam splitter to detect the information of the statistics of incoming particles can be applied for detection of the spin-entanglement (see Figure 1.18). Two particles, which are initially unentangled, are fed into the entangler region, which entangles these two particles in a certain way. Here we consider the case of the spin-singlet and -triplet entanglement, and they come out separately into 1 and 2 to further go through a beam splitter. These two particles finally reach the detection points 3 and 4.

The currents at 3 and 4 carry the information of the entangled incoming states, and the correlations between the output currents can explicitly differentiate the incoming spin-singlet and triplet states. The current correlations are given by

$$S_{\alpha\beta}(t) = \langle \delta I_\alpha(t) \delta I_\beta(0) \rangle \,, \tag{1.68}$$

where $\delta I_\alpha(t) = I_\alpha(t) - \langle I_\alpha \rangle$ is the fluctuation of the currents at outgoing port $\alpha = 3, 4$. This correlation can be Fourier transformed, and its zero frequency component give the shot noise, which is given by

$$S_{33} = S_{44} = -S_{34} \propto T(1-T)(1 \pm \delta_{\varepsilon_1, \varepsilon_2}) \,, \tag{1.69}$$

where T is the transmission probability through the beam splitter, and ε_i is the energy of incoming state, and $+(-)$ sign refers to the spin-singlet (triplet). For the triplet case, the sign is $-$, and the noise completely vanishes. This means that two incoming triplet states always split into two separate outgoing ports. This makes the current fluctuation to vanish, and consequently the noise vanishes. On the other hand, the singlet state corresponds to $+$ sign, so the noise is enhanced, which means the two particles forming a spin-singlet tend to go into the same outgoing port to increase the current fluctuation. Here, we observe the bunching effect on the spin-singlet, and ani-bunching effect for the spin-triplet states, and these difference is explicitly manifested in the distinction in the output noise structure [BLS00].

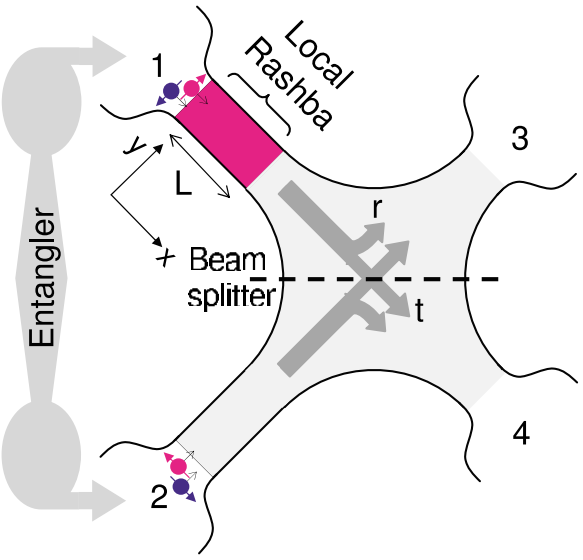

Figure 1.19: The top figure shows the beam splitter structure with Rasha spin-orbit interaction region near the incoming port 1. r and t are the reflection and transmission through the beam splitter. The figure is taken from [EBL02]

This method of the distinguishing the entangled states via a beam splitter was extended by introducing a region with Rashba spin-orbit interaction of the form $H_R = -\alpha k \sigma_y$ at one of the incoming ports [EBL02, EBS05]. The spin of the state coming into 1 is rotated by angle $\theta_R = 2\alpha m^* L/\hbar^2$ due to the region with the Rashba spin-orbit interaction. Two particles

forming entangled spin singlet (S) and triplet (T) states and unentangled triplet ($\uparrow\uparrow, \downarrow\downarrow$) states are injected in the separate incoming port 1 and 2. Due to the Rashba interaction, these states are mixed and produces the output noise which depends on the rotation angle θ_R.

The auto-correlation is given by

$$S_{33} = \frac{2e^2}{h\nu} T(1-T) f_X \,, \tag{1.70}$$

where f_X is the Fano factor for $X = S, T, \uparrow\uparrow, \downarrow\downarrow$ incoming states. The Fano factor can differentiate different incoming states as in

$$\begin{aligned} f_S &= 1 + \cos\theta_R \delta_{\varepsilon_1,\varepsilon_2} \,, \\ f_T^y &= 1 - \cos\theta_R \delta_{\varepsilon_1,\varepsilon_2} \,, \\ f_T^z &= f_{\sigma\sigma_y} = 1 - \delta_{\varepsilon_1,\varepsilon_2} \,, \\ f_{\sigma\sigma}^z &= 1 - \cos\theta_R \delta_{\varepsilon_1,\varepsilon_2} \,. \end{aligned} \tag{1.71}$$

Here, f_T^y corresponds to the triplet T state of the spin basis in y direction, $f_{\sigma\sigma}^z$ is for $\uparrow\uparrow$ and $\downarrow\downarrow$ states in z basis. Therefore, introducing the Rashba spin-orbit interaction provides a further advantage in distinguishing entangled spin-singlet and triplet states and unentangled triplet states.

Another method of differentiating the spin singlet and triplet states were realized by a double-quantum-dot system connected in between superconductor reservoirs [CBL00]. The Figure 1.20(a) shows two quantum dots in between two s-wave superconductor reservoirs. The energy states of the double dots depends on whether they are coupled in the spin singlet or triplet states. This type of double-dot structure J can be connected in parallel to a normal Josephson junction J' as shown in Figure 1.20(b). Further, magnetic flux Φ is applied in the center region to form a SQUID structure. The Josephson current I_S through this SQUID structure depends on the spin states of the double-dot, therefore the measurement of the Josephson current can distinguish the spin states of the quantum dots.

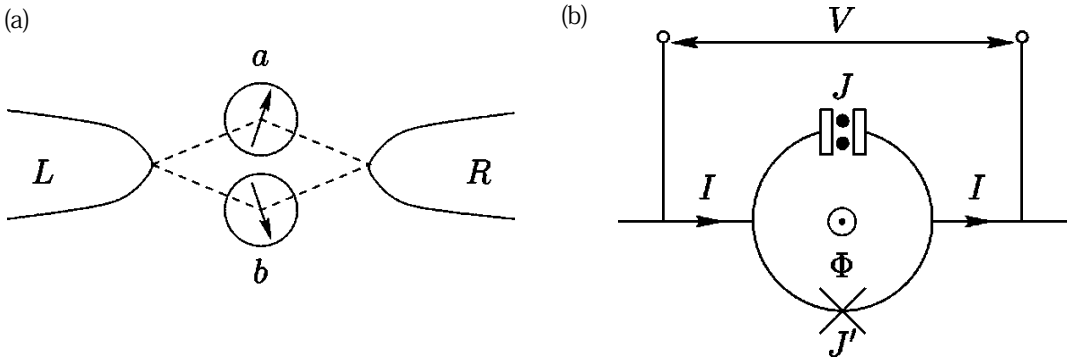

Figure 1.20: (a): Two quantum dots are connected to two s-wave superconductor reservoir. (b): The system in double-dot in junction with superconductor in (a) (J in the figure (b)) is connected in parallel to an ordinary Josephson junction J to form a SQUID structure. The figures are taken from [CBL00]

1.3.3 Cooper-Pair Splitter

The beam splitter structure introduced in the previous section provides a mean to distinguish the entangled spin-singlet and triplet state by the measurement of the output shot noise. This type of system relies on some mechanisms that can entangle the incoming particles before going into the beam splitter, and the details of how this can be done still remains to be answered. The key idea is to extract already spin-entangled electrons from s-wave superconductor (SC). The ground state of a s-wave superconductor is formed by Cooper-pairs (CP) that are in spin-singlet entangled states.

The key physics for extracting a CP from SC is Andreev reflection [BTK82], which occurs at a superconductor-normal metal interface. When an electron is incident from a normal-metal to a superconductor, a hole can be reflected in the normal metal, which is the result of taking out an electron from the metal and putting it in the superconductor. The incident electron and the electron taken out from the metal form a Cooper-pair in the superconductor. This process is called local Andreev reflection because the incident electron and hole reflection occurs at the same interface.

It turns out that Andreev reflection is not restricted to only a local case, but it can also happen nonlocally. An incident electron can create a hole at a distant location from the point of incident, and consequently an electron taken out there can form a Cooper-pair with the incident electron. This nonlocal Andreev reflection, also known as crossed Andreev reflection (CAR), can be viewed as the process of two electrons forming a Cooper-pair tunnel out to two separate locations of the normal metal [BWL04, RKK05, KBT09]. Since these two electrons are correlated over the Copper-pair correlation length ξ, the separation of these two points cannot exceed ξ in order for CAR to happen.

Utilizing CAR, two electrons initially forming a Cooper-pair can be extracted at spatially separate locations. A Cooper-pair splitter is a device to perform such separation of a pair of entangled electrons. Various ideas of Cooper-pair splitters were proposed in the form of a superconductor in junction with normal metal fork geometry [LMB01], quantum dots [RSL01, RL03], Luttinger liquid wires [RL02], and carbon nanotubes [BVB02].

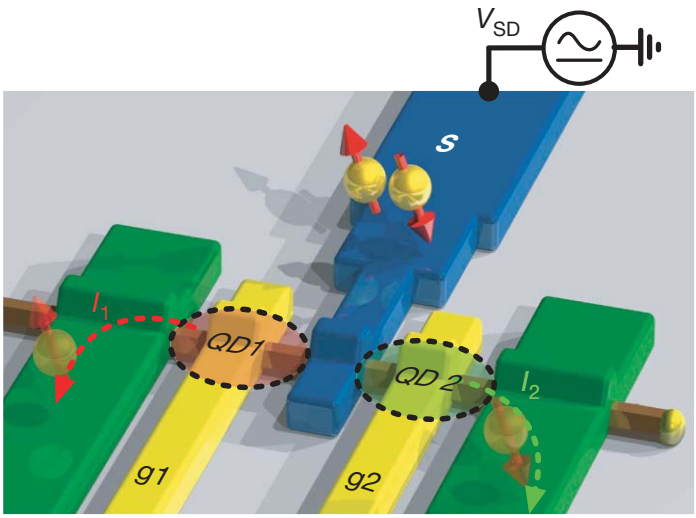

Figure 1.21: A s-wave superconductor is connected to two quantum dots that are spatially apart. Cooper-pairs from the superconductor can tunnel through the dots and go into the leads. The figure is taken from [HCN09].

The first experimental realization of a quantum dot based CP splitter was achieved through s-wave superconductor in junction with InAs quantum wires acting as quantum dots [HCN09, HCB11] (see Figure 1.21). They measured the conductance ΔG_1 through one of the dots as a function of the gate voltage on the second dot. The conductance ΔG_1 closely follows the change of G_2, and this signal vanishes when the superconductor in conjunction with those dots become a normal state as the applied magnetic field exceeds the superconducting critical field value. This indicates that the electrons coming from the superconductor split into two dots in a correlated fashion, which supports the picture of spatially separating two electrons from a CP. Furthermore, the experiments on CP splitter based on carbon nanotubes (which act as quantum dots) were performed [HPR10, HBH12]. In more recently work, the splitting of CP was achieved the efficiency closed to unity [SBS12].

1.3.3.1 Quantum Dot and Luttinger Liquid based CP Splitter

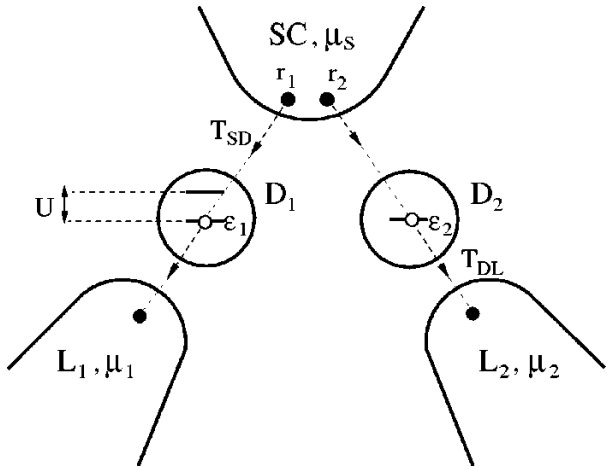

Figure 1.22: A s-wave superconductor (SC) is tunnel coupled to two quantum dots D_1 and D_2., and each quantum dot is further coupled to a lead. Two spin-entangled electrons forming a Cooper-pair in the SC tunnel from r_1 and r_2 to two quantum dots via Andreev tuenneling. The figure is taken from [RSL01].

Here, the CP splitter with quantum dots and Luttinger liquid wires will be discussed in some details for their relevancy to the rest of the thesis. The quantum dot based CP splitter setting is shown in the Figure 1.22, where a s-wave superconductor is connected to two quantum dots by tunnel coupling T_{SD}, and the dots are further connected to leads with coupling T_{DL} [RSL01]. The dots have energy levels $\varepsilon_{1,2}$ respectively, and the charging energy U of the dots is considered for the Coulomb blockade effect. The premise of a CP splitter relies on its capability in spatially separating a pair of entangled electrons, hence the parameters of the setup need to be carefully tuned in the appropriate regime.

First of all, the bias between the superconductor (SC) and the outgoing leads $\Delta\mu = \mu_s - \mu_l$ must be smaller than the SC energy gap Δ, so that no quasiparticle excitations occur in the SC. Two electrons from a CP tunnel from SC to dots with time delay around $\hbar/\Delta$. One possibility is that both electrons tunnel through the same dot, and another case is that two electrons go through different dots. In order to spatially separate the initially entangled electrons, the latter case is of the interest. In order to avoid the tunneling of both electrons into the same dot, the charging energy U should be sufficiently large so that double occupancy on one dot is suppressed. If the SC to lead bias is set lower than the charging energy $U > \delta\mu$, such process is reduced.

The spin entanglement of the incoming electrons is harmed if there is a spin flip process through the dots. One way to prevent such spin flip is to have the number of electrons on the dots to be even, so that their net spin is zero. Another source of loss of the entanglement due to spin flip is that as an electron enters a given dot, and another electron with opposite spin, which was already in the dot, leaves into the lead. This type of spin flip process is suppressed if the energy level spacing of the dot, $\delta\varepsilon$, is larger than $k_B T$ and $\Delta\mu$.

There is other type of loss of the entanglement, which comes from electron-hole excitations in the leads. It turns out such many-body contribution is suppressed if resonance width of the lead γ_l is smaller than $\Delta\mu$. Furthermore, the most efficient setting to achieve separation of entangled pair is to work in almost empty dot, which is ensured by $|T_{SD}| < |T_{DL}|$, meaning an electron on a dot is drained faster into the lead than being supplied from SC. Of course,

the temperature should be smaller than any of the energy scale so that thermal fluctuations don't smear the entanglement. In summary, the condition for separating two electrons from SC into different dots states

$$\Delta, U, \delta\varepsilon > \Delta\mu > \gamma_l, k_B T\,, \qquad \gamma_l > \gamma_s\,. \tag{1.72}$$

The current from the SC to the leads is calculated by Fermi's golden rule with T matrix approach. The current I_1 when each of the two entangled electrons tunnel through different dot is given by

$$I_1 = \frac{e\gamma_s^2\gamma}{(\varepsilon_1+\varepsilon_2)^2+\gamma^2/4}\left[\frac{\sin(k_F\delta r)}{k_F\delta r}\right]^2 e^{-2\delta r/\pi\xi}\,, \tag{1.73}$$

where $\gamma_s = 2\pi\nu_s|T_{DS}|$ is the resonance width coming from SC to dot coupling, γ is the energy broadening coming from dot to lead coupling, δr is the separation of the two points that two entangled electron pair leave SC, and ξ is the SC coherence length. The algebraic and exponential suppression over the separation distance δr are from the effect of the SC. It is obvious that δr cannot be too large, because if it exceeds the coherence length, Cooper-pair coherence is lost. The current can be further maximized if we choose the energy level of two dots to be $\varepsilon_1 = -\varepsilon_2$.

On the other hand, the current when two electrons go through the same dot is given by

$$I_2 = 2e\gamma_s\gamma\left(\frac{\pi\Delta+U}{\pi\Delta U}\right)^2\,. \tag{1.74}$$

In this case, there is no suppression due to the effect of the CP coherent length because both electrons tunnel from the same location, namely $\delta r = 0$. When $U \ll \Delta$, $I_2 \sim U^{-2}$. The larger the gap is, the shorter the delay time between the two electron tunneling events. If Δ is large, soon after the first electron comes in to one of the dots, the second electron also hops into the same dot. Then, the dot is doubly occupied to experience charging energy U, and the main cause of the suppression of the current hence becomes U. In the other limit, $U \gg \Delta$, $I_2 \sim \Delta^{-2}$. The current suppression comes from the penalty in leaving the SC in an exited state for the time Δ^{-1}.

In order to split the two electron for a CP, we need $I_1 > I_2$, which leads to the condition

$$\frac{I_1}{I_2} = \frac{2}{\gamma^2}\left(\frac{\pi\Delta U}{\pi\Delta + U}\right)^2 \left[\frac{\sin(k_F\delta r)}{k_F\delta r}\right]^2 e^{-2\delta r/\pi\xi} > 1\,, \tag{1.75}$$

then the desired regime is obtained when $\pi\Delta U/\gamma(\pi\Delta + U) > k_F\delta r$, and $\delta r < \xi$. Since ξ can be in the order of μm, the second condition is easy to satisfy. If the charging energy is very large, and taking $\gamma \sim \gamma_l$, then the condition is approximately $\Delta/\gamma_l > k_F\delta r$. The right hand side of the inequality can be made small by choosing small δr and small density, and the left hand side can be made large by choosing SC with large gap value and slowing down the draining rate from the dot to lead.

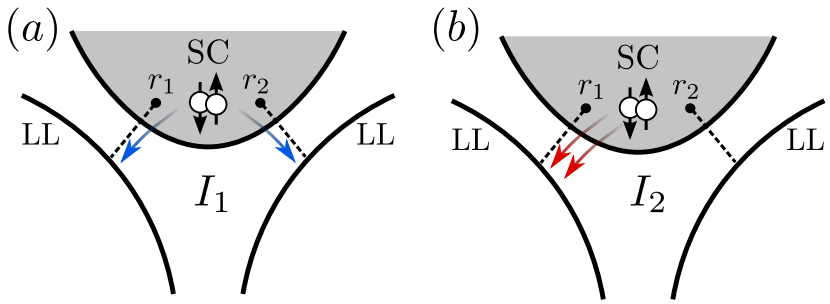

Figure 1.23: A s-wave superconductor is tunnel coupled to two Luttinger liquid wires. r_1 and r_2 are the points where two spin-entangled electrons from a Cooper-pair (CP) tunnel. Two electrons forming a CP can tunnel into (a)two separate wires or (b)the same wire to produce current I_1 and I_2 respectively.

Another interesting realization of a CP splitter is a s-wave superconductor connected to two Luttinger liquid wires [RL02] (see Figure 1.23). In one-dimensional system, the effect of electron-electron interaction becomes important, and the conventional approach of Fermi liquid theory fails to work. Such an interacting one-dimensional system is dealt by Luttinger liquid, where a single-particle picture is replaced by collective bosonic excitations to capture the effect of interaction. The electronic fields are expressed in terms of exponetiated bosonic fields by bosonization procedure. Injection of CP's into such wires are considered here. Two electrons from the SC can again either tunnel into two separate wires or into the same wire producing current I_1 and I_2 respectively.

For the case two electrons tunneling into separate wires (see Figure 1.23(a)), the current I_1 is given by

$$I_1 \sim \left[\frac{\sin(k_F\delta r)}{k_F\delta r}\right]^2 e^{-2\delta r/\pi\xi} V^{2\gamma+1}\,, \tag{1.76}$$

where V is the bias difference between the SC and wires, and $\gamma = (g + g^{-1} - 2)/4$ (g is the interaction parameter of the charge sector of the spinful Luttinger liquid). $g = 1$ for the non-interaction system. Here $g < 1$ for repulsive interaction is considered. The factor with $\sin k_F\delta r/k_F\delta r e^{-2\delta r/\pi\xi}$ is due to the presence of the SC. In comparison to the quantum dot case, the present case with Luttinger liquid picks up the power law dependence on the bias. This is one of the characteristics of Luttinger liquid system. As the system becomes more interacting, γ becomes larger, and the current is suppressed more due to the effect of interaction.

The current I_2 for two electron tunneling into the same wire is given by

$$I_2 \sim V^{2\gamma+1}\left[A_+\left(\frac{eV}{\Delta}\right)^{2\gamma} + A_-\left(\frac{eV}{\Delta}\right)^{2(g^{-1}-g)/4}\right]. \tag{1.77}$$

In this case, additional algebraic suppression in the ratio of eV/Δ is imposed on top of the different wire current I_1 Meanwhile, the exponential and algebraic suppression due to the SC is not present because of $\delta r = 0$. Since $(g^{-1} - g)/4 = \gamma + (1 - g)/2 > \gamma$, the suppression coming from A_- term is more significant since $eV > \Delta$, which meas that A_+ term is more dominant in Eq. (1.77). Finally, the condition for splitting a CP into different leads is $I_1 > I_2$, which leads to

$$A_+\left(\frac{eV}{\Delta}\right)^{2\gamma} < \frac{1}{(k_F\delta r)^2}\,, \tag{1.78}$$

where the exponential suppression was ignored because it can be made reasonably small when ξ is sufficiently large. Hence, larger γ (more effect of the electron-electron interaction) helps to satisfy the condition for splitting the CP.

CHAPTER 2

Cooper-Pair Injection into Quantum Spin Hall Insulator

2.1 Introduction

The quest for solid-state medium providing means to produce, transport, manipulate, and detect quantum entanglement has been fueling tremendous research activity in recent years. Many of the practical proposals rely upon an innately quantum-mechanical electron spin as an elementary building block for quantum bits and ultimately quantum computation [LD98]. The promise for spin-based quantum manipulations hinges on its relatively long relaxation and coherence times, in contrast to charge-based degrees of freedom that are naturally more susceptible to various decoherence processes inherent to a solid-state environment. An alternative fault-tolerant charge-based quantum computation relies on topological protection of braiding statistics of non-Abelian anyons in certain quantum Hall states [NSS08], although the experimental situation there still offers a formidable challenge [DHU08]. In this Letter, we propose to utilize spin-dependent topological properties of newly-discovered two-dimensional quantum spin Hall insulators (QSHI) [KM05b, KWB07, QZ10] in combination with spin entanglement of Cooper pairs (CP's) in superconductors as a starting point for spin-based macroscopic quantum manipulations [BLS00, RSL01, LMB01, RL02, BVB02, KVF04]. Recent experimental strides in realizing mesoscopic CP splitters [HCN09, HPR10] and measuring their cross correlations [WC10] show the feasibility of our proposal.

While spins appear to be good candidates for initialization (e.g., by spin-exchange or superconducting correlations) and local gating (both by magnetic and electric fields) of

quantum bits, the transport and detection remain more challenging. For the latter, some kind of spin-to-charge conversion appears to be necessary at present [HKP07]. In this Letter, we utilize topological helicity of the QSHI edge states to convert spin entanglement into measurable charge-current correlations, which are amenable to modern experimental capabilities [BB00]. While we will not study here the feasibility of using the same system to transport spin entanglement, its potential to this end should also be clear from our discussion. Our proposal exploits the ideas [RL02, BVB02, KVF04] for injecting CP's into two Luttinger-liquid (LL) wires. A key role will be played by electron-electron interactions along the edges away from the contacts with the superconductor (SC), which govern nonchiral LL charge fractionalization and interactions with Fermi-liquid contacts [SS95] as well as suppress same-edge tunneling [RL02, BVB02]. The tunneling cross correlations thus contain a wealth of information about LL effects, SC spin pairing (especially when dealing with unconventional SC's [SU91]), and topological properties of the QSHI.

2.2 Tunneling between SC and Helical Edge States

At sufficiently low voltages and temperatures (on the scale set by the superconducting gap Δ), two electrons that initially constitute a CP on the superconducting side are injected into the QSHI coherently, with a time delay of up to $\sim \Delta^{-1}$. The larger this delay, the weaker the LL effects on the suppression of the tunneling into the same edge [RL02]. Since this does not affect the low-energy tunneling exponent, however, we can use a simplified model of equal-time CP injection [BVB02], reinserting the delay effects [RL02] via the appropriate energy normalization by Δ when necessary. The (equal-time) tunneling Hamiltonian has two pieces corresponding to the CP injection into the same ($\bar{H}'$) or different ($\check{H}'$) edges at $x = 0$:

$$\bar{H}' = \bar{\Gamma} e^{-i2eVt} \left[\psi_\uparrow^{(u)} \psi_\downarrow^{(u)}(0) + \psi_\uparrow^{(l)} \psi_\downarrow^{(l)}(0) \right] + \text{H.c.}\,, \tag{2.1}$$

$$\check{H}' = \check{\Gamma} e^{-i2eVt} \left[\psi_\uparrow^{(u)} \psi_\downarrow^{(l)}(0) - \psi_\downarrow^{(u)} \psi_\uparrow^{(l)}(0) \right] + \text{H.c.}\,, \tag{2.2}$$

where V is the voltage applied between the SC and QSHI and u/l label electrons in

the upper/lower edges. $\psi^{(u,l)}_{\uparrow,\downarrow}(x)$ are electronic field operators for the helical edge modes. Figure 2.1 shows a schematic of our setup. Since the CP density of states in the SC is a delta function at the Fermi level, the effective tunneling Hamiltonian above determines the total current injected from the SC. We will focus on the weak-tunneling limit, where the overlap between different CP's injected in the QSHI is negligible and the spin-singlet entanglement is maximized.

In Eq. (2.1), we assumed symmetric tunneling into the two edges and in the second equation, we accounted for singlet pairing of the CP's. It should be clear that any asymmetry in the two tunneling contacts would enhance the relative role of the same-edge tunneling. The electron-electron repulsion, on the other hand, can reverse this tendency toward the different-edge tunneling [RSL01, RL02, BVB02]. There are at least two factors, however, that may hinder this most interesting scenario. First of all, the cross-edge tunneling amplitude $\check{\Gamma}$ is suppressed exponentially for the edge separations d larger than the superconducting coherence length ξ. Even more problematically, CP injection into different edges is suppressed as a power law in $k_F d$ (where k_F is the SC's Fermi wave number) due to destructive Friedel-like interference for electrons tunneling from the SC into different contacts [RL02]. This issue can be overcome by injecting CP's via an intermediate layer of material with a longer Fermi wavelength and proximity-induced SC gap [HCN09].

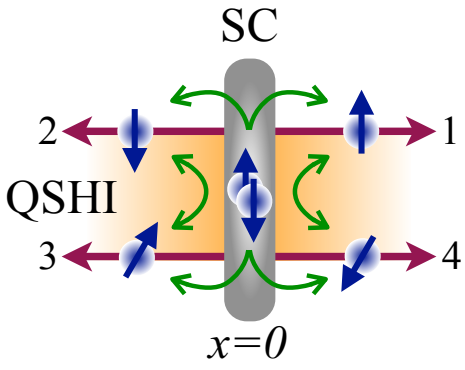

Figure 2.1: Same-edge ($\bar{H}'$) and cross-edge ($\check{H}'$) singlet electron-pair injection processes from the superconductor into the upper and lower QSHI edges.

Electron tunneling into different edges is spin symmetric if the full structure is inversion symmetric. The latter can be affected by, e.g., applying a local strain or gate voltage to one of the edges, thus locally modifying its spin-orbit coupling. We will account for this tunable asymmetry by a relative angle θ between spin-quantization axes at the two contacts as seen in Figure 2.1, where we can see the quantization axis at the bottom edge is tilted relatively to the top one. Tunneling Hamiltonian (2.2) then has to be modified by a relative spin rotation at, say, the lower edge:

$$\psi^{(l)}_{\uparrow,\downarrow} \to \cos(\theta/2)\psi^{(l)}_{\uparrow,\downarrow} \pm \sin(\theta/2)\psi^{(l)}_{\downarrow,\uparrow}\,. \tag{2.3}$$

In comparison to Ref. [BVB02], our θ in Eq. (2.3) has a similar effect on the edge-current cross correlations as spin filtering in carbon nanotubes along axes misaligned by θ. The key practical difference here is that such spin filtering is difficult and has not yet been achieved experimentally, while our proposal is based on measuring unfiltered charge currents. In other words, an analog of spin filtering is already built into helicity of the edge states.

2.3 Helical Edge States with Interaction

The effective edge-state Hamiltonian for the QSHI, including the interband and intraband forward-scattering processes near the Fermi points is [Gia04, WBZ06, SJ09]

$$H_0 = v \sum_{k=u,l} \int \frac{dx}{2\pi} \left[\frac{1}{g} \left(\partial_x \phi^{(k)}\right)^2 + g \left(\partial_x \theta^{(k)}\right)^2 \right] . \tag{2.4}$$

Here, $\phi^{(k)} \equiv (\phi^{(k)}_{\uparrow} + \phi^{(k)}_{\downarrow})/2$ and $\theta^{(k)} \equiv \pm(\phi^{(k)}_{\uparrow} - \phi^{(k)}_{\downarrow})/2$ for $k = u/l$ are linear combinations of the "spin-s" bosonic density operators $\phi^{(k)}_s$, such that the bosonization identity for the fermionic field operators along the upper edge with the spin-up/down electrons moving to the right/left is $\psi^{(u)}_s(x) \propto e^{is\phi^{(u)}_s(x)}$. Since the relationship between the spin and orbital chirality reverses at the opposite edge, $\psi^{(l)}_s(x) \propto e^{-is\phi^{(l)}_s(x)}$. In our convention, the commutation relations are $[\theta^{(k)}(x), \phi^{(k)}(x')] = (i\pi/2)\mathrm{sign}(x - x')$. g in Eq. (4.3) parametrizes the strength of the electron-electron interactions ($g = 1$ for free electrons and $0 < g < 1$ for repulsive interactions). Interband scattering between the right and left movers within a given edge

leads to nontrivial correlation effects (i.e., $g \neq 1$), making the QSHI fundamentally distinct from an integer quantum Hall insulator with chiral edge states [Wen92]. In the special case of equal-strength interband and intraband scattering, $v = v_F/g$, in terms of the bare Fermi velocity v_F. In the general case with broken Galilean invariance, however, g and v are independent phenomenological parameters governed by the interplay between band-structure and correlation effects [Gia04]. A rough estimate [SJ09] gives $g \gtrsim 0.5$ for helical edge states in a HgTe quantum well [KWB07], corresponding to moderate interaction effects while the two-electron disorder and umklapp backscattering are still irrelevant [WBZ06].

2.4 Current-Current Correlations

In order to measure current cross correlations, we place current sensors along the edges at points 1, 2, 3, and 4, as shown in Figure 2.1. Alternatively, we can divert edge currents into voltage probes [DHU08] and measure low-frequency voltage correlations $\langle \delta V_i \delta V_j \rangle$. Note, however, that the Fermi-liquid voltage probes would affect incoming currents, effectively masking the LL charge fractionalization at low voltages [SS95]. Using bosonic representation for the current operators along the edges, $I^{(k)} = vg\partial_x \theta^{(k)}/\pi$, we evaluate the symmetrized noise spectrum

$$S_{ij}(\omega) = S_{ji}(-\omega) = \int_{-\infty}^{\infty} dt e^{i\omega t} \langle \{\delta I_i(t), \delta I_j(0)\} \rangle \ , \tag{2.5}$$

where $\delta I_i(t) \equiv I_i - \langle I_i(t) \rangle$. i labels four outgoing channels: $i = 1$, upper right; 2, upper left; 3, lower left; and 4, lower right branches. To this end, we use standard Keldysh formalism [CFW96]. Note that when calculating noise correlations to the leading (second) order in the tunneling coefficients Γ_i, we do not distinguish between the noise $\langle \delta I_i \delta I_j \rangle$ and current $\langle I_i I_j \rangle$ correlators, since the difference $\langle I_i \rangle \langle I_j \rangle$ enters at the fourth order in tunneling. The current direction is always chosen away from the SC.

Let us first discuss the most interesting regime, when a CP injected from a SC tunnels into two separate edges. This is governed by Eq. (2.2) and sketched by the cross-edge right- and left-moving electron pairs in Figure 2.1. A finite θ, furthermore, leads to correlations

between leads 1 and 3 as well as 2 and 4. Initial spin-singlet entanglement is thus converted into the θ-dependent cross-edge current correlations. In addition to this, there is a purely LL entanglement stemming from the injected charge fractionalization [SS95], which has to be included on equal footing with the spin entanglement. This is sketched in Figure 2.3: A single electron injected into a given edge sets off a counterpropagating nondispersive charge wave, which eats up a fraction $(1-g)/2$ of the elementary electron charge e.

Putting these superconducting and LL correlations together, we find for the low-frequency noise cross correlators $S_{14} = S_{23} = \check{S}_+$:

$$\begin{aligned}\frac{\check{S}_+}{eV} &\propto |\check{\Gamma}|^2 \left(\frac{eV}{\epsilon_F}\right)^{2\gamma} \left[\left(e_+^2 + e_-^2\right)\cos^2\frac{\theta}{2} + 2e_+e_-\sin^2\frac{\theta}{2}\right] \\ &= |\check{\Gamma}|^2 \left(\frac{eV}{\epsilon_F}\right)^{2\gamma} e^2 \frac{1+g^2\cos\theta}{2}\,. \end{aligned} \tag{2.6}$$

We are focusing on the low-temperature regime, $k_BT \ll eV$, so that thermal noise can be neglected. ϵ_F is the characteristic bandwidth of the LL, typically of the order of the Fermi energy, and $\gamma \equiv (g+g^{-1})/2 - 1$ is the spinless nonchiral LL bulk exponent for a single-electron injection [Gia04]. Apart from the generic LL tunneling anomaly, there are two types of interesting factors in Eq. (2.6): LL factors $e_+^2 + e_-^2 = e^2(1+g^2)/2$ and $2e_+e_- = e^2(1-g^2)/2$ reflecting charge fractionalization [SS95] and trigonometric factors $\cos^2(\theta/2)$ and $\sin^2(\theta/2)$ reflecting spin-singlet entanglement. Similarly, we find for $S_{13} = S_{24} = \check{S}_-$:

$$\begin{aligned}\frac{\check{S}_-}{eV} &\propto |\check{\Gamma}|^2 \left(\frac{eV}{\epsilon_F}\right)^{2\gamma} \left[\left(e_+^2 + e_-^2\right)\sin^2\frac{\theta}{2} + 2e_+e_-\cos^2\frac{\theta}{2}\right] \\ &= |\check{\Gamma}|^2 \left(\frac{eV}{\epsilon_F}\right)^{2\gamma} e^2 \frac{1-g^2\cos\theta}{2}\,. \end{aligned} \tag{2.7}$$

The geometric part of $\check{S}_\pm$ containing $1 \pm g^2\cos\theta$ can be also obtained by considering the process of charge fractionalization. As a right-moving electron is injected in Luttinger liquid with interaction strength g, it fractionalizes into a right-moving state with charge $e_+ = (1+g)/2$ and a left-moving state with charge $e_- = (1-g)/2$ as shown in Figure 2.2.

For the total interedge correlation $S_{ul} \equiv \langle I_u I_l\rangle = S_{13} + S_{14} + S_{23} + S_{24} = 2(\check{S}_+ + \check{S}_-)$, we have $S_{ul}/V \propto V^{2\gamma}$, independent of the charge fractionalization and angle θ. The self-

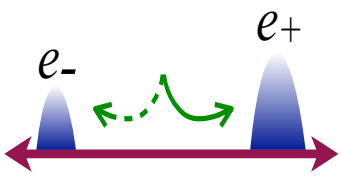

Figure 2.2: A single right-moving electron injected into an edge LL "pumps" a charge of $e(1-g)/2$ to the left. The net fractionalized charges propagating to the right (left) are thus respectively given by $e_\pm = e(1 \pm g)/2$ [SS95].

correlators are determined by the respective average currents, as generally expected for the Poissonian statistics in the tunneling regime:

$$S_{ii} = 2\left(e_+^2 + e_-^2\right)\langle I_i\rangle/e = (1+g^2)e\langle I_i\rangle\,. \tag{2.8}$$

In the special case when $\theta = 0$ and $g = 1$, there is a perfect positive cross correlation of currents at contacts 1, 4 and 2, 3 (i.e., $\check{S}_+ = S_{ii}$) and zero correlation at contacts 1, 3 and 2, 4 (i.e., $\check{S}_- = 0$). The former is certainly a manifestation of many-body entanglement, since noninteracting electrons are required to have nonpositive cross correlations in general multiterminal structures [BB00]. According to Eqs. (2.6) and (2.7), the LL parameter g can be measured in the inversion-symmetric configuration (so that $\theta = 0$) using

$$g = \sqrt{\left(\check{S}_+ - \check{S}_-\right)/\left(\check{S}_+ + \check{S}_-\right)}\,. \tag{2.9}$$

If θ is unknown and not precisely controlled, but can, nonetheless, be swept over the half-period $(0,\pi)$, g will be found by maximizing the absolute value of the right-hand side in Eq. (2.9), which equals $g\sqrt{\cos\theta}$ according to Eqs. (2.6), (2.7). The same g experimentally extracted from Eqs. (2.8) and (2.9) would provide direct evidence of spin entanglement as manifested by the interedge correlations (even if g turns out to be trivial, i.e., close to 1).

2.5 Discussion

Detrimental to the above formulation would be any backscattering along the edges. While the time-reversal symmetry protects against backscattering on nonmagnetic impurities, there

would inevitably be interactions of the edge modes with nearby Fermi liquids (such as electrostatic gates, metallic contacts etc.), and the edges would terminate somewhere, possibly merging with a Fermi-liquid continuum. As was already mentioned above, the Fermi-liquid probes measuring current fluctuations would conceal the LL fractionalization [SS95], effectively removing positive cross correlations associated with the LL physics. In this case, we would expect g in Eqs. (2.6)-(2.9) to be close to unity. More problematically, backscattering engendered by charge fluctuations on nearby gates or other metallic regions, which would scramble ballistic propagation of edge states, needs to be eliminated from a practical implementation of our proposal. It should be clear, however, that various backscattering and boundary-related effects should not affect the finite-frequency correlations on time scales shorter than those at which they set in while still longer than Δ^{-1}, so that the CP tunneling delay is not resolved.

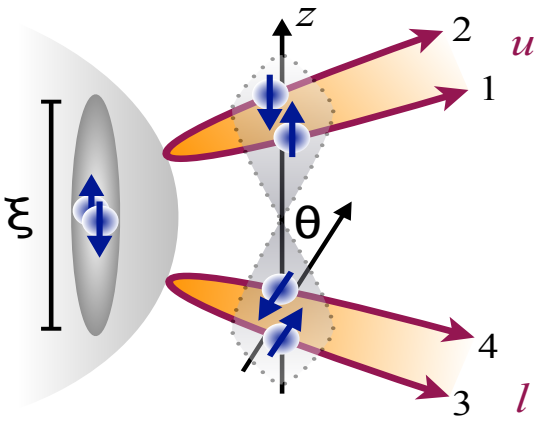

Figure 2.3: A schematic bending of the edges shows a close analogy of our model to the proposed entangled CP injection into carbon nanotubes [BVB02]. The essential differences stem from the LL correlations along the edges vs those at carbon nanotubes' ends and the natural spin filtering provided by the edge-state helicity in the QSHI.

In the absence of the LL fractionalization, $g = 1$, the noise $\check{S}_{\pm} \propto (1 \pm \cos\theta)/2$ has the same angular dependence as the spin-current noise in the carbon-nanotube proposal of Ref. [BVB02]. The θ dependence here is the same, in turn, as in the Einstein-Podolsky-

Rosen thought experiment [EPR35] on a delocalized spin-singlet state of two electrons. It is instructive to understand a close relationship between our setup and that of Ref. [BVB02] by schematically folding two sides of either infinite QSHI edge into a semi-infinite "wire," as sketched in Figure 2.3. This wire is then formally identical to a semi-infinite spinful LL, only without interactions between spins up (down) moving in opposite directions as well as between spins up and down moving in the same direction. There is still, however, a nontrivial interaction between spins up and down moving in opposite directions, which corresponds to $g \neq 1$ in our original model shown in Figure 2.1. Hypothetical spin filtration [BVB02] in semi-infinite carbon nanotubes is thus provided in our system by effectively unfolding the 1D modes of such semi-infinite wires into infinite edges, with half the number of 1D bands and helical spin character (i.e., spins up and down going in opposite directions).

Owing to the difference in the interaction channels here and in Ref. [BVB02], we find a hierarchy of the tunneling exponents that is more similar to that discussed in Ref. [RL02] for infinite LL wires. Injecting a CP into opposite QSHI edges is characterized by the exponent $2\gamma = g + g^{-1} - 2$, as has already been discussed above [Eqs. (2.6) and (2.7)]. We find that the same-edge tunneling of a singlet CP is suppressed by an additional factor $\sim (eV/\Delta)^{2(\gamma'-\gamma)}$ with respect to Eqs. (2.6) and (2.7), where $\gamma' \equiv g^{-1} - 1$ is the end-tunneling exponent for a nonchiral spinless LL [Gia04]. The fact that $\gamma' > \gamma$ for $g < 1$ insures that the split-tunneling dominates at low energies [RL02, BVB02] over the same-edge tunneling, which is parasitic for our purposes. In particular, the same-edge tunneling would introduce large positive cross correlations S_{12} and S_{34}, while not contributing to the interedge correlations.

The situation is quite different in the case of unconventional SC's with triplet spin pairing [SU91]. For example, a CP in the equal-spin pairing phase could be injected into the same (left- or right-moving) edge mode, in the case of the same-edge tunneling, which is governed by the LL exponent $4\gamma + 2$ vs 2γ for the cross-edge tunneling. The relative suppression factor here is $\sim (eV/\Delta)^{2\gamma+2}$, with the quadratic factor stemming from the Pauli exclusion that hinders injection of two same-spin electrons into the same edge band [Fis94]. For a finite θ, there are also nontrivial interedge correlations, dictated by the superconducting

spin pairing. In this context, we can speculate, furthermore, that a QSHI not only provides a fruitful medium for injecting and subsequently manipulating spin-entangled CP's, but can also serve as a probe for spin pairing, which can thus be manifested via current cross correlations along the edges.

We finally note that our setup is distinct from that of the Hanbury Brown and Twiss correlations of CP's in the QSHI discussed recently in Ref. [Cho10]. In the latter implementation, CP's are injected ballistically from an edge portion that opens a gap due to a strong proximity effect to a nearby SC. The induced superconductivity provides perfect Andreev reflection for electrons incoming from the normal region of the edge. Time-reversal symmetry prohibits normal scattering in this situation. This Andreev reflection is found to induce ordinary (i.e., negative) current cross correlations with the second edge that is connected to the first by a point contact [Cho10]. In the present situation, on the other hand, the contact between the SC and the QSHI is weak and the electrons are thus passing along the edges almost ballistically with little Andreev scattering. Those electrons that rarely undergo Andreev reflection, in turn, scatter to a different edge as holes, which is called crossed Andreev reflection (while the same-edge Andreev reflection is suppressed by the LL correlations). This effective flipping of the scattered carrier charge reconciles our positive cross correlations with the Hanbury Brown and Twiss perspective of Ref. [Cho10].

CHAPTER 3

Crossed Andreev reflection in quantum wires with strong spin-orbit interaction

3.1 Introduction

One of the key features and resources of quantum mechanics is entanglement, particularly in the particle spin sector, which has been an enticing subject since the Einstein-Podolsky-Rosen thought experiment [EPR35] and, more recently, fueled by the modern proposals for spin-based quantum information processing and computation [LD98, DL99]. In order to use an entangled pair of electrons for quantum information technology in a scalable semiconductor setting, it is essential to have a solid-state system that can separate the entangled electrons over appreciable distance. Detecting electron spin entanglement is possible via bunching or antibunching correlations in beam splitters [BLS00] and transport through Coulomb-blockaded quantum dots forming a Josephson junction [CBL00]. A conceptual headway came with a proposal to spatially separate spin-singlet Cooper pairs (CP's) injected from an s-wave superconductor via crossed Andreev reflection (CAR) [DF00] in a quantum dot setup [RSL01] and in a normal-metal fork [LMB01]. Later, more elaborate considerations for an s-wave superconductor in junction with quantum wires [RL02, BVB02], quantum beam splitter [SSB04], and quantum dots [SFM04] have been put forward. CAR is essential in all these proposals, and it has been experimentally manifested in the negative nonlocal differential resistance in the system of a superconductor in junction with normal metal [BWL04, RKK05, WC10]. CP splitter experiments have been recently performed with quantum dots [HCN09] and carbon nanotubes [HPR10]. As another form of CP

splitter, we theoretically proposed the system with a superconductor straddling a strip of two-dimensional quantum spin Hall insulator (QSHI) [SLT10], to inject a CP into its gapless edge states. Utilizing the helical Luttinger-liquid character of the QSHI edges (where each electron moves in the opposite direction to its time-reversed Kramers partner with opposite spin), the spin entanglement can be converted into nonlocal charge-current cross correlations.

In this paper, we consider CP injection into quantum wires with strong spin-orbit interaction (SOI), such as self-doped (and possibly backgated, to control their electron density) InAs nanowires. If only SOI is considered, the spin degeneracy at the Γ point ($k = 0$) is preserved because of the time-reversal symmetry. However, this degeneracy can be lifted by external magnetic field (facilitated in InAs by a large g factor of electrons and generally enhanced by electron-electron interactions [BJK10]). When the chemical potential is set in the corresponding gap at the Γ point, gapless states which propagate in the opposite directions with almost opposite spins can be realized at the Fermi points. Note that such a system can closely resemble the helical edge state of the QSHI [KM05a, KM05b, BZ06]. We consider s-wave superconductor connected to a pair of such semiconductor wires in the regime where two CP electrons split into different wires, in the presence of electron-electron repulsion. Effective spin-quantization axes for the left- and right-moving electrons injected into the Fermi points of the two wires are tilted—in one wire relative to the other—by their geometric misalignment. Such tilt affects the current cross correlations in the wires in a way that is similar to the tunable breaking of the inversion symmetry discussed in Ref. [SLT10].

When temperatures and voltage bias between the superconductor and the wires are smaller than the superconductor gap Δ, single-particle injection into the wires is suppressed. In this regime, transport is dominated by the CP tunneling. This process, however, is exponentially suppressed if the distance between the wires exceeds the coherence length of a CP and algebraically on the scale of the Fermi wavelength in the superconductor (depending sensitively on its spatial dimensionality) [RL02], posing a potentially serious constraint on the interwire separation. Very importantly, furthermore, if the applied voltage and temperature are smaller than Δ, the parasitic tunneling of two CP electrons into the same wire is

suppressed with a power law that is governed by the Luttinger-liquid correlations [RL02]. In this work, we thus focus on the regime where a CP splits ejecting electrons into the different wires. There is a time lag of $\sim\Delta^{-1}$ between two such tunneling events, the longer it is the weaker the Luttinger-liquid suppression of the same-wire CP tunneling. However, when two electrons are forced to split and enter different wires at low energies, the leading-order tunneling rates are independent of this time delay (neglecting any interwire interactions) [RL02]. Therefore, we consider a simplified model with equal-time CP injection of two electrons into two different wires [BVB02].

This paper is organized as follows. In Sec. 3.2, we introduce the Hamiltonian for the quantum wire with spin-orbit coupling and magnetic field, and discuss tunneling matrix elements. We consider both Rashba and Dresselhaus SOI with the wire oriented in the xy plane under the magnetic field in the z direction. In Sec. 3.3, we calculate the noise spectrum of the currents in the wires with Keldysh formalism. (Details of the computation are relegated to the appendices.) Final remarks on possible extensions of our theory and experimental feasibility are provided in Sec. 3.4.

3.2 Hamiltonian for Quantum Wires

For the wires, Rashba and Dresselhaus SOI in combination with the Zeeman splitting are considered. Lateral confinement in the wire governs subbands, of which we suppose (at sufficiently low temperature and appropriate backgate bias) only the lowest one is occupied, whose Kramers pairs are split by the lack of both time-reversal and inversion symmetries. In this system, the one-dimensional effective Hamiltonian for a wire oriented along the x axis is given by [SEL03, SGS07, GSS08]

$$H_0 = \frac{\hbar^2 k^2}{2m^*} + \alpha k\hat{\sigma}_y + \beta k\hat{\sigma}_x - \xi\hat{\sigma}_z\,, \tag{3.1}$$

where m^* is the effective mass of electron, α (β) is the strength of the Rashba (Dresselhaus) SOI, and k is the electron wave number. The Dresselhaus part is for the case when a zinc-blende heterostructure is grown in the [001] crystallographic direction, while the wire is

oriented in the [100] direction [SKK08, WCW09]. $2\xi = g\mu_B B$ is the Zeeman energy gap at $k = 0$, with magnetic field B applied along the z axis, g is the g factor, and μ_B the Bohr magneton. $\hat{\boldsymbol{\sigma}} = (\hat{\sigma}_x, \hat{\sigma}_y, \hat{\sigma}_z)$ are Pauli matrices. Other wire and magnetic field orientations are discussed in Sec. IV.

Defining the k-dependent effective field $\mathbf{R}(k) = (\beta k, \alpha k, -\xi)$, the Hamiltonian can be written as

$$H_0 = \frac{\hbar^2 k^2}{2m^*} + \mathbf{R}(k) \cdot \hat{\boldsymbol{\sigma}} \,, \tag{3.2}$$

and the eigenspinors are found by rotating spinors such that $\mathbf{R}(k)\cdot\hat{\boldsymbol{\sigma}}|\chi_\pm(\mathbf{k})\rangle = \pm R(k)|\chi_\pm(k)\rangle$, where $R(k) = \sqrt{k^2(\alpha^2+\beta^2)+\xi^2}$. The subscripts $\pm$ here label spin up/down along $\mathbf{R}(k)$. The energy eigenstates are thus given by $\psi_\pm(k) = \chi_\pm(k)e^{ikx}$, with energy $\epsilon_\pm(k) = \hbar^2k^2/2m^* \pm R(k)$. The upper and lower ($\epsilon_+$ and ϵ_-) bands are sketched in Fig. 4.1. When the chemical potential μ is set within the gap, we can linearize the remaining left and right-moving ϵ_- branches within a Luttinger-liquid picture. This requires $(eV, k_BT) \ll \xi$ and electron-electron interactions that are not strong enough to hybridize the $\epsilon_\pm$ bands. On the other hand, we require the magnetic field to be weak enough on the scale set by H_c of the superconductor (which can be enhanced in mesoscopic structures up to the paramagnetically-limited value of order Δ/μ_B [TMS70]).

Inversion asymmetry between the two wires is introduced by tilting the lower wire (which is otherwise defined along the same crystallographic axis), which rotates the spin quantization axis at each Fermi point of the ϵ_- band. The upper wire is along the x axis, whereas we suppose the lower wire is placed in the xy plane at an angle θ with respect to the x axis, as shown in Fig. 4.2. (This may in practice be realized by growing both wires parallel to each other on an unstrained crystal, and then distorting the crystal in the xy plane to effectively tilt the wires; depending on the interwire separation, a finite θ may not require a large strain, whose additional effect on the SOI is neglected.) The SOI in the lower wire is thus given by

$$H_{\rm SO} = \alpha k \left(\cos\theta\hat{\sigma}_y - \sin\theta\hat{\sigma}_x\right) + \beta k \left(\cos\theta\hat{\sigma}_x + \sin\theta\hat{\sigma}_y\right) \,. \tag{3.3}$$

Reflecting this rotation of the lower wire, the effective fields for the upper (u) and lower (d)

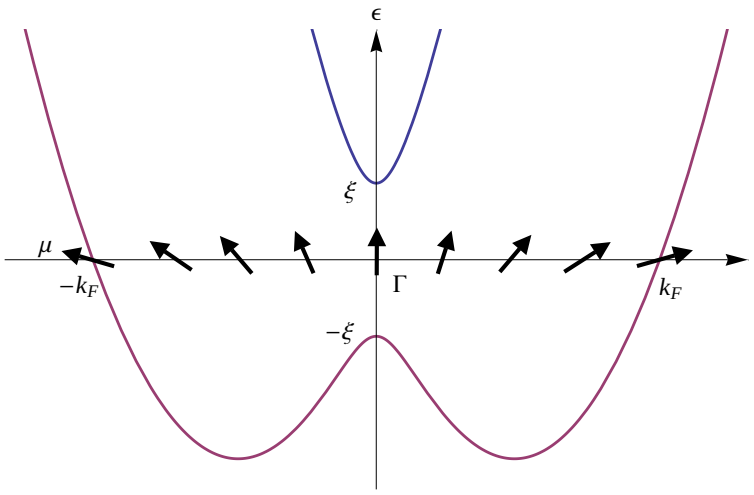

Figure 3.1: Single-particle electron dispersion with Rashba and Dresselhaus SOI. Zeeman splitting 2ξ is induced at $k = 0$ by a magnetic field in the z direction, and the chemical potential is set in this gap. One-dimensional effective theory is then linearized near $\pm k_F$, which define respectively the right- and left-moving electron branches.

wires are given by

$$\begin{aligned}
\mathbf{R}^{(u)}(k) &\equiv \mathbf{R}(k, \theta = 0) = (\beta k, \alpha k, -\xi)\,, \\
\mathbf{R}^{(d)}(k) &\equiv \mathbf{R}(k, \theta) \\
&= [k(-\alpha \sin\theta + \beta\cos\theta), k(\alpha\cos\theta + \beta\sin\theta), -\xi]\ . \qquad (3.4)
\end{aligned}$$

The corresponding Fermi-point eigenspinors are $|\chi^{(u,d)}_{r,l}\rangle \equiv |\chi^{(u,d)}(\pm k_F)\rangle$, which solve

$$\mathbf{R}^{(n)}_{r,l} \cdot \hat{\boldsymbol{\sigma}} |\chi^{(n)}_{r,l}\rangle = -R^{(n)}_{r,l} |\chi^{(n)}_{r,l}\rangle \qquad (3.5)$$

for $\mathbf{R}^{(u,d)}_{r,l} \equiv \mathbf{R}^{(u,d)}(\pm k_F)$. We will assume electronic correlations are not strong enough to significantly affect these Fermi-point spinors. Anticipating tunneling of electrons with well-defined spins from the superconductor into the Fermi points of our wires, we can effectively decompose the fermionic field operators $\psi^{(n)}_\sigma$ ($\sigma = \uparrow, \downarrow$) in terms of the right (left) movers $\psi^{(n)}_{r,l}$ in the nth wire as [SGS07]

$$\psi^{(n)}_\sigma = \langle \chi^{(n)}_r | \sigma \rangle \psi^{(n)}_r + \langle \chi^{(n)}_l | \sigma \rangle \psi^{(n)}_l\,. \qquad (3.6)$$

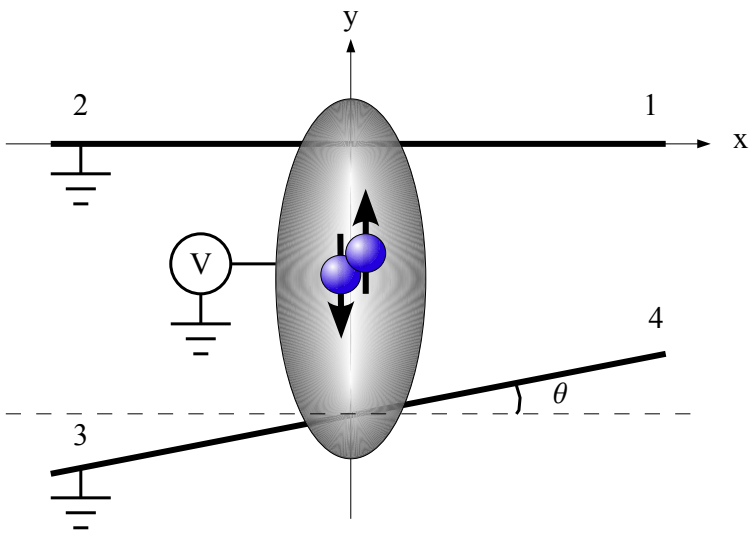

Figure 3.2: S-wave superconductor bridging two identical wires. The lower wire is rotated by angle θ with respect the upper wire. The superconductor is biased by V with respect to the wires.

The full wire Hamiltonian (4.3) is bosonized [Gia04] near the Fermi points to give an essentially helical (so long as the Zeeman term ξ is weak) Luttinger-liquid: [SJ09]

$$H_0 = v \sum_{n=u,d} \int \frac{dx}{2\pi} \left[\frac{1}{g} \left(\partial_x \phi^{(n)} \right)^2 + g \left(\partial_x \theta^{(n)} \right)^2 \right], \tag{3.7}$$

where $\phi^{(n)}, \theta^{(n)} = (\phi_r^{(n)} \pm \phi_l^{(n)})/2$ obey commutation relations $[\theta^{(n)}(x), \phi^{(m)}(y)] = (i\pi/2)\ \mathrm{sgn}(x-y)\delta_{nm}$. $\phi_{r,l}^{(n)}$ parametrize fermionic operators as $\psi_{r,l}^{(n)} \propto e^{\pm i\phi_{r,l}^{(n)}}$.

The tunneling Hamiltonian, which describes nonlocal injection of the spin singlet CP from an s-wave superconductor into the two quantum wires is given by [BVB02]

$$H_T = \mathcal{T} e^{-2eVt} \left[\psi_\uparrow^{(u)} \psi_\downarrow^{(d)}(0) - \psi_\downarrow^{(u)} \psi_\uparrow^{(d)}(0) \right] + \text{H.c.}\,. \tag{3.8}$$

In this model, two electrons from a singlet CP split and tunnel simultaneously into the upper and lower wires at their respective origins. V is the voltage applied between the superconductor and the wires, which is set to be smaller than Δ to preclude quasiparticle excitations. Expanding spin-dependent operators $\psi_{\uparrow/\downarrow}^{(n)}$ in terms of the chiral modes pertinent

to the wires as in Eq. (3.6), we can rewire the tunneling Hamiltonian (4.4) as

$$\psi_{\uparrow}^{(u)}\psi_{\downarrow}^{(d)} - \psi_{\downarrow}^{(u)}\psi_{\uparrow}^{(d)} = \sum_{\mu,\nu=r,l} K_{\mu\nu}\psi_{\mu}^{(u)}\psi_{\nu}^{(d)}\,, \tag{3.9}$$

where $K_{\mu\nu}$ are the complex-valued expansion coefficients, which are given by

$$K_{\mu\nu} = \langle\chi_{\mu}^{(u)}|\uparrow\rangle\langle\chi_{\nu}^{(d)}|\downarrow\rangle - \langle\chi_{\mu}^{(u)}|\downarrow\rangle\langle\chi_{\nu}^{(d)}|\uparrow\rangle\,. \tag{3.10}$$

In Section 3.3, the current-current correlations are calculated, which depend on $|K_{\mu\nu}|^2$ (reflecting spin-rotational symmetry of a singlet CP):

$$|K_{\mu\nu}|^2 = 1 - |\langle\chi_{\mu}^{(u)}|\chi_{\nu}^{(d)}\rangle|^2 = \frac{1}{2}\left(1 - \hat{\mathbf{R}}_{\mu}^{(u)}\cdot\hat{\mathbf{R}}_{\nu}^{(d)}\right)\,. \tag{3.11}$$

Here, $\hat{\mathbf{R}}_{\mu}^{(n)} = \mathbf{R}_{\mu}^{(n)}/R_{\mu}^{(n)}$, and $|K_{\mu\nu}|^2$ can be evaluated using Eq. (3.4). $R_{\mu}^{(n)} = \sqrt{k_F^2(\alpha^2+\beta^2)+\xi^2}$, for $n = u, l$ and $\mu = \pm$, independent of the orientation of the wire or electron chirality. Furthermore, since $\mathbf{R}_{\mu}^{(u)}\cdot\mathbf{R}_{\nu}^{(d)} = \mu\nu k_F^2(\alpha^2+\beta^2)\cos\theta + \xi^2$ (where μ and $\nu = \pm$ respectively for r, l), we find that $|K_{++}|^2 = |K_{--}|^2$ and $|K_{+-}|^2 = |K_{-+}|^2$. Lumping Zeeman and SOI energies into a dimensionless parameter $\lambda = \xi/k_F\sqrt{\alpha^2+\beta^2}$, we finally arrive at a rather simple expression for Eq. (3.11):

$$|K_{\mu\nu}|^2 = \frac{1-\mu\nu\cos\theta}{2(1+\lambda^2)}\,. \tag{3.12}$$

3.3 Noise spectrum

In this section, the current-current correlations at the four end points of the two wires in Fig. 4.2 are considered. The symmetrized noise spectrum,

$$S_{ij}(\omega) = S_{ji}(-\omega) = \int_{-\infty}^{\infty} dt e^{i\omega t}\langle\{\delta I_i(t), \delta I_j(0)\}\rangle\,, \tag{3.13}$$

is calculated using Keldysh formalism [CFW96, SLT10]. Here $\delta I_i(t) = I_i(t) - \langle I_i(t)\rangle$ are the current fluctuations, i labeling four outgoing channels in the wires ($i = 1$, upper right; 2 upper left; 3, lower left; and 4, lower right branches)(see Fig. 4.2). We henceforth bosonize

the current operators (with details of the computation provided in Section 3.5.1), finally obtaining the following expressions for the noise spectra at zero frequency ($\omega = 0$):

$$\begin{aligned}
S_{13} = S_{31} = S_{24} = S_{42} &= eI(1 + g^2 \cos\theta) \equiv S_+ \,, \\
S_{14} = S_{41} = S_{23} = S_{32} &= eI(1 - g^2 \cos\theta) \equiv S_- \,, \\
S_{11} = S_{22} = S_{33} = S_{44} &= eI(1 + g^2) \,, \\
S_{12} = S_{21} = S_{34} = S_{43} &= eI(1 - g^2) \,.
\end{aligned} \tag{3.14}$$

Here, I is the average current flowing though each of the four branches, which is given by Eq. (3.23). This current vanishes in the limit $\lambda \gg 1$, when both wires become fully spin polarized thus blocking the CP tunneling. Notice that the magnetic field did not scramble helical structure of the interwire cross correlations, which are the same [apart from the overall suppression by $(1 + \lambda^2)$] as the case of the time-reversal symmetric QSHI [SLT10]. This is one of the key results of this paper.

The interwire cross-correlation spectra (4.10) are given by

$$S_\pm(\theta, \lambda) \propto \frac{1 \pm g^2 \cos\theta}{1 + \lambda^2} \,, \tag{3.15}$$

which are modified from those in Ref. [SLT10] only by the magnetic-field suppression factor of $(1 + \lambda^2)^{-1}$. In Ref. [SLT10], the angle θ dependence for the CP injection into the helical edge states of a QSHI is due to a tunable asymmetry between two edges (induced by a local application of strain or gate voltage to an otherwise inversion-symmetric system). Here, θ dependence comes from the mechanical rotation of the lower wire by the angle θ. Notice that the definitions for S_+ and S_- are interchanged here in comparison to Ref. [SLT10]. This is because the quantum wires considered here do not have the inversion symmetry of helical edge states on the opposite sides of a QSHI strip. Despite this fundamental difference, we can clearly see the same structure in the CP noise cross correlations for both the present quantum-wire system and the helical QSHI edges. According to Eq. (3.15), we can extract the Luttinger-liquid interaction parameter g (which is typically [AYP02, ASY05] $g \sim 0.1 - 1$ in semiconducting wires) from the interwire cross correlations: $g^2 \cos\theta = (S_+ - S_-)/(S_+ + S_-)$.

While in Ref. [SLT10] the angle θ is a parameter that may not be precisely known, in the present setup the rotation angle θ of the lower wire can be experimentally well defined, so that g can be found by measuring S_+ and S_- for an arbitrary value of θ that is away from $\pi/2$.

3.4 Conclusion and discussion

The backscattering caused by disorder in the wire scrambles the ballistic transport and smears the correlations pertaining to entangled electron pairs, which could hinder practical implementation of our proposal. The nonlocal charge cross correlations thus have to be detected on the length scales shorter than the mean free path. Partitioning of electrons accordingly to their spin is the key feature for our result, which was obtained by setting the chemical potential in the gap to probe into a single band. If it is set otherwise, for instance, in the region of multiple bands, this feature is lost.

In the discussion so far, we were considering only one specific crystallographic orientation of the wires. Namely, the heterostructure growth is in the [001] crystallographic direction and each wire is defined (e.g., electrostatically) along the [100] direction. However, while the Rashba SOI is rotationally invariant around the normal axis, the Dresselhaus SOI is sensitive to the wire orientation on a crystal's surface [MSS07, SKK08]. Suppose that with the same crystal growth direction of [001], the wire is defined at an angle θ_D from the [100] direction. In this case, the Dresselhaus SOI part of the Hamiltonian is given by [SKK08]

$$H_D = \beta k \left[\cos(2\theta_D)\hat{\sigma}_x - \sin(2\theta_D)\hat{\sigma}_y\right] . \tag{3.16}$$

This crystallographic orientation and the associated Hamiltonian are now chosen for the upper wire, with our coordinate system still placed (as in Fig. 4.2) with the x direction collinear with the wire. The corresponding effective-field vector is then $\mathbf{R}^{(u)}(k) = [\beta k \cos(2\theta_D), \alpha k - \beta k \sin(2\theta_D), -\xi]$. Since the lower wire is rotated in the xy plane by the angle θ with respect to the upper wire, $\mathbf{R}^{(l)}$ obtained by the corresponding rotation on $\mathbf{R}^{(u)}$ is given by $\mathbf{R}^{(l)} = [-\alpha k \sin\theta + \beta k \cos(2\theta_D - \theta), \alpha k \cos\theta - \beta k \sin(2\theta_D - \theta), -\xi]$. The ab-

solute value of $\mathbf{R}^{(u,l)}$ is modified by θ_D: $R^{(u,l)} = \sqrt{k^2[\alpha^2+\beta^2-2\alpha\beta\sin(2\theta_D)]+\xi^2}$. Both the direction and the magnitude of $\mathbf{R}^{(u,l)}$ are thus modified, affecting $K_{\mu\nu}$ in Eq. (3.11). We still have $|K_{++}|^2 = |K_{--}|^2$ and $|K_{+-}|^2 = |K_{-+}|^2$ according to Eq. (3.11). In fact, the modification of $|K_{\mu\nu}|^2$ can be absorbed by redefining λ entering Eq. (3.12) as $\lambda = \xi/k_F\sqrt{\alpha^2+\beta^2-2\alpha\beta\sin(2\theta_D)}$, with all subsequent relations for the noise spectra unmodified. In particular, apart from the modified geometric spin factor λ, which suppresses the overall strength of the CAR, $S_\pm$ in Eq. (3.15) remain the same. This means we can choose any wire orientation on the crystal surface without altering the essence of the noise cross correlations. One special point is $\theta_D = \pi/4$ when $\alpha = \beta$ (or $\theta_D = -\pi/4$ when $\alpha = -\beta$), corresponding to the "persistent spin helix" [SEL03, BZ06], where λ blows up and the CAR is fully blocked (reflecting exact cancellation of the SOI terms).

Let us also comment on a possible triplet pairing of the injected electrons, e.g., if the two terms in the tunneling Hamiltonian (4.4) acquire a relative phase difference: $e^{i\delta/2}\psi_\uparrow^{(u)}\psi_\downarrow^{(d)} - e^{-i\delta/2}\psi_\downarrow^{(u)}\psi_\uparrow^{(d)}$. We can rewrite it as $\cos(\delta/2)(\psi_\uparrow^{(u)}\psi_\downarrow^{(d)} + \psi_\downarrow^{(u)}\psi_\uparrow^{(d)}) - i\sin(\delta/2)(\psi_\uparrow^{(u)}\psi_\downarrow^{(d)} + \psi_\downarrow^{(u)}\psi_\uparrow^{(d)})$. The corresponding modification of $|K_{\mu\nu}|^2$ in Eq. (3.12) can be accounted for by the replacement $\theta \to \theta - \delta$, with the same δ shift of θ appearing in the noise expressions. Interestingly, the phase difference in the tunneling terms has the same effect on the current correlations as a mechanical rotation of the wires. Such a triplet component in tunneling can be effectively induced by tunneling away from the Fermi points at finite temperature and/or voltage, and artificially enhanced in more complex tunneling setups [VR12].

Another concern to be mentioned is that, if the superconductor is in a slab shape, the perpendicular critical field is reduced. This issue can be mitigated by applying an in-plane magnetic field. For the case of a thin-film superconductor, the critical field is further enhanced (up to its paramagnetic limit [TMS70]) when the magnetic penetration depth is greater than its thickness. $\mathbf{R}$ in Eq. (3.4) needs to be modified accordingly. Since the magnetic-field and SOI contributions to $\mathbf{R}$ are not generally perpendicular to each other, the resulting energy band is not symmetric as in Fig. 4.1. In turn, $|K_{\mu\nu}|^2$ in Eq. (3.12) and the formula in Eq. (4.10) acquire certain corrections. In the limit of $\lambda \ll 1$, the correc-

tions are small, however, and we recover the same noise behavior as in Eq. (3.15). In the strong-field limit, $\lambda \gtrsim 1$, on the other hand, a more careful analysis would be warranted.

Now let us return to Eq. (3.15) to see the feasibility of this theory in an experiment. A very large magnetic splitting (on the scale of the SOI) in the wires, $\lambda \gg 1$, blocks Andreev reflection [JB95], when the Fermi level is inside the Γ-point gap. The SOI is large in the InAs-based heterostructures and wires, where the Rashba parameter is $\alpha \lesssim 10^{-11}$ eV m (being tunable by electrostatic gating) [NAT97, KNA02, DSS09, EAS10], $\beta \ll \alpha$, and g factor is ≈ 15. For electron densities in the range of $10 - 100$ μm^{-1}, this gives for the magnetic field $B \sim 0.1 - 1$ T corresponding to $\lambda \sim 1$. Both α and g factor can be considerably lower (both up to two orders of magnitude) in InGaAs-based heterostructures, which can make also $\alpha \sim \beta$ [MSS07], while the corresponding magnetic field range remains roughly the same. This gives us a favorable operational bound for the magnetic field, which opens the Γ-point gap without compromising the strength of the CAR, while also not exceeding the paramagnetically-limited critical field (with $T_c \gtrsim 1$ K). Taking everything into account, this means the experiments can be done at temperatures close to 1 K.

3.5 Supplementary Calculations

3.5.1 Average current and noise spectrum

We evaluate the average current in each wire and current-current correlations, Eq. (3.13). Tunneling of Cooper pairs is treated perturbatively with the Keldysh formalism. Using Luttinger-liquid bosonization formalism [Gia04, SJ09], the fermionic field is expressed as

$$\psi_\mu^{(n)}(x) = \frac{1}{\sqrt{2\pi a}} e^{i\mu[k_F x + \phi_\mu^{(n)}(x)]} ,$$

where a is the short-distance cutoff. The Klein factor is omitted here as it has no effect on the final results derived below. $\mu = r, l = \pm$ labels the left- and right-moving branches. In

this bosonized representation, the tunneling Hamiltonian, Eq. (4.4), becomes

$$H_T = \frac{\mathcal{T}}{2\pi a} e^{-i\omega_0 t} \sum_{\mu,\nu=r,l} K_{\mu\nu} e^{i[\mu\phi_\mu^{(u)}(0)+\nu\phi_\nu^{(d)}(0)]} + \text{H.c.}\,.$$

Here, $\omega_0 = 2eV/\hbar$ is the Josephson frequency corresponding to the bias V applied between the superconductor and the wires, and $K_{\mu\nu}$ is given in Eq. (3.9).

We define the current to be positive as it flows away from the superconductor. The bosonized current operators at distance $x \gg a$ from the superconductor, along branches 1 through 4 in Fig. 4.2, are given by [Gia04]

$$\begin{aligned} I_{1,2} &= \pm I^{(u)}(\pm x) = \pm e(vg/\pi)\partial_x \theta^{(u)}(\pm x)\,, \\ I_{4,3} &= \pm I^{(d)}(\pm x) = \pm e(vg/\pi)\partial_x \theta^{(d)}(\pm x)\,. \end{aligned}$$

The average current and the noise spectrum are given by [CFW96, CGD03]

$$\begin{aligned} I^{(n)}(x,t) &= \frac{1}{2}\sum_\eta \left\langle T_c e^{-\frac{i}{\hbar}\int_c dt'' H_T(t'')} I^{(n)}(x,t,\eta)\right\rangle, \\ S^{(nm)}(x,t;x',t') &\approx \sum_\eta \left\langle T_c e^{-\frac{i}{\hbar}\int_c dt'' H_T(t'')} I^{(n)}(x,t,\eta) I^{(m)}(x',t',-\eta)\right\rangle, \end{aligned}$$

respectively, where T_c is the Keldysh contour-ordering operator, $\eta = \pm$ labels the upper (lower) branch of the Keldysh contour for the field operators, and the time evolution of the operators on the right-hand side is given in the interaction picture. Since to the leading order in tunneling the average current I is proportional to $|\mathcal{T}|^2$, we have dropped the $\langle I_i(t)\rangle\langle I_j(0)\rangle$ term in the noise spectrum, which is of order $|\mathcal{T}|^4$. When calculating the noise spectrum, it is convenient to exponentiate the operator $\theta^{(n)}$ in the following way:

$$\partial_x \theta^{(n)}(x,t) = \partial_x(-i\partial_\lambda) e^{i\lambda\theta^{(n)}(x,t)}\big|_{\lambda=0}\,.$$

Up to the second order in $\mathcal{T}$, we finally find

$$I^{(n)}(x,t) = -\mathrm{sgn}(x)|\mathcal{T}|^2\frac{evg}{4\pi a^2h^2}\sum_{\substack{\mu,\nu,\varepsilon\\ \eta,\eta_1,\eta_2}}|K_{\mu\nu}|^2\eta_1\eta_2\partial_x(-i\partial_\lambda)\int_{-\infty}^{\infty}dt_1dt_2e^{-\varepsilon i\omega_0(t_1-t_2)}$$
$$\times\left\langle T_c e^{i\lambda\theta^{(n)}(x,t,\eta)}e^{i\varepsilon[\mu\phi_\mu^{(u)}(0,t_1,\eta_1)+\nu\phi_\nu^{(d)}(0,t_1,\eta_1)]}e^{-i\varepsilon[\mu\phi_\mu^{(u)}(0,t_2,\eta_2)+\nu\phi_\nu^{(d)}(0,t_2,\eta_2)]}\right\rangle\Big|_{\lambda=0}, \quad (3.17)$$

$$S^{(nm)}(x,t;x',t') = -\mathrm{sgn}(x)\mathrm{sgn}(x')\frac{1}{2}\left(\frac{evg|\mathcal{T}|}{\pi ah}\right)^2\sum_{\substack{\mu,\nu,\varepsilon\\ \eta,\eta_1,\eta_2}}|K_{\mu\nu}|^2\eta_1\eta_2\partial_x\partial_{x'}\partial_{\lambda_1}\partial_{\lambda_2}\int_{-\infty}^{\infty}dt_1dt_2e^{-i\varepsilon\omega_0(t_1-t_2)}$$
$$\times\left\langle T_c e^{i\lambda_1\theta^{(n)}(x,t,\eta)}e^{-i\lambda_2\theta^{(m)}(x',t',-\eta)}e^{i\varepsilon[\mu\phi_\mu^{(u)}(0,t_1,\eta_1)+\nu\phi_\nu^{(d)}(0,t_1,\eta_1)]}e^{-i\varepsilon[\mu\phi_\mu^{(u)}(0,t_2,\eta_2)+\nu\phi_\nu^{(d)}(0,t_2,\eta_2)]}\right\rangle\Big|_{\lambda_1,\lambda_2=0}. \quad (3.18)$$

Here, $\varepsilon = \pm$ corresponds to the annihilation (creation) part of H_T and h is the Planck's constant. The above expression is then evaluated using standard bosonic operator identities [Gia04], giving

$$I^{(n)}(x,t) = -i\mathrm{sgn}(x)\frac{evg|\mathcal{T}|^2}{4\pi a^2h^2}\sum_{\substack{\mu,\nu,\varepsilon\\ \eta,\eta_1,\eta_2}}\varepsilon|K_{\mu\nu}|^2\eta_1\eta_2\int_{-\infty}^{\infty}dt_1\int_{-\infty}^{\infty}dt_2e^{-\varepsilon i\omega_0(t_1-t_2)}$$
$$\times\sum_\kappa(\delta_{n,u}\delta_{\mu,\kappa}+\delta_{n,d}\delta_{\nu,\kappa})P_{\eta_1\eta_2}(t_1-t_2)\left[Q_{\kappa,\eta\eta_1}(x,t-t_1)-Q_{\kappa,\eta\eta_2}(x,t-t_2)\right], \quad (3.19)$$

$$S^{(nm)}(x,t;x',t') = \mathrm{sgn}(x)\mathrm{sgn}(x')\frac{1}{2}\left(\frac{evg|\mathcal{T}|}{\pi ah}\right)^2\sum_{\substack{\mu,\nu,\varepsilon\\ \eta,\eta_1,\eta_2}}|K_{\mu\nu}|^2\eta_1\eta_2\int_{-\infty}^{\infty}dt_1\int_{-\infty}^{\infty}dt_2e^{-i\varepsilon\omega_0(t_1-t_2)}\sum_{\lambda,\kappa}L_{nm,\lambda\kappa}$$
$$\times P_{\eta_1\eta_2}(t_1-t_2)\left[Q_{\lambda,\eta\eta_1}(x,t-t_1)-Q_{\lambda,\eta\eta_2}(x,t-t_2)\right]\left[Q_{\kappa,-\eta\eta_1}(x',t'-t_1)-Q_{\kappa,-\eta\eta_2}(x',t'-t_2)\right], \quad (3.20)$$

where $L_{nm,\lambda\kappa} = (\delta_{u,n}\delta_{\mu,\lambda}+\delta_{d,n}\delta_{\nu,\lambda})(\delta_{u,m}\delta_{\mu,\kappa}+\delta_{d,m}\delta_{\nu,\kappa})$ and $P_{\eta\eta'}(t)$ and $Q_{\mu,\eta\eta'}(x,t)$ are expressed in terms of the Green's functions of $\phi^{(n)}(x,t)$ and $\theta^{(n)}(x,t)$:

$$P_{\eta\eta'}(t) = \prod_{n=u,d}\exp\left[G^{(n)\phi\phi}_{\eta\eta'}(0,t)+G^{(n)\theta\theta}_{\eta\eta'}(0,t)\right], \quad Q_{\mu,\eta\eta'}(x,t) = \mu\partial_xG^{(n)\theta\phi}_{\eta\eta'}(x,t)+\partial_xG^{(n)\theta\theta}_{\eta\eta'}(x,t). \quad (3.21)$$

Here [Gia04],

$$\begin{aligned}
G^{(n)\phi\phi}_{\eta\eta'}(x,t) &= \langle T_c\phi^{(n)}(x,t,\eta)\phi^{(n)}(0,0,\eta')-\phi^{(n)}(0,0)^2\rangle = -\frac{g}{4}\sum_{r=\pm}\ln\left[1+iD_{\eta\eta'}(t)\left(vt-rx\right)/a\right],\\
G^{(n)\theta\theta}_{\eta\eta'}(x,t) &= \langle T_c\theta^{(n)}_\eta(x,t)\theta^{(n)}_{\eta'}(0,0)-\theta^{(n)}(0,0)^2\rangle = -\frac{1}{4g}\sum_{r=\pm}\ln\left[1+iD_{\eta\eta'}(t)\left(vt-rx\right)/a\right],\\
G^{(n)\phi\theta}_{\eta\eta'}(x,t) &= \langle T_c\phi^{(n)}_\eta(x,t)\theta^{(n)}_{\eta'}(0,0)\rangle = G^{(n)\theta\phi}_{\eta\eta'}(x,t)\\
&= \langle T_c\theta^{(n)}_\eta(x,t)\phi^{(n)}_{\eta'}(0,0)\rangle = -\frac{1}{4}\sum_{r=\pm}r\ln\left[1+iD_{\eta\eta'}(t)\left(vt-rx\right)/a\right], \quad (3.22)
\end{aligned}$$

where $D_{\eta\eta'}(t) = \Theta(\eta\eta')\mathrm{sgn}(\eta' t) + \Theta(-\eta\eta')\mathrm{sgn}(\eta')$.

We finally obtain the current as

$$\begin{aligned} I^{(n)}(x) \quad &= i\mathrm{sgn}(x)\frac{evg}{4\pi a^2 h^2}|\mathcal{T}|^2 \sum_{\mu,\nu,\kappa} |K_{\mu\nu}|^2 (\delta_{n,u}\delta_{\mu,\kappa} + \delta_{n,d}\delta_{\nu,\kappa}) \\ &\quad \times \big[Q_{\kappa,++}(x) - Q_{\kappa,+-}(x) + Q_{\kappa,-+}(x) - Q_{\kappa,--}(x)\big] \\ &\quad \times \big[P_{+-}(\omega_0) - P_{+-}(-\omega_0) - P_{-+}(\omega_0) + P_{-+}(-\omega_0)\big] \\ &= \mathrm{sgn}(\omega_0)\frac{1}{1+\lambda^2}\frac{2\pi e|\mathcal{T}|^2}{v^2 h^2 \Gamma(2\gamma+2)}\left(\frac{|\omega_0|a}{v}\right)^{2\gamma}|\omega_0|\,, \end{aligned} \tag{3.23}$$

where $P_{\eta\eta'}(\omega)$ and $Q_{\mu,\eta\eta'}(x) \equiv Q_{\mu,\eta\eta'}(x, \omega = 0)$ denotes the Fourier transform and $\gamma = (g + g^{-1} - 2)/2$. $K_{\mu\nu}$ here is taken from Eq. (3.12). Similarly for the noise spectrum, we get:

$$\begin{aligned} &S^{(nm)}(x, x', \omega = 0) \\ &= -\mathrm{sgn}(x)\mathrm{sgn}(x')\frac{1}{2}\left(\frac{evg|\mathcal{T}|}{\pi a h}\right)^2 \sum_{\mu\nu}|K_{\mu\nu}|^2 \sum_{\lambda,\kappa} L_{nm,\lambda\kappa}\big[P_{-+}(\omega_0) + P_{-+}(-\omega_0) + P_{+-}(\omega_0) + P_{+-}(-\omega_0)\big] \\ &\times\big\{\big[Q_{\lambda,++}(x) - Q_{\lambda,+-}(x)\big]\big[Q_{\kappa,-+}(x') - Q_{\kappa,--}(x')\big] + \big[Q_{\lambda,-+}(x) - Q_{\lambda,--}(x)\big]\big[Q_{\kappa,++}(x') - Q_{\kappa,+-}(x')\big]\big\} \\ &\quad = eI\big[\delta_{n,m}F_1(x,x') + \delta_{n,-m}F_2(x,x')\big]\,, \end{aligned} \tag{3.24}$$

where

$$F_1(x,x') = 1 + g^2\mathrm{sgn}(x)\mathrm{sgn}(x') \;\; (\text{for } n = m)\,, \quad F_2(x,x') = 1 - g^2\cos\theta\,\mathrm{sgn}(x)\mathrm{sgn}(x') \;\; (\text{for } n \neq m)\,,$$

and I is given by the absolute value of the current in Eq. (3.23).

3.5.2 Relevant integrals

The evaluation of the average current and the noise spectrum in Eqs. (3.23) and (3.24) reduces to finding $P_{\eta\eta'}(\omega)$ and $Q_{\mu,\eta\eta'}(x, \omega = 0) = Q_{\mu,\eta\eta'}(x)$, which are the Fourier transforms of the functions defined in Eq. (3.21). Using the Green's functions in Eq. (3.22), we find

$$\begin{aligned} P_{\eta\eta'}(t) &= \frac{1}{\left[1 + iD_{\eta\eta'}(t)vt/a\right]^{2\gamma+2}}\,, \\ Q_{\mu,\eta\eta'}(x,t) &= i\sum_{r=\pm}\frac{r+\mu g}{4ag}\frac{D_{\eta\eta'}(t)}{1 + iD_{\eta\eta'}(t)(vt - rx)/a}\,. \end{aligned}$$

$P_{-+}(\omega)$ can be evaluated by noting the integral:

$$\int_{-\infty}^{\infty} dt \frac{e^{i\omega t}}{(\delta + it)^{\nu}} = \frac{2\pi}{\Gamma(\nu)} |\omega|^{\nu-1} e^{-|\omega|\delta} \Theta(\omega) \,.$$

Furthermore, we see $P_{+-}(\omega) = P_{-+}(-\omega)$, and the expression appearing in Eqs. (3.23) and (3.24) become

$$\begin{aligned} &P_{-+}(\omega_0) - P_{-+}(-\omega_0) - P_{+-}(\omega_0) + P_{+-}(-\omega_0) \\ &= \frac{4\pi}{\Gamma(2\gamma+2)} \left(\frac{a}{v}\right)^{2\gamma+2} |\omega_0|^{2\gamma+1} e^{-|\omega_0|a/v} \mathrm{sgn}(\omega_0) \,, \end{aligned}$$

and

$$\begin{aligned} &P_{-+}(\omega_0) + P_{-+}(-\omega_0) + P_{+-}(\omega_0) + P_{+-}(-\omega_0) \\ &= \frac{4\pi}{\Gamma(2\gamma+2)} \left(\frac{a}{v}\right)^{2\gamma+2} |\omega_0|^{2\gamma+1} e^{-|\omega_0|a/v} \,. \end{aligned}$$

To be internally consistent with the low-energy Luttinger-liquid description, we henceforth drop the factor $e^{-|\omega_0|a/v}$. The remaining relevant terms entering Eqs. (3.23) and (3.24) are

$$\begin{aligned} &Q_{\mu,++}(x) - Q_{\mu,+-}(x) = Q_{\mu,-+}(x) - Q_{\mu,--}(x) \\ &= i \sum_r \frac{r + \mu g}{4g} \int_0^{\infty} dt \left[\frac{1}{a + i(vt - rx)} + \frac{1}{a - i(vt - rx)} \right] \\ &= i \sum_r \frac{r + \mu g}{2gv} \left[\frac{\pi}{2} - \tan^{-1}\left(-\frac{rx}{a}\right) \right] \approx \frac{i\pi}{2vg} \left[\mu g + \mathrm{sgn(x)} \right] \,. \end{aligned}$$

CHAPTER 4

Detection of entanglement by helical Luttinger liquids

4.1 Introduction

Controlled generation, manipulation, and detection of entangled quantum states are crucial ingredients for quantum computation [NC00], quantum teleportation [BBC93], and quantum cryptography [BB84, Eke91, GRT02]. The Einstein-Podolsky-Rosen (EPR) thought experiment similarly relied on the control of entangled states [EPR35]. One of the ways to test quantum entanglement is to observe a violation of a Bell inequality [Bel66, CHS69]. Although this has been achieved with a high accuracy using entangled-photon sources [AGR81, AGR82, Fra89, KMW95], performing such experiment with electrons is a challenging task, because of electron-electron interactions and dephasing due to the solid-state environment. Nonetheless, Bell tests based on electron spin entanglement [Kaw01, CBL02, LLB05], orbital entanglement [SSB03], and electron-hole entanglement [BEK03] have been proposed, where a Bell inequality is built upon charge current correlations.

Sources of entangled particles and mechanisms to spatially separate them are essential requirements for performing a Bell test. This task can be achieved by a Cooper-pair (CP) splitter, which spatially separates a spin-entangled CP by sending a weak current from a superconductor (SC) into a pair of quantum dots, wires, or carbon nanotubes [LMB01, RSL01, RL02, BVB02, RL03, SSB04]. An s-wave SC provides an excellent source of spin-entangled electrons from CP's, which are condensed at the Fermi level of its ground state. Spatial separation of a CP can be achieved through crossed Andreev reflection [BWL04, RKK05, WC10], as has been recently demonstrated using double quantum dot structures in single-wall car-

bon nanotubes [HPR10, HBH12] and InAs semiconductor nanowires [HCN09, HCB11]. The efficiency of CP splitting was shown to approach unity [SBS12], which encourages further pursuit of superconducting heterostructures toward Bell tests and, in time, scalable quantum measurements.

After a spin-entangled pair of electrons is spatially separated, their spins need to be read out. Traditionally, the information on spin is extracted by a spin-to-charge conversion [EHB04, HKP07], where a spin state governs charge current via spin filtering controlled by a local magnetic field or exchange correlations. This, however, requires intricate fine-tuning and could generally suffer from low efficiency and parasitic backscattering. Recent discovery of two-dimensional topological insulators (TI) [KM05a, KM05b, BZ06, BHZ06, HK10, QZ11], also called quantum spin-Hall insulators (QSHI), could provide robust means for the purpose of spin-to-charge conversion, owing to its special edge states. Experimentally it is established in inverted-band HgTe quantum-well heterostructures [KWB07, RBB09]. The edge states of a QSHI are robust against time-reversal symmetric perturbations, and their spins and momenta are tightly correlated. A given edge of a QSHI supports a Kramers pair of counter-propagating gapless modes with opposite spins, which we call helical edge states. A CP splitter utilizing such helical edge states as charge carriers has been proposed [SLT10], where it was shown that the entangled spin-singlet state from CP imprints a characteristic signature in the current-current correlations. Quasi-one-dimensional semiconductor wires with strong spin-orbit coupling, such as InAs, subject to an external magnetic field can provide a way to emulate the helical states [SLT12], which shares many features and functionalities of helical edge states. Such a CP splitter utilizing a helical electron system was recently suggested as a mean to perform a Bell test based on nonlocal current correlations along the edges of two QSHI's [CSS12].

In this paper, we study a Bell test implemented by an electron-pair splitter based on the interacting helical edge states of a QSHI. Each edge state is deformed to form a beam splitter, as seen in Fig. 4.1, replacing a spin filter in a conventional Bell-test experiment. It

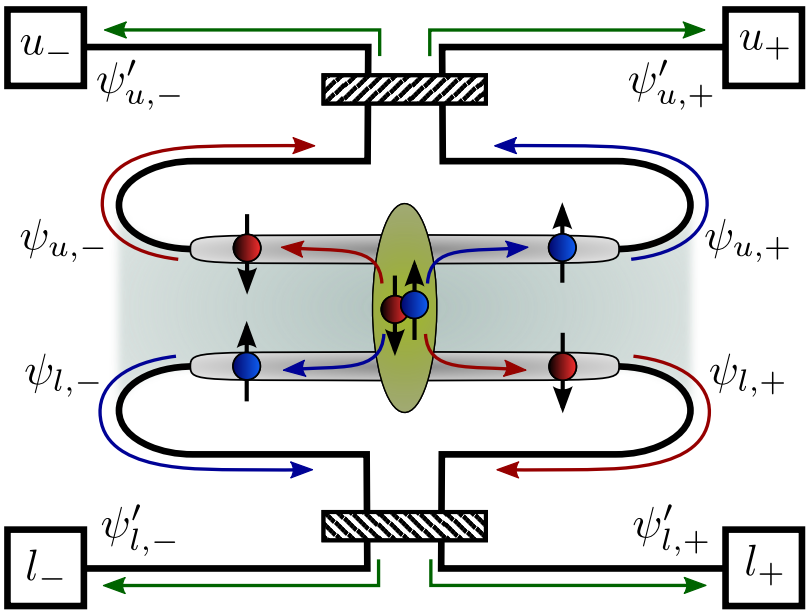

Figure 4.1: An s-wave SC is coupled to a QSHI. Two electrons forming a CP split into top and bottom helical edge states. The electron-electron interaction is finite in the grey regions around SC and vanishes outside of these regions. Two beam splitters are formed at the edges, which are indicated by the striped regions. The charge currents are detected at the end points labeled by $u_\pm$ and $l_\pm$. $\psi_{n,r}$ with $n = u, l$ and $r = \pm$ indicate the incoming electron states moving to the right (+) and left (-) along the upper (u) and lower (l) edges, and $\psi'_{n,r}$ are the outgoing states perturbed by the beam splitters.

is important to consider electron-electron interactions in the helical edge states, since they are crucial for separating a CP into different edges of the QSHI [RL02]. The edge states are treated as inhomogeneous helical Luttinger liquids (LL's), whose segments in the proximity to the SC have sizable interactions, while the outside regions, which form beam splitters, are noninteracting Fermi gases. Although a LL wire connected to Fermi-liquid reservoirs is known to mask the effect of electron-electron interactions in transport [MS95, SS95], we show that the low-frequency current-current correlations can be used to construct a Bell inequality. A violation of the inequality can be achieved by controlling scattering through the beam splitters via external means, such as electrostatic gating or magnetic field. At finite

temperatures, the electron-electron interaction in LL leads to decoherence due to charge fractionalization [Le 05, Le 06], suppressing signatures of the CP entanglement.

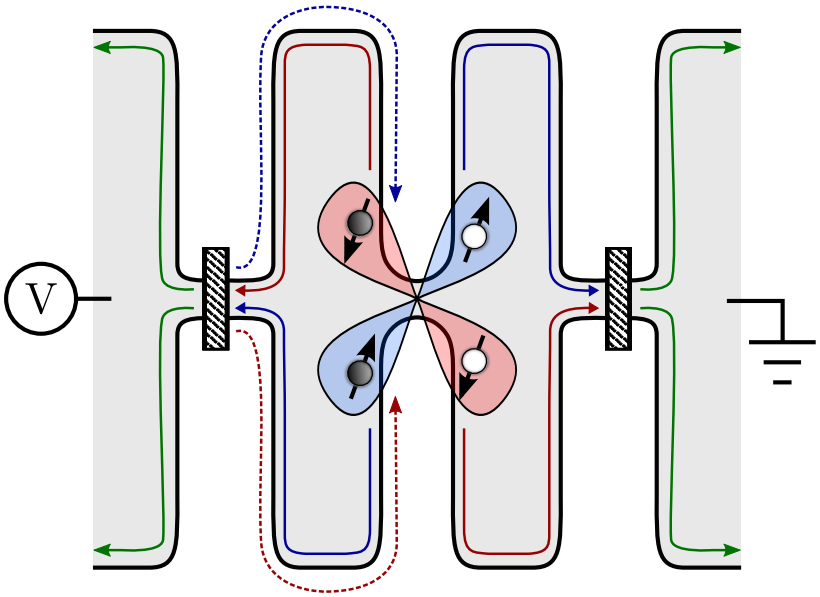

Figure 4.2: Alternatively to the CP splitter schematically shown in Fig. 4.1, an entangled electron-hole pair can be injected across the QSHI edges through the constriction in the middle, by biasing the left reservoir relative to the right reservoir. Blue (red) lobe indicates an electron-hole pair created by spin up (down) incoming state from the left reservoir, denoted by blue (red) dashed trajectories. These entangled electrons-hole pairs then propagate along the edges toward the two beam splitters (shaded regions).

So far, we have focused on the spin-entangled electrons entering different edges and going through beam splitters as in Fig. 4.1. Alternatively, entangled electron-hole pairs can be produced via weak tunneling between the upper and lower edges analogously to Ref. [BEK03]. The corresponding system is sketched in Fig. 4.2. The entangled electron and hole go through the beam splitter without backscattering, and the current-current correlations at the output ports of the beam splitter can be used for constructing a Bell test. As this type of system based on injecting electron-hole pairs instead of CP's can in principle be operated very similarly to the device shown in Fig. 4.1, we will henceforth limit our discussion ex-

clusively to the latter. The advantage of the proposals based on Figs. 4.1 or 4.2 to those of Refs. [SSB03, BEK03] is that the interedge tunneling naturally creates maximally entangled quasiparticle pairs of the form $(|\uparrow\downarrow\rangle \mp |\downarrow\uparrow\rangle)/\sqrt{2}$ (spin here corresponding to chirality of edge index, respectively). Ballistic nature of helical wires furthermore protects against strong orbital dephasing, such that the QSHI would be advantageous even in the setting of Ref. [SSB03], where the CP's are injected by local Andreev processes. It is important to mention that in the models depicted in Figs. 4.1 and 4.2, we assume structural inversion symmetry in the central, tunneling region, in addition to the time-reversal symmetry (thus dictating effective spin conservation on tunneling [SLT10]). In contrast, momentum conservation is assumed for the beam splitters, which requires locally lifting inversion symmetry (e.g., by a Rashba coupling) or time-reversal symmetry (e.g., by a magnetic or exchange field), in order to allow for interedge scattering.

4.2 Model and Hamiltonian

We consider a CP splitter formed by tunnel coupling an s-wave SC to the helical edge states of a QSHI. The total Hamiltonian of the system is $H = H_0 + H_T$, where H_0 describes the unperturbed edge states, including electron-electron interactions, and the tunneling from the SC is given by the Hamiltonian H_T. Since the spin and momentum of the edge states are locked by their helical structure, the LL branches can be labelled by chiral index, $r = \pm$, for the right- and left-moving states, respectively, with the spin index being redundant. We suppose the spin-up (down) states circulate clockwise (counterclockwise) around the QSHI sample, as sketched in Fig. 4.1. Hence, we can denote electron field operators for the left and right-moving LL branches on the upper (u) and lower (l) edges by

$$\psi_{u,\uparrow(\downarrow)} \equiv \psi_{u,\pm}\,, \quad \psi_{l,\uparrow(\downarrow)} \equiv \psi_{l,\mp}\,, \tag{4.1}$$

where (dropping Klein factor and the trivial phase factor $e^{irk_F x}$ associated with the Fermi wave number k_F)

$$\psi_{n,r} \propto \frac{e^{i(\theta_n + r\phi_n)}}{\sqrt{2\pi\delta}}\,, \tag{4.2}$$

in terms of bosonic fields ϕ and θ, subjected to a short-distance cutoff δ [Gia04]. In our convention, the commutation relation for the bosonic operators is given by $[\theta_n(x), \phi_{n'}(y)] = i(\pi/2)\delta_{nn'}\mathrm{sgn}(x-y)$. The effective LL Hamiltonian of the helical edge states in terms of the bosonic operators reads

$$H_0 = \sum_{n=u,l} \int \frac{dx}{2\pi} v(x) \left[\frac{1}{g(x)} (\partial_x \phi_n)^2 + g(x) (\partial_x \theta_n)^2 \right] , \tag{4.3}$$

where g is the interaction parameter and v is the renormalized velocity of the plasmonic excitations, both position dependent for an inhomogeneous LL. For both edges, we take $x = 0$ as the point where electrons tunnel from the SC, and we let the interacting region be $|x| \leq L$ with $g(x) = g < 1$ (repulsive interaction). Exterior of this region ($|x| > L$) is noninteracting, where we set $g(x) = 1$. Correspondingly, the velocity is $v(x) = v_F$ for $|x| > L$ and $v(x) = v$ for $|x| \leq L$. In addition, the left and right ends of each edge are connected through a beam splitter (see Fig. 1), which will be treated using scattering-matrix formalism.

The temperature $k_B T$ and the voltage bias eV between the SC and QSHI are set below the superconducting energy gap Δ to prevent quasiparticle tunneling. We will be interested in the low-temperature regime, $k_B T \ll eV$, when the electric shot noise dominates over the thermal noise. In order to achieve CP splitting into different QSHI edges, their separation should be less than the superconducting coherence length. Furthermore, the electron-electron (here, LL) interaction is necessary to suppress the same-edge tunneling [RL02]. Large enough interaction strength $1 - g$ and gap Δ allow for the different-edge tunneling to become the dominant transport process. This allows one to employ a simple model of equal-time cross-edge tunneling of spin-singlet electron pairs. As the spin-singlet wave function corresponds to $\psi_{u,\uparrow}\psi_{l,\downarrow} - \psi_{u,\downarrow}\psi_{l,\uparrow}$, one obtains the following tunneling Hamiltonian (assuming structural inversion symmetry [SLT10]):

$$\begin{aligned} H_T &= \Gamma e^{-i\omega_0 t} \left[\psi_{u,+}(0)\psi_{l,+}(0) - \psi_{u,-}(0)\psi_{l,-}(0) \right] + \text{H.c.} \\ &= \sum_{r,\varepsilon=\pm} \varepsilon r \Gamma^{\varepsilon} e^{-i\varepsilon\omega_0 t} \psi^{\varepsilon}_{u,r}(0)\psi^{\varepsilon}_{l,r}(0) \, . \end{aligned} \tag{4.4}$$

Here, Γ is a CP tunneling coefficient, $\omega_0 = 2eV/\hbar$ is the Josephson frequency, and ε labels Hermitian conjugate: $\psi^+ = \psi$ and $\psi^- = \psi^\dagger$. Similar electron-hole tunneling Hamiltonian

can be constructed for the set-up of Fig. 4.2, even in the absence of any LL correlations, with $\omega_0 = eV/\hbar$. Electron-electron interactions will, however, always be present and thus need to be included for completeness, particularly in order to understand intrinsic dephasing mechanisms.

4.3 Beam Splitters

The ends of each edge of the QSHI, where the interaction vanishes ($g = 1$), are connected to a beam splitter as in Fig. 4.1. The regions forming the beam splitters are made sufficiently long (on the scale of the Fermi wavelength), making the wave number conserved. Hence, we assume no backscattering occurs from the beam splitters. In a given edge, the right- and left-moving incoming and outgoing states through the beam splitter are related by

$$\begin{pmatrix} \psi'_{n,+} \\ \psi'_{n,-} \end{pmatrix} = \begin{pmatrix} \cos\frac{\varphi_n}{2} & -\sin\frac{\varphi_n}{2} \\ \sin\frac{\varphi_n}{2} & \cos\frac{\varphi_n}{2} \end{pmatrix} \begin{pmatrix} \psi_{n,+} \\ \psi_{n,-} \end{pmatrix} , \tag{4.5}$$

where $\psi'_{n,\pm}$ and $\psi_{n,\pm}$ refer to the right (left)-moving outgoing and incoming states, respectively, along the nth edge. φ_n is the beam-splitter scattering angle, which can be controlled by local electromagnetic or elastic means [LOY98, OKL99].

The transport current operators at the detection points at $u_\pm$ and $l_\pm$ in Fig. 4.1 can be readily expressed in terms of the outgoing filed operators $\psi'_{n,r}$. Defining the currents to be positive away from the beam splitters, the current operator $I^n_\pm$ at the edge $n = u, l$ for the right (+) and left (−) detection points is given by

$$I^n_\pm = ev_F \psi'^\dagger_{n,\pm}\psi'_{n,\pm} = I^n_{\pm,+} + I^n_{\pm,-} + I^n_{\pm,i} \, , \tag{4.6}$$

where v_F is the Fermi velocity in the noninteracting leads. Using Eq. (4.5), three different terms appearing in Eq. (4.6) are given by

$$\begin{aligned} I^n_{\pm,r} &= \frac{ev_F}{2}(1 \pm r\cos\varphi_n)\psi^\dagger_{n,r}\psi_{n,r} \, , \\ I^n_{\pm,i} &= \mp\frac{ev_F}{2}\sin\varphi_n \left(\psi^\dagger_{n,+}\psi_{n,-} + \text{H.c.}\right) , \end{aligned} \tag{4.7}$$

where $\psi_{n,+}$ and $\psi_{n,-}$ are evaluated at some reference points $x > L$ and $x < -L$, respectively, before reaching the beam splitters. There are two types of contributions to the currents, namely the incoherent current, $I^n_{\pm,r}$, which is insensitive to dephasing along the edges, and the interference current, $I^n_{\pm,i}$, which carries the crucial quantum-phase information.

4.4 Current and Noise

Two spin-entangled electrons initially constituting a CP are spatially separated into the top and bottom edges, with the currents produced by such entangled electrons being correlated accordingly to the edge helicity. Thus, the ensuing current-current correlations reflect the entanglement of the injected electron pair. In the following, we calculate the average current and the low-frequency noise, to the leading order in tunneling.

The expectation value of current $\bar{I}^n_\pm$ along the nth edge ($n = u, l$) is given perturbatively by

$$\begin{aligned}\bar{I}^n_\pm &= \left\langle I^n_\pm(t)\right\rangle = \left\langle T_c e^{-\frac{i}{\hbar}\int_c dt' H_T(t')} I^n_\pm(t,+)\right\rangle \\ &\approx -\frac{1}{2\hbar^2}\sum_{\eta_1,\eta_2=\pm}\eta_1\eta_2\int dt_1 dt_2 \\ &\quad\times\left\langle T_c H_T(t_1,\eta_1)H_T(t_2,\eta_2)I^n_\pm(t,+)\right\rangle . \end{aligned} \tag{4.8}$$

The time evolution of the operators here is given in the interaction picture by $A(t) = e^{iH_0 t/\hbar}Ae^{-iH_0 t/\hbar}$. T_c stands for the Keldysh contour ordering and η labels its branches, with $\eta = \pm$ for the upper (lower) branch. Using Eq. (4.4) and (4.7), the above Eq. (4.8) can be expressed in terms of the incoming fermionic operators. Following the standard bosonization scheme, we proceed by expressing the fermionic operators in terms of the bosonic operators following Eq. (4.2), and the chiral electron density appearing in the current operators can be written as $\psi^\dagger_{n,r}\psi_{n,r} = \partial_x(\phi_n + r\theta_n)/2\pi$ [Gia04].

A detailed calculation for the average current is, for completeness, included in Appendix 4.7.2. The final expression is given in terms of the Green's functions for bosonic fields that incorporate the appropriate boundary conditions for the inhomogeneous LL, Eqs. (4.27)

and (4.30). The current reads

$$\bar{I}^n_{\pm} = \left\langle I^n_{\pm,+}(t) + I^n_{\pm,-}(t) \right\rangle = \frac{e}{h} \left(\frac{|\Gamma|}{\hbar v} \right)^2 P(\omega_0) \equiv \bar{I}\,, \tag{4.9}$$

where $P(\omega)$, which is defined in terms of the Fourier transform of the function $P_{\pm\mp}(t)$, Eq. (4.35), is proportional to the product of the tunneling densities of states of the edge LL's and independent of the beam splitter scattering angle φ_n. Note that $\left\langle I^n_{\pm,i} \right\rangle = 0$ for our forward-scattering beam splitter.

As an electron tunnels in the interacting region ($|x| \leq L$), resulting plasmonic charge-density waves go trough multiple reflections between the interfaces of interacting and non-interacting regions (at $x = \pm L$), for which the interacting region acts as a Fabry-Pérot resonator [SS95]. Such reflections are seen as multiple oscillations in the bosonic Green's functions, as in Eqs. (4.27) and (4.30), and the fermionic Green's functions oscillate in turn. The propagation time $t_L = L/v$ of the plasmonic excitations across the interacting region sets the time scale of the Fabry-Pérot oscillation. The function $P_{\pm\mp}(t)$ is a product of the part related to the Green's function in the absence of noninteracting leads (i.e., $L \to \infty$) and the factor containing the effect of the Fabry-Pérot resonator. The applied bias V sets the time scale $t_V = \hbar/eV = 2\omega_0^{-1}$. When $t_V \ll t_L$ (large bias), the phase $e^{i\omega_0 t}$ in the Fourier transform of $P_{\pm\mp}(t)$ oscillates more rapidly than the time scale of the Fabry-Pérot oscillation. In this limit, the effect of the resonator is washed out, and we can evaluate $P(\omega_0)$ in the absence of the noninteracting leads [LCM05], to find $P(\omega_0) \propto \omega_0^{2\gamma+1}$. Here, $\gamma = (g + g^{-1} - 2)/2$ is the single-particle tunneling density of states exponent in a bulk LL.

The symmetrized current-current correlators between the upper and lower edges are given by

$$\begin{aligned} S_{\alpha\beta}(t,t') &= \left\langle \{\delta I^u_\alpha(t), \delta I^l_\beta(t')\} \right\rangle \\ &= \sum_{\eta=\pm} \left\langle T_c e^{-\frac{i}{\hbar}\int_c dt'' H_T(t'')} I^u_\alpha(t,\eta) I^l_\beta(t',-\eta) \right\rangle\,, \end{aligned} \tag{4.10}$$

where $\delta I^n_\alpha(t) = I^n_\alpha(t) - \bar{I}^n$ is the current fluctuation. The above correlation is evaluated up to second order in Γ. The current correlations come in various combinations of the aforementioned current contributions: the incoherent currents, $I^n_{\alpha,+}$ and $I^n_{\alpha,-}$, and the interference

current $I^n_{\alpha,i}$. Let us decompose the noise, $S_{\alpha\beta}(t,t') = \sum_{\mu,\nu=\pm,i} S^{\mu\nu}_{\alpha\beta}(t,t')$, into terms corresponding to different current combinations of the upper-edge current $I^u_{\alpha,\mu}$ and the lower-edge current $I^l_{\beta,\nu}$:

$$\begin{aligned} &S^{\mu\nu}_{\alpha\beta}(t,t') \\ &= \sum_{\eta=\pm} \left\langle T_c e^{-\frac{i}{\hbar}\int_c dt'' H_T(t'')} I^u_{\alpha,\mu}(t,\eta) I^l_{\beta,\nu}(t',-\eta) \right\rangle . \end{aligned} \tag{4.11}$$

The cross terms between $I_{\alpha,i}$ and $I_{\alpha,\pm}$ give no contribution. The terms involving only $I^n_{\alpha,\pm}$ result in

$$\tilde{S}^{(0)}_{\alpha\beta} \equiv \sum_{\mu,\nu=\pm} \tilde{S}^{\mu\nu}_{\alpha\beta} = e\bar{I}\left(1 + \alpha\beta\cos\varphi_u \cos\varphi_l\right) . \tag{4.12}$$

Here, $\tilde{S}^{\mu\nu}_{\alpha\beta} \equiv S^{\mu\nu}_{\alpha\beta}(\omega = 0)$ is the zero-frequency Fourier transform of $S^{\mu\nu}_{\alpha\beta}(t-t')$. Lastly, we find the correlation involving only the interference terms $I^n_{\alpha,i}$ as

$$\tilde{S}^{(i)}_{\alpha\beta} = \alpha\beta C(\omega_0) e\bar{I} \sin\varphi_u \sin\varphi_l . \tag{4.13}$$

$C(\omega)$ is the Fourier transform of $C(t)$ given in Eq. (4.43). It characterizes dephasing and ranges $0 \le C(\omega_0) \le 1$. When $g = 1$ (i.e., the edges are everywhere noninteracting), $C(\omega_0) = 1$, which means the nonlocal spin entanglement of the electron pair persists until the currents are measured. In this ideal case, the total noise is given by (for $r = \pm$)

$$\tilde{S}_{r,\pm r} = e\bar{I}\left[1 \pm \cos(\varphi_u - \varphi_l)\right] . \tag{4.14}$$

This noise reminds us of spin correlations in the EPR thought experiment, where a spin-singlet state decays into two counter-propagating particles, whose resulting beams pass through two distant polarizers before being detected. The coincidence signal correlations in the distant detectors depend sinusoidally on the relative angle of the polarizers. In Eq. (4.14), our current correlations similarly depend on the relative scattering angle of the beam splitters.

LL is known to exhibit a charge fractionalization [PGL00, LHY08, SBY08], where a chiral single-particle state, say a right-moving electron, breaks down into a charge $e(1 + g)/2$ moving to the right and $e(1 - g)/2$ moving to the left. At finite temperature, these

counter-propagating states cease to overlap after a time $\tau = \pi k_B T\gamma/\hbar$, as is reflected in the exponential decay (dephasing) of a single-particle propagator for the right-moving branch [Le 05, Le 06]. The interference effect is likewise exponentially suppressed. For instance, exponential suppression in the Aharonov-Bohm oscillation of the tunneling current between two LL wires has been studied in Ref. [Le 05].

When the electron temperature is above the finite-size crossover temperature, $T \gg T_0 \equiv \hbar v/2\pi k_B L$, the interference in an LL system of size $2L$ decays exponentially. If $T \ll T_0$, the suppression occurs in a power-law form in a complicated fashion depending on the hierarchy of the relevant energy scales: ambient temperature, $k_B T$, bias, eV, and the crossover temperature, $k_B T_0$. In our case, this dephasing affects C appearing in Eq. (4.13), which is expected to show similar reduction at finite temperatures. Using the Green's functions in Eqs. (4.27) and (4.30), we can extract the exponentially decaying part, which is given by $C(L, \omega_0) \propto e^{-2\gamma T/T_0}$. Such exponential suppression does not affect $\tilde{S}^{(0)}_{\alpha\beta}$ pertaining to the incoherent current, as a consequence of the conservation of charge. In the opposite, low-temperature regime, $T \ll T_0$, $C(\omega_0)$ is instead expected to show a power-law behavior, with details depending on the relative strength of the bias with respect to the crossover energy scale (i.e., $k_B T \ll eV \ll k_B T_0$ or $k_B T \ll k_B T_0 \ll eV$) [GL97, Le 06].

4.5 Bell inequality

In optical experiments, a violation of a Bell inequality is tested by coincidence counting of the simultaneous arrival of a pair of entangled photons at remote locations. On the other hand, it is more natural to measure current correlations in solid-state devices, which could be used to construct a Bell inequality in beam-splitter based systems [Kaw01, CBL02]. The time window for a current measurement should be short enough so that no more than a single Cooper pair is detected at a time and the $1/f$ noise can be neglected, but it should also be sufficiently long on the scale of the inverse voltage and the transport time along the edges such that the zero-frequency approximation for the shot noise is adequate [CBL02].

Under these conditions, the current-current correlations can be combined to give the Clauser-Horne-Shimony-Holt Bell inequality [CHS69]. As shown in the previous section, the total zero-frequency noise is (evaluating C at ω_0 throughout)

$$\tilde{S}_{\alpha\beta} = e\bar{I}\left[1 + \alpha\beta\left(\cos\varphi_u \cos\varphi_d + C\sin\varphi_u \sin\varphi_d\right)\right] . \tag{4.15}$$

The Bell inequality then is given by

$$\begin{aligned} B &\equiv \left|F(\varphi_u, \varphi_l) - F(\varphi_u, \varphi_l') + F(\varphi_u', \varphi_l) + F(\varphi_u', \varphi_l')\right| \\ &\leq 2\,, \end{aligned} \tag{4.16}$$

where the correlation functions in the inequality are directly related to the noise spectra by

$$\begin{aligned} F(\varphi_u, \varphi_d) &= \frac{\tilde{S}_{++} - \tilde{S}_{+-} - \tilde{S}_{-+} + \tilde{S}_{--}}{\tilde{S}_{++} + \tilde{S}_{+-} + \tilde{S}_{-+} + \tilde{S}_{--}} \\ &= \cos\varphi_u \cos\varphi_l + C\sin\varphi_u \sin\varphi_l\,. \end{aligned} \tag{4.17}$$

The noninteracting ($g = 1$) zero-temperature case gives maximally-entangled result with $C = 1$ and $F(\varphi_u, \varphi_d) = \cos(\varphi_u - \varphi_d)$. A choice of the angles maximizing B is $\varphi_u = \pi/4$, $\varphi_d = \pi/2$, $\varphi_u' = 3\pi/4$, and $\varphi_d' = \pi$, leading to $B = 2\sqrt{2}$.

Even in the presence of dephasing, i.e., $C < 1$, by adjusting the four angles, φ_u, φ_u', φ_l, and φ_l', the maximum value of the Bell parameter [SSB03]

$$B = 2\sqrt{1 + C^2} \tag{4.18}$$

still exceeds 2. This means that the Bell inequality can in principle be violated for arbitrary nonzero C. The optimal violation angles are given by [SSB03]

$$\begin{aligned} &\tan\varphi_u = -C\cot\varphi_s\,, \quad \tan\varphi_u' = C\tan\varphi_s\,, \\ &\tan\frac{\varphi_l - \varphi_l'}{2} = \mathrm{sgn}(\cos\varphi_u)\sqrt{\frac{\tan^2\varphi_s + C^2}{C^2\tan^2\varphi_s + 1}}\,, \end{aligned} \tag{4.19}$$

where $\varphi_s \equiv (\varphi_l + \varphi_l')/2$ is arbitrary. Although it is possible to observe a violation of the Bell inequality under a finite dephasing, the range of angles that can achieve a violation shrinks as $C \to 0$.

4.6 Discussion and Conclusion

We discussed the construction of a Bell inequality via the current-current correlations between different edges of a QSHI equipped with beam splitters. The entanglement is produced by coherently injecting electron Cooper pairs from a superconductor or electron-hole pairs from a normal Fermi-liquid reservoir biased by a constant voltage V with respect to the QSHI. Adjusting the transmission matrix through the beam splitters by local electric or magnetic fields, a violation of the Bell inequality can be achieved even in the presence of a moderate dephasing, parametrized by C (with $C = 1$ corresponding to maximal entanglement with no dephasing and $C = 0$ to complete dephasing and classical correlations).

The edge states of a QSHI are modeled as helical LL's. Electron-electron interactions are essential ingredient in order to achieve tunneling of two electrons forming a CP into different edges. On the other hand, the charge fractionalization furnished by LL causes dephasing at finite temperature when $T > T_0 = \hbar v/2\pi k_B 2L$. In this high-temperature regime, the dephasing parameter suffers exponential decay as $C \propto e^{-2\gamma T/T_0}$. In the low-temperature limit, $T < T_0$, C does not decay exponentially, but is expected to follow power-law scaling characteristic of LL's. Even with the reduction of the dephasing parameter below unity, the entanglement of quasiparticle (electron-electron or electron-hole) pairs is visible through the violation of the Bell inequality, albeit it becomes progressively more difficult to tune the beam splitters to achieve the violation as C vanishes.

The QSHI edge states thus provide a promising medium for production and manipulation of quantum information in mesoscopic systems, even in the absence of any correlations (as in Fig. 4.2). In our minimal model, we have only considered dephasing due to internal electronic interactions along the edges. Collective or quasiparticle modes present in the solid-state environment can generally be expected to provide additional detrimental dephasing sources that need to be studied and mitigated.

4.7 Supplementary Calculations

4.7.1 Green's functions

Evaluation of the current and noise in Eqs. (4.8) and (4.10) is based on several bosonic Green's functions. Since the system of interest here is an inhomogeneous LL where the interaction parameter g depends on the position, we need to impose appropriate boundary conditions to obtain the Green's functions.

First, we identify the Lagrangian for the bosonic fields ϕ and θ from Eq. (4.3) as

$$\mathcal{L} = \frac{1}{\pi}\partial_x\theta\partial_t\phi - \frac{v}{2\pi}\left[\frac{1}{g}(\partial_x\phi)^2 + g(\partial_x\theta)^2\right] . \tag{4.20}$$

The effective Lagrangian for the ϕ or θ field can be found by integrating out the θ or ϕ field, respectively:

$$\begin{aligned}\mathcal{L}_\phi &= \frac{1}{2\pi g}\left[\frac{1}{v}(\partial_t\phi)^2 - v(\partial_x\phi)^2\right] ,\\ \mathcal{L}_\theta &= \frac{g}{2\pi}\left[\frac{1}{v}(\partial_t\theta)^2 - v(\partial_x\theta)^2\right] .\end{aligned} \tag{4.21}$$

The spatial dependence of the velocity and the interaction parameter are $v(x) = v_F$ and $g(x) = g_l = 1$ for $|x| > L$, and $v(x) = v$ and $g(x) = g$ for $|x| \le L$. For electrons injected at $x = 0$, the retarded Green's functions are found to satisfy the following differential equations:

$$\begin{aligned}\frac{1}{\pi}\left[\frac{\omega^2}{g(x)v(x)} + \partial_x\left(\frac{v(x)}{g(x)}\partial_x\right)\right] G_R^{\phi\phi}(x,\omega) &= \delta(x) ,\\ \frac{1}{\pi}\left[\frac{g(x)\omega^2}{v(x)} + \partial_x\left(v(x)g(x)\partial_x\right)\right] G_R^{\theta\theta}(x,\omega) &= \delta(x) ,\end{aligned} \tag{4.22}$$

with the appropriate boundary conditions: (1) the solutions in the leads are moving away from $x = 0$, (2) $G_R(x,\omega)$ is continuous at $x = \pm L, 0$, (3) the following expressions at $x = \pm L$ are continuous:

$$\begin{aligned}\frac{v(x)}{g(x)}\partial_x G_R^{\phi\phi}(x,\omega)\Big|_{x=\pm L+0^-}^{x=\pm L+0^+} &= 0 ,\\ v(x)g(x)\partial_x G_R^{\theta\theta}(x,\omega)\Big|_{x=\pm L+0^-}^{x=\pm L+0^+} &= 0 ,\end{aligned}$$

and (4) the derivative at the location of the delta function $x = 0$ is discontinuous as

$$\frac{v(x)}{g(x)}\partial_x G_R^{\phi\phi}(x,\omega)\Big|_{x=0^-}^{x=0^+} = \pi\,,$$
$$v(x)g(x)\partial_x G_R^{\theta\theta}(x,\omega)\Big|_{x=0^-}^{x=0^+} = \pi\,.$$

Neglecting electron backscattering, we suppose that both fermionic branches have continuous displacement fields at the interface, thus making the fields θ and ϕ continuous. The boundary conditions are then obtained from the continuity of their time derivatives, which are calculated using the bosonic commutation relations. Microscopically, this assumes that the electronic Hamiltonian is smooth on the scale of the Fermi wavelength, which makes the transport ballistic at the Fermi level.

We look for the solutions of the form

$$G_R^{\phi\phi,\theta\theta}(x,\omega) = \begin{cases} Ae^{-i\omega x/v_F} & \text{for } x < -L \\ Be^{i\omega x/v} + Ce^{-i\omega x/v} & \text{for } -L \le x \le 0 \\ De^{i\omega x/v} + Ee^{-i\omega x/v} & \text{for } 0 \le x \le L \\ Fe^{i\omega x/v_F} & \text{for } L < x \end{cases}, \tag{4.23}$$

which, after imposing the above boundary conditions, we find

$$G_R^{\phi\phi}(x,\omega) = A_\phi g \begin{cases} a_t e^{i\omega(|x|-L)/v_F} & \text{for } L < |x| \\ e^{i\omega(|x|-L)/v} + a_r e^{-i\omega(|x|-L)/v} & \text{for } |x| \le L \end{cases}, \quad A_\phi = -i\frac{\pi}{2\omega}\frac{e^{i\omega L/v}}{1-a_r e^{i2\omega L/v}}\,,$$
$$G_R^{\theta\theta}(x,\omega) = A_\theta \begin{cases} g_l^{-1} a_t e^{i\omega(|x|-L)/v_F} & \text{for } L < |x| \\ g^{-1}e^{i\omega(|x|-L)/v} - a_r e^{-i\omega(|x|-L)/v} & \text{for } |x| \le L \end{cases}, \quad A_\theta = -i\frac{\pi}{2\omega}\frac{e^{i\omega L/v}}{1+a_r e^{i2\omega L/v}}\,. \tag{4.24}$$

Here, $a_t = 2g_l/(g_l+g)$ and $a_r = (g_l-g)/(g_l+g)$ are the transmission and reflection coefficients for the bosonic fields between regions with different interaction parameter strengths. Given the retarded Green's functions, the greater and lesser Green's functions can be found by the standard relationships

$$G_> = i2[1+n_B(\omega)]\mathrm{Im}G_R\,,\;\; G_< = i2n_B(\omega)\mathrm{Im}G_R\,, \tag{4.25}$$

where $n_B(\omega) = 1/(e^{\beta\hbar\omega} - 1)$ is the bosonic distribution function.

In the calculation of the current and noise, we encounter the Keldysh contour ordered Green's functions. The following conventions are used: $G^{AB}_{\eta\eta'}(x,t) = \langle T_c A(x,t,\eta)B(0,0,\eta')\rangle$, where

$$\begin{aligned}
G^{AB}_{-+}(x,t) &= G^{AB}_{>}(x,t) = -i\,\langle A(x,t)B(0,0)\rangle\ , \\
G^{AB}_{+-}(x,t) &= G^{AB}_{<}(x,t) = -i\,\langle B(0,0)A(x,t)\rangle\ , \\
G^{AB}_{++}(x,t) &= \Theta(t)G_{>}(x,t) + \Theta(-t)G_{<}(x,t)\,, \\
G^{AB}_{--}(x,t) &= -\Theta(-t)G_{>}(x,t) - \Theta(t)G_{<}(x,t)\,,
\end{aligned} \tag{4.26}$$

for arbitrary bosonic operators A and B.

The finite-temperature Green's functions at $|x| > L$ (noninteracting region) are found to be

$$\begin{aligned}
iG^{\phi\phi}_{\eta\eta'}(x,t) &= \langle T_c\phi(x,t,\eta)\phi(0,0,\eta')\rangle \to -\frac{g}{4}a_t\sum_{n=0}^{\infty}a_r^n\sum_{s=\pm}G_{n,s}(x,t)\,, \\
iG^{\theta\theta}_{\eta\eta'}(x,t) &= \langle T_c\phi(x,t,\eta)\phi(0,0,\eta')\rangle \to -\frac{1}{4}a_t\sum_{n=0}^{\infty}(-a_r)^n\sum_{s=\pm}G_{n,s}(x,t)\,, \\
iG^{\theta\phi}_{\eta\eta'}(x,t) &= \langle \theta(x,t,\eta)\phi(0,0,\eta')\rangle \to \mathrm{sgn}(x)\frac{g}{4}a_t\sum_{n=0}^{\infty}a_r^n\sum_{s=\pm}sG_{n,s}(x,t)\,, \\
iG^{\phi\theta}_{\eta\eta'}(x,t) &= \langle \phi(x,t,\eta)\theta(0,0,\eta')\rangle \to \mathrm{sgn}(x)\frac{1}{4}a_t\sum_{n=0}^{\infty}(-a_r)^n\sum_{s=\pm}sG_{n,s}(x,t)\,,
\end{aligned} \tag{4.27}$$

where $D_{\eta\eta'}(t) = \Theta(\eta\eta')\mathrm{sgn}(\eta' t) + \Theta(-\eta\eta')\mathrm{sgn}(\eta')$ and

$$G_{n,s}(x,t) = \ln\sin\left\{\frac{\pi}{\hbar\beta}\left[\frac{\delta}{v} + iD_{\eta\eta'}(t)\left(t - s\frac{L(2n+1)}{v} - s\frac{|x|-L}{v_F}\right)\right]\right\}\,. \tag{4.28}$$

The arrow in the above equations indicate that the divergent terms on the right hand side are left out, since they can be regularized out. From the Lagrangian in Eq. (4.20), the first

two Green's functions are related to the last two by

$$G^{\theta\phi}_{>,<}(x,\omega) = i\,\langle T_c\theta(x,t,\mp)\phi(0,0,\pm)\rangle = -i\frac{v}{g\omega}\partial_x G^{\phi\phi}_{>,<}(x,\omega)\,,$$
$$G^{\phi\theta}_{>,<}(x,\omega) = i\,\langle T_c\phi(x,t,\mp)\theta(0,0,\pm)\rangle = -i\frac{vg}{\omega}\partial_x G^{\theta\theta}_{>,<}(x,\omega)\,. \tag{4.29}$$

We further need the Green's functions for $x = 0$ case, which are given by

$$iG^{\phi\phi}_{\eta\eta'}(x=0,t) \to -\frac{g}{2}\bar{G}_{0,s}(x,t) - \frac{g}{2}\sum_{n=1}^{\infty}\sum_{s=\pm} a_r^n \bar{G}_{n,s}(x,t)\,,$$
$$iG^{\theta\theta}_{\eta\eta'}(x=0,t) \to -\frac{1}{2g}\bar{G}_{0,s}(x,t) - \frac{1}{2g}\sum_{n=1}^{\infty}\sum_{s=\pm}(-a_r)^n \bar{G}_{n,s}(x,t)\,, \tag{4.30}$$

where

$$\bar{G}_{n,s}(x,t) = \ln\sin\left[\frac{\pi}{\hbar\beta}\left(\frac{\delta}{v} + iD_{\eta\eta'}(t)\left(t + sn\frac{2L}{v}\right)\right)\right]\,. \tag{4.31}$$

By Eqs. (4.24), and (4.29), we can show $G^{\theta\phi}_{\eta\eta'}(0,t) = G^{\phi\theta}_{\eta\eta'}(0,t) = 0$.

A bosonic mode created at $x = 0$ propagates in the interacting region, $|x| < L$, before it hits the boundary between the interacting and noninteracting regions at $x = \pm L$. Some part of the wave is transmitted into the noninteracting region, whereas the rest is reflected back into the interacting region. This process of transmission and reflection is repeated, establishing a Fabry-Pérot resonator structure. The above Green's functions are in the form of the sum of these transmitted and reflected parts.

4.7.2 Current

The average current in Eq. (4.9) up to second order in the tunneling coefficient in terms of the fermionic fields is given by

$$\langle I^n_{\pm}(t)\rangle = \langle T_c e^{-\frac{i}{\hbar}\int_c dt'' H_T(t'')} I^n(x,t,+)\rangle \approx \frac{|\Gamma|^2}{2\hbar^2}\sum_{\eta_1,\eta_2,\varepsilon,\sigma=\pm}\eta_1\eta_2\int_{-\infty}^{\infty}dt_1\int_{-\infty}^{\infty}dt_2 e^{-i\varepsilon\omega_0(t_1-t_2)}$$
$$\times\,\langle T_c\psi^{\varepsilon}_{u,\sigma}(0,t_1,\eta_1)\psi^{\varepsilon}_{l,\sigma}(0,t_1,\eta_1)\psi^{-\varepsilon}_{u,\sigma}(0,t_2,\eta_2)\psi^{-\varepsilon}_{l,\sigma}(0,t_2,\eta_2)I^n_{\pm}(t,+)\rangle\,. \tag{4.32}$$

Bosonizing field operators, $\psi_{n,r} = e^{i(\theta_n + r\phi_n)}/\sqrt{2\pi\delta}$, where θ_n and ϕ_n are boson fields given in Eq. (4.3) with the commutation relation $[\theta_n(x),\phi_{n'}(y)] = i(\pi/2)\delta_{nn'}\mathrm{sgn}(x-y)$. $r = +(-)$

labels the right-(left-)moving state. The current operators $I^n_{\pm,r}$ ($r = \pm$) in Eq. (4.7) involve fermionic operators in the combination $\psi^\dagger_{n,r}\psi_{n,r}$, which can be expressed in terms of bosonic operators as

$$\psi^\dagger_{n,r}(x,t)\psi_{n,r}(x,t) = \frac{1}{2\pi}\partial_x[r\theta_n(x,t)+\phi_n(x,t)] = \frac{1}{2\pi}\partial_x(-i\partial_\lambda)e^{i\lambda[r\theta_n(x,t)+\phi_n(x,t)]}\Big|_{\lambda=0}. \quad (4.33)$$

The expectation value of $I^n_{\pm,i}$ can be shown to vanish, since there are always operators that cannot be contracted. By summing the contributions from $I^n_{\pm,+}$ and $I^n_{\pm,-}$, the following result is obtained:

$$\begin{aligned}\bar{I} = \left\langle I^n_\pm(t)\right\rangle =& -\frac{e}{h}\frac{v_F|\Gamma|^2}{8\pi\hbar^2v^2}\sum_{r,\varepsilon,\sigma,\eta_1,\eta_2=\pm}(1\pm r\cos\varphi_n)\eta_1\eta_2\varepsilon \\ &\times\left[r\tilde{Q}^\theta_{+\eta_1,\sigma}(r) - r\tilde{Q}^\theta_{+\eta_2,\sigma}(r) + \sigma\tilde{Q}^\phi_{+\eta_1,\sigma}(r) - \sigma\tilde{Q}^\phi_{+\eta_2,\sigma}(r)\right]P_{\eta_1\eta_2}(-\varepsilon\omega_0) \\ =& \frac{e}{h}\left(\frac{|\Gamma|}{\hbar v}\right)^2[P_{-+}(\omega_0) - P_{+-}(-\omega_0)] = \mathrm{sgn}(\omega_0)\frac{e}{h}\left(\frac{|\Gamma|}{\hbar v}\right)^2 P(\omega_0)\,. \end{aligned} \quad (4.34)$$

Here, $\tilde{Q}_{\eta\eta';\sigma}(r) \equiv Q_{\eta\eta';\sigma}(x,\omega=0)$, which depend only on $r \equiv \mathrm{sgn}(x)$. The corresponding real-time expressions for Q and P are given by

$$\begin{aligned} Q^\theta_{\eta\eta';\sigma}(x,t) &= \partial_x G^{\theta\theta}_{\eta\eta'}(x,t) + \sigma\partial_x G^{\theta\phi}_{\eta\eta'}(x,t) \\ Q^\phi_{\eta\eta';\sigma}(x,t) &= \partial_x G^{\phi\phi}_{\eta\eta'}(x,t) + \sigma\partial_x G^{\phi\theta}_{\eta\eta'}(x,t)\,, \\ P_{\eta_1\eta_2}(t) &= \frac{hv^2}{(2\pi\delta)^2}e^{i2\left[G^{\theta\theta}_{\eta_1\eta_2}(0,t)+G^{\phi\phi}_{\eta_1\eta_2}(0,t)-G^{\theta\theta}(0,0)-G^{\phi\phi}(0,0)\right]}\,. \end{aligned} \quad (4.35)$$

We can show that $P_{\mp\pm}(\omega) = \Theta(\pm\omega)P(\omega)$, hence $P_{-+}(\omega_0) - P_{+-}(\omega_0) = \mathrm{sgn}(\omega_0)P(\omega_0)$. Furthermore, the relations

$$\tilde{Q}^{\theta/\phi}_{++,\sigma}(x) - \tilde{Q}^{\theta/\phi}_{+-,\sigma}(x) = \tilde{Q}^{\theta/\phi}_{-+,\sigma}(x) - \tilde{Q}^{\theta/\phi}_{--,\sigma}(x) = \frac{\pi}{2v_F}[\mathrm{sgn}(x)+\sigma] \quad (4.36)$$

turn out to be independent of temperature.

4.7.3 Zero-frequency noise

With the current in Eq. (4.7) and tunneling Hamiltonian in Eq. (4.4), the current-current correlations between the upper and lower edges Eq. (4.10), up to second order in the tunneling

coefficient, are given by

$$S_{\alpha\beta}(t,t') = \sum_{\mu,\nu=\pm,i} S^{\mu\nu}_{\alpha\beta}(t,t') \tag{4.37}$$

$$\begin{aligned} &= -\frac{1}{2\hbar^2} \sum_{\mu,\nu=\pm,i} \sum_{\eta,\eta_1,\eta_2,\sigma_1,\sigma_2,\varepsilon_1,\varepsilon_2=\pm} \Gamma^{\varepsilon_1}\Gamma^{\varepsilon_2}\varepsilon_1\varepsilon_2\sigma_1\sigma_2\eta_1\eta_2 \int_{-\infty}^{\infty} dt_1 dt_2 e^{-i\omega_0(\varepsilon_1 t_1+\varepsilon_2 t_2)} \\ &\quad \times \langle T_c I^u_{\alpha,\mu}(t,\eta) I^l_{\beta,\nu}(t',-\eta) \psi^{\varepsilon_1}_{u\sigma_1}(0,t_1,\eta_1) \psi^{\varepsilon_1}_{l\sigma_1}(0,t_1,\eta_1) \psi^{\varepsilon_2}_{u\sigma_2}(0,t_2,\eta_2) \psi^{\varepsilon_2}_{l\sigma_2}(0,t_2,\eta_2)\rangle \,, \end{aligned} \tag{4.38}$$

where $S^{\mu\nu}_{\alpha\beta}$ is the correlation between the currents $I^u_{\alpha,\mu}$ and $I^d_{\beta,\nu}$.

First, we calculate the contributions from $I^n_{\alpha,+}$ and $I^n_{\alpha,-}$:

$$\begin{aligned} &\sum_{\mu,\nu=\pm} S^{\mu\nu}_{\alpha\beta}(t,t') \\ &= \frac{|\Gamma|^2}{2\hbar^2} \sum_{\mu,\nu=\pm} \sum_{\eta,\eta_1,\eta_2,\sigma,\varepsilon=\pm} \eta_1\eta_2 \int_{-\infty}^{\infty} dt_1 dt_2 e^{-i\varepsilon\omega_0(t_1-t_2)} \\ &\quad \times \langle T_c I^u_{\alpha,\mu}(t,\eta) I^l_{\beta,\nu}(t',-\eta) \psi^{\varepsilon}_{u,\sigma}(0,t_1,\eta_1) \psi^{\varepsilon}_{l,\sigma}(0,t_1,\eta_1) \psi^{-\varepsilon}_{u,\sigma}(0,t_2,\eta_2) \psi^{-\varepsilon}_{l,\sigma}(0,t_2,\eta_2)\rangle \\ &= \frac{|\Gamma|^2}{2\hbar^2} \left(\frac{ev_F}{2\pi}\right)^2 \sum_{\mu,\nu=\pm} \frac{1}{4}(1+\alpha\mu\cos\varphi_u)(1+\beta\nu\cos\varphi_l) \sum_{\eta,\eta_1,\eta_2,\sigma,\varepsilon=\pm} \eta_1\eta_2 \int_{-\infty}^{\infty} dt_1 dt_2 e^{-i\varepsilon\omega_0(t_1-t_2)} \\ &\quad \times \left(\frac{1}{2\pi\delta}\right)^2 \partial_x \partial_{x'} \langle T_c[\mu\theta_u(x,t,\eta)+\phi_u(x,t,\eta)][\nu\theta_l(x',t',-\eta)+\phi_l(x',t',-\eta)] \\ &\quad e^{i\varepsilon[\theta_u(0,t_1,\eta_1)+\sigma\phi_u(0,t_1,\eta_1)]} e^{i\varepsilon[\theta_l(0,t_1,\eta_1)+\sigma\phi_l(0,t_1,\eta_1)]} e^{-i\varepsilon[\theta_u(0,t_2,\eta_2)+\sigma\phi_u(0,t_2,\eta_2)]} e^{i\varepsilon[\theta_l(0,t_2,\eta_2)+\sigma\phi_l(0,t_2,\eta_2)]} \Big|^{x\to\mu}_{x'\to\nu} \\ &= \frac{|\Gamma|^2}{2\hbar^2} \left(\frac{ev_F}{2\pi}\right)^2 \frac{1}{4hv^2} \sum_{\mu,\nu=\pm} (1+\alpha\mu\cos\varphi_u)(1+\beta\nu\cos\varphi_l) \sum_{\eta,\eta_1,\eta_2,\sigma,\varepsilon=\pm} \eta_1\eta_2 \int_{-\infty}^{\infty} dt_1 dt_2 e^{-i\varepsilon\omega_0(t_1-t_2)} \\ &\quad \times \left[\mu Q^{\theta}_{\eta\eta_1,\sigma}(\mu,t-t_1) - \mu Q^{\theta}_{\eta\eta_2,\sigma}(\mu,t-t_2) + \sigma Q^{\phi}_{\eta\eta_1,\sigma}(\mu,t-t_1) - \sigma Q^{\phi}_{\eta\eta_2,\sigma}(\mu,t-t_2)\right] \\ &\quad \times \left[\nu Q^{\theta}_{-\eta\eta_1,\sigma}(\nu,t'-t_1) - \nu Q^{\theta}_{-\eta\eta_2,\sigma}(\nu,t'-t_2) + \sigma Q^{\phi}_{-\eta\eta_1,\sigma}(\nu,t'-t_1) - \sigma Q^{\phi}_{-\eta\eta_2,\sigma}(\nu,t'-t_2)\right] \\ &\quad \times P_{\eta_1\eta_2}(t_1-t_2) \end{aligned} \tag{4.39}$$

Here, $Q^{\theta/\phi}_{\eta\eta'}(x,t)$ and $P_{\eta\eta'}(t)$ are defined in Eq. (4.35). The zero-frequency component of the

Fourier transform of the above expression is given by

$$\begin{aligned}\sum_{\mu,\nu=\pm}\tilde{S}^{\mu\nu}_{\alpha\beta} &= \frac{e^2}{h}\frac{|\Gamma|^2}{2\hbar^2v^2}\frac{v_F^2}{4\pi^2}\frac{1}{4}\sum_{\mu,\nu=\pm}(1+\alpha\mu\cos\varphi_u)(1+\beta\nu\cos\varphi_l)\sum_{\eta,\eta_1,\eta_2,\sigma,\varepsilon=\pm}\eta_1\eta_2 \\ &\times\left[\tilde{\mu}Q^{\theta}_{\eta\eta_1,\sigma}(\mu)-\tilde{\mu}Q^{\theta}_{\eta\eta_2,\sigma}(\mu)+\sigma\tilde{Q}^{\phi}_{\eta\eta_1,\sigma}(\mu)-\sigma\tilde{Q}^{\phi}_{\eta\eta_2,\sigma}(\mu)\right] \\ &\times\left[\tilde{\nu}Q^{\theta}_{-\eta\eta_1,\sigma}(\nu)-\tilde{\nu}Q^{\theta}_{-\eta\eta_2,\sigma}(\nu)+\sigma\tilde{Q}^{\phi}_{-\eta\eta_1,\sigma}(\nu)-\sigma\tilde{Q}^{\phi}_{-\eta\eta_2,\sigma}(r'l)\right]2P_{\eta_1\eta_2}(-\varepsilon\omega_0) \\ &= \frac{e^2}{h}\left(\frac{|\Gamma|}{\hbar v}\right)^2(1+\alpha\beta\cos\varphi_u\cos\varphi_l)\,P(\omega_0)=\tilde{S}^{(0)}_{\alpha\beta}\,. \end{aligned} \tag{4.40}$$

In the last line, we used $P(\omega_0)=P_{+-}(\omega_0)+P_{-+}(\omega_0)$. All the temperature and bias dependence is in $P(\omega_0)$. Therefore,

$$\tilde{S}^{(0)}_{\alpha\beta}=e\bar{I}\,(1+\alpha\beta\cos\varphi_u\cos\varphi_l)\,P(\omega_0)\,. \tag{4.41}$$

The correlations between $I^u_{\pm,+(-)}$ and $I^l_{\pm,i}$ vanish. Finally, the correlation between I^u_i and I^l_i is given by

$$\begin{aligned}S^{(i)}_{\alpha\beta}(t,t') =& -\frac{1}{2\hbar^2}\sum_{\eta}\sum_{\substack{\sigma_1,\varepsilon_1,\eta_1\\ \sigma_2,\varepsilon_2,\eta_2}}\Gamma^{\varepsilon_1}\Gamma^{\varepsilon_2}\varepsilon_1\varepsilon_2\sigma_1\sigma_2\eta_1\eta_2\int_{-\infty}^{\infty}dt_1\int_{-\infty}^{\infty}dt_2e^{-i\omega_0(\varepsilon_1t_1+\varepsilon_2t_2)} \\ &\times\langle T_cI^u_0(l,t,\eta)I^l_0(l,t',-\eta)\psi^{\varepsilon_1}_{u,\sigma_1}(0,t_1,\eta_1)\psi^{\varepsilon_1}_{l,\sigma_1}(0,t_1,\eta_1)\psi^{\varepsilon_2}_{u,\sigma_2}(0,t_2,\eta_2)\psi^{\varepsilon_2}_{l,\sigma_2}(0,t_2,\eta_2)\rangle \\ =&\alpha\beta\frac{e^2v_F^2|\Gamma|^2}{8\hbar^2}\sin\varphi_u\sin\varphi_l\sum_{\eta,\eta_1,\eta_2,\varepsilon,r=\pm}\eta_1\eta_2\int_{-\infty}^{\infty}dt_1\int_{-\infty}^{\infty}dt_2e^{-i\varepsilon\omega_0(t_1-t_2)} \\ &\times\langle T_c\psi^{\dagger}_{u,r}(rl,t,\eta)\psi_{u,-r}(-rl,t,\eta)\psi^{\varepsilon}_{u,\varepsilon r}(0,t_1,\eta_1)\psi^{-\varepsilon}_{u,-\varepsilon r}(0,t_2,\eta_2)\rangle \\ &\times\langle T_c\psi^{\dagger}_{l,r}(rl,t',-\eta)\psi_{l,-r}(-rl,t',-\eta)\psi^{\varepsilon}_{l,\varepsilon r}(0,t_1,\eta_1)\psi^{-\varepsilon}_{l,-\varepsilon r}(0,t_2,\eta_2)\rangle\,. \end{aligned} \tag{4.42}$$

l is taken to be a reference point located between the end of the interacting region ($x=L$) and the location of the beam splitter. After defining

$$\begin{aligned}C(t-t') =&\frac{|\Gamma|^2ev_F^2}{4\hbar^2\bar{I}}\sum_{\eta,\eta_1,\eta_2,\varepsilon,r=\pm}\eta_1\eta_2\int_{-\infty}^{\infty}dt_1\int_{-\infty}^{\infty}dt_2e^{-i\varepsilon\omega_0(t_1-t_2)} \\ &\times\langle T_c\psi^{\dagger}_{u,r}(rl,t,\eta)\psi_{u,-r}(-rl,t,\eta)\psi^{\varepsilon}_{u,\varepsilon r}(0,t_1,\eta_1)\psi^{-\varepsilon}_{u,-\varepsilon r}(0,t_2,\eta_2)\rangle \\ &\times\langle T_c\psi^{\dagger}_{l,r}(rl,t',-\eta)\psi_{l,-r}(-rl,t',-\eta)\psi^{\varepsilon}_{l,\varepsilon r}(0,t_1,\eta_1)\psi^{-\varepsilon}_{l,-\varepsilon r}(0,t_2,\eta_2)\rangle \end{aligned} \tag{4.43}$$

and Fourier transforming the noise, we finally get

$$\tilde{S}^{(i)}_{\alpha\beta}=\alpha\beta C(\omega_0,L)e\bar{I}\sin\varphi_u\sin\varphi_l\,. \tag{4.44}$$

References

[AA81] H. Aoki and T. Ando. "Effect of localization on the hall conductivity in the two-dimensional system in strong magnetic fields." *Solid State Communications*, **38**(11):1079 – 1082, 1981.

[AAL79] E. Abrahams, P. W. Anderson, D. C. Licciardello, and T. V. Ramakrishnan. "Scaling Theory of Localization: Absence of Quantum Diffusion in Two Dimensions." *Phys. Rev. Lett.*, **42**:673–676, Mar 1979.

[AGR81] Alain Aspect, Philippe Grangier, and Gérard Roger. "Experimental Tests of Realistic Local Theories via Bell's Theorem." *Phys. Rev. Lett.*, **47**:460–463, Aug 1981.

[AGR82] Alain Aspect, Philippe Grangier, and Gérard Roger. "Experimental Realization of Einstein-Podolsky-Rosen-Bohm *Gedankenexperiment* : A New Violation of Bell's Inequalities." *Phys. Rev. Lett.*, **49**:91–94, Jul 1982.

[ASY05] O. M. Auslaender, H. Steinberg, A. Yacoby, Y. Tserkovnyak, B. I. Halperin, K. W. Baldwin, L. N. Pfeiffer, and K. W. West. "Spin-Charge Separation and Localization in One Dimension." *Science*, **308**(5718):88–92, 2005.

[AYP02] O. M. Auslaender, A. Yacoby, R. de Picciotto, K. W. Baldwin, L. N. Pfeiffer, and K. W. West. "Tunneling Spectroscopy of the Elementary Excitations in a One-Dimensional Wire." *Science*, **295**(5556):825–828, 2002.

[B88] M. Büttiker. "Absence of backscattering in the quantum Hall effect in multiprobe conductors." *Phys. Rev. B*, **38**:9375–9389, Nov 1988.

[B92] M. Büttiker. "Scattering theory of current and intensity noise correlations in conductors and wave guides." *Phys. Rev. B*, **46**:12485–12507, Nov 1992.

[BB84] C. H. Bennett and G. Brassard. "Quantum Cryptography: Public Key Distribution and Coin Tossing." In *Proceedings of the IEEE International Conference on Computers, Systems and Signal Processing*, pp. 175–179, New York, 1984. IEEE Press.

[BB00] Ya.M. Blanter and M. Büttiker. "Shot noise in mesoscopic conductors." *Physics Reports*, **336**:1–166, 2000.

[BBC93] Charles H. Bennett, Gilles Brassard, Claude Crépeau, Richard Jozsa, Asher Peres, and William K. Wootters. "Teleporting an unknown quantum state via dual classical and Einstein-Podolsky-Rosen channels." *Phys. Rev. Lett.*, **70**:1895–1899, Mar 1993.

[BEK03] C. W. J. Beenakker, C. Emary, M. Kindermann, and J. L. van Velsen. "Proposal for Production and Detection of Entangled Electron-Hole Pairs in a Degenerate Electron Gas." *Phys. Rev. Lett.*, **91**:147901, Oct 2003.

[Bel66] John S. Bell. "On the Problem of Hidden Variables in Quantum Mechanics." *Rev. Mod. Phys.*, **38**:447–452, Jul 1966.

[BEL00] Guido Burkard, Hans-Andreas Engel, and Daniel Loss. "Spintronics and Quantum Dots for Quantum Computing and Quantum Communication." *Fortschritte der Physik*, **48**(9-11):965–986, 2000.

[BHZ06] B. Andrei Bernevig, Taylor L. Hughes, and Shou-Cheng Zhang. "Quantum Spin Hall Effect and Topological Phase Transition in HgTe Quantum Wells." *Science*, **314**(5806):1757–1761, 2006.

[BIL85] M. Büttiker, Y. Imry, R. Landauer, and S. Pinhas. "Generalized many-channel conductance formula with application to small rings." *Phys. Rev. B*, **31**:6207–6215, May 1985.

[BJK10] Bernd Braunecker, George I. Japaridze, Jelena Klinovaja, and Daniel Loss. "Spin-selective Peierls transition in interacting one-dimensional conductors with spin-orbit interaction." *Phys. Rev. B*, **82**:045127, Jul 2010.

[BLS00] Guido Burkard, Daniel Loss, and Eugene V. Sukhorukov. "Noise of entangled electrons: Bunching and antibunching." *Phys. Rev. B*, **61**:R16303–R16306, Jun 2000.

[BTK82] G. E. Blonder, M. Tinkham, and T. M. Klapwijk. "Transition from metallic to tunneling regimes in superconducting microconstrictions: Excess current, charge imbalance, and supercurrent conversion." *Phys. Rev. B*, **25**:4515–4532, Apr 1982.

[Bur07] Guido Burkard. "Spin-entangled electrons in solid-state systems." *Journal of Physics: Condensed Matter*, **19**(23):233202, 2007.

[BVB02] Cristina Bena, Smitha Vishveshwara, Leon Balents, and Matthew P. A. Fisher. "Quantum Entanglement in Carbon Nanotubes." *Phys. Rev. Lett.*, **89**:037901, Jun 2002.

[BWL04] D. Beckmann, H. B. Weber, and H. v. Löhneysen. "Evidence for Crossed Andreev Reflection in Superconductor-Ferromagnet Hybrid Structures." *Phys. Rev. Lett.*, **93**:197003, Nov 2004.

[BZ06] B. Andrei Bernevig and Shou-Cheng Zhang. "Quantum Spin Hall Effect." *Phys. Rev. Lett.*, **96**:106802, Mar 2006.

[CBL00] Mahn-Soo Choi, C. Bruder, and Daniel Loss. "Spin-dependent Josephson current through double quantum dots and measurement of entangled electron states." *Phys. Rev. B*, **62**:13569–13572, Nov 2000.

[CBL02] Nikolai M. Chtchelkatchev, Gianni Blatter, Gordey B. Lesovik, and Thierry Martin. "Bell inequalities and entanglement in solid-state devices." *Phys. Rev. B*, **66**:161320, Oct 2002.

[CFW96] C. de C. Chamon, D. E. Freed, and X. G. Wen. "Nonequilibrium quantum noise in chiral Luttinger liquids." *Phys. Rev. B*, **53**:4033–4053, Feb 1996.

[CGD03] A. Crépieux, R. Guyon, P. Devillard, and T. Martin. "Electron injection in a nanotube: Noise correlations and entanglement." *Phys. Rev. B*, **67**:205408, May 2003.

[CGP09] A. H. Castro Neto, F. Guinea, N. M. R. Peres, K. S. Novoselov, and A. K. Geim. "The electronic properties of graphene." *Rev. Mod. Phys.*, **81**:109–162, Jan 2009.

[Cho10] M.-S. Choi. "Hanbury Brown and Twiss Correlations of Cooper Pairs in Helical Liquids." *ArXiv e-prints*, February 2010.

[CHS69] John F. Clauser, Michael A. Horne, Abner Shimony, and Richard A. Holt. "Proposed Experiment to Test Local Hidden-Variable Theories." *Phys. Rev. Lett.*, **23**:880–884, Oct 1969.

[CSS12] Wei Chen, R. Shen, L. Sheng, B. G. Wang, and D. Y. Xing. "Electron Entanglement Detected by Quantum Spin Hall Systems." *Phys. Rev. Lett.*, **109**:036802, Jul 2012.

[DF00] Guy Deutscher and Denis Feinberg. "Coupling superconducting-ferromagnetic point contacts by Andreev reflections." *Applied Physics Letters*, **76**(4):487–489, 2000.

[DHU08] M. Dolev, M. Heiblum, V. Umansky, Ady Stern, and D. Mahalu. "Observation of a quarter of an electron charge at the [ngr] = 5/2 quantum Hall state." *Nature*, **452**(7189):829–834, 2008.

[DL99] David P. DiVincenzo and Daniel Loss. "Quantum computers and quantum coherence." *J. Magn. Magn. Mater.*, **200**:202, Oct 1999.

[DP08] S. Das Sarma and A. Pinczuk. *Perspectives in Quantum Hall Effects: Novel Quantum Liquids in Low-Dimensional Semiconductor Structures*. John Wiley & Sons, 2008.

[DSS09] Sajal Dhara, Hari S. Solanki, Vibhor Singh, Arjun Narayanan, Prajakta Chaudhari, Mahesh Gokhale, Arnab Bhattacharya, and Mandar M. Deshmukh. "Magnetotransport properties of individual InAs nanowires." *Phys. Rev. B*, **79**:121311, Mar 2009.

[EAS10] S. Estévez Hernández, M. Akabori, K. Sladek, Ch. Volk, S. Alagha, H. Hardtdegen, M. G. Pala, N. Demarina, D. Grützmacher, and Th. Schäpers. "Spin-orbit

coupling and phase coherence in InAs nanowires." *Phys. Rev. B*, **82**:235303, Dec 2010.

[EBL02] J. Carlos Egues, Guido Burkard, and Daniel Loss. "Rashba Spin-Orbit Interaction and Shot Noise for Spin-Polarized and Entangled Electrons." *Phys. Rev. Lett.*, **89**:176401, Oct 2002.

[EBS05] J. Carlos Egues, Guido Burkard, D. S. Saraga, John Schliemann, and Daniel Loss. "Shot noise and spin-orbit coherent control of entangled and spin-polarized electrons." *Phys. Rev. B*, **72**:235326, Dec 2005.

[EHB04] J. M. Elzerman, R. Hanson, L. H. Willems van Beveren, B. Witkamp, L. M. K. Vandersypen, and L. P. Kouwenhoven. "Single-shot read-out of an individual electron spin in a quantum dot." *Nature*, **430**(6998):431–435, July 2004.

[Eke91] Artur K. Ekert. "Quantum cryptography based on Bell's theorem." *Phys. Rev. Lett.*, **67**:661–663, Aug 1991.

[EPR35] A. Einstein, B. Podolsky, and N. Rosen. "Can Quantum-Mechanical Description of Physical Reality Be Considered Complete?" *Phys. Rev.*, **47**:777–780, May 1935.

[ERH06] H.-A. Engel, E. I. Rashba, and B. I. Halperin. "Theory of Spin Hall Effects in Semiconductors." *eprint arXiv:cond-mat/0603306*, March 2006.

[Eza00] Z.F. Ezawa. *Quantum Hall Effects: Field Theoretical Approach and Related Topics*. World Scientific, 2000.

[Fis94] Matthew P. A. Fisher. "Cooper-pair tunneling into a quantum Hall fluid." *Phys. Rev. B*, **49**:14550–14553, May 1994.

[FK06] Liang Fu and C. L. Kane. "Time reversal polarization and a Z_2 adiabatic spin pump." *Phys. Rev. B*, **74**:195312, Nov 2006.

[Fra89] J. D. Franson. "Bell inequality for position and time." *Phys. Rev. Lett.*, **62**:2205–2208, May 1989.

[Gia04] T. Giamarchi. *Quantum Physics in One Dimension*. International Series of Monographs on Physics. Oxford University Press, USA, 2004.

[Gir99] S. M. Girvin. "Course 2: The Quantum Hall Effect: Novel Excitations and Broken Symmetries." In A. Comtet, T. Jolicoeur, S. Ouvry, and F. David, editors, *Topological Aspects of Low Dimensional Systems*, p. 53, 1999.

[GL97] Michael R. Geller and Daniel Loss. "Aharonov-Bohm effect in the chiral Luttinger liquid." *Phys. Rev. B*, **56**:9692–9706, Oct 1997.

[Goe09] M. O. Goerbig. "Quantum Hall Effects." *ArXiv e-prints*, September 2009.

[Goe11] M. O. Goerbig. "Electronic properties of graphene in a strong magnetic field." *Rev. Mod. Phys.*, **83**:1193–1243, Nov 2011.

[GRT02] Nicolas Gisin, Grégoire Ribordy, Wolfgang Tittel, and Hugo Zbinden. "Quantum cryptography." *Rev. Mod. Phys.*, **74**:145–195, Mar 2002.

[GSS08] Suhas Gangadharaiah, Jianmin Sun, and Oleg A. Starykh. "Spin-orbital effects in magnetized quantum wires and spin chains." *Phys. Rev. B*, **78**:054436, Aug 2008.

[GWW91] Martin Greiter, Xiao-Gang Wen, and Frank Wilczek. "Paired Hall state at half filling." *Phys. Rev. Lett.*, **66**:3205–3208, Jun 1991.

[Hal82] B. I. Halperin. "Quantized Hall conductance, current-carrying edge states, and the existence of extended states in a two-dimensional disordered potential." *Phys. Rev. B*, **25**:2185–2190, Feb 1982.

[Hal88] F. D. M. Haldane. "Model for a Quantum Hall Effect without Landau Levels: Condensed-Matter Realization of the "Parity Anomaly"." *Phys. Rev. Lett.*, **61**:2015–2018, Oct 1988.

[HBH12] L. G. Herrmann, P. Burset, W. J. Herrera, F. Portier, P. Roche, C. Strunk, A. Levy Yeyati, and T. Kontos. "Spectroscopy of non-local superconducting correlations in a double quantum dot." *ArXiv e-prints*, May 2012.

[HCB11] L. Hofstetter, S. Csonka, A. Baumgartner, G. Fülöp, S. d'Hollosy, J. Nygård, and C. Schönenberger. "Finite-Bias Cooper Pair Splitting." *Phys. Rev. Lett.*, **107**:136801, Sep 2011.

[HCN09] L. Hofstetter, S. Csonka, J. Nygard, and C. Schonenberger. "Cooper pair splitter realized in a two-quantum-dot Y-junction." *Nature*, **461**(7266):960–963, October 2009.

[Hir99] J. E. Hirsch. "Spin Hall Effect." *Phys. Rev. Lett.*, **83**:1834–1837, Aug 1999.

[HK10] M. Z. Hasan and C. L. Kane. "*Colloquium* : Topological insulators." *Rev. Mod. Phys.*, **82**:3045–3067, Nov 2010.

[HKP07] R. Hanson, L. P. Kouwenhoven, J. R. Petta, S. Tarucha, and L. M. K. Vandersypen. "Spins in few-electron quantum dots." *Rev. Mod. Phys.*, **79**:1217–1265, Oct 2007.

[HOS99] M. Henny, S. Oberholzer, C. Strunk, T. Heinzel, K. Ensslin, M. Holland, and C. Schnenberger. "The Fermionic Hanbury Brown and Twiss Experiment." *Science*, **284**(5412):296–298, 1999.

[HPR10] L. G. Herrmann, F. Portier, P. Roche, A. Levy Yeyati, T. Kontos, and C. Strunk. "Carbon Nanotubes as Cooper-Pair Beam Splitters." *Phys. Rev. Lett.*, **104**:026801, Jan 2010.

[HT56] R. Hanbury Brown and R. Q. Twiss. "A Test of a New Type of Stellar Interferometer on Sirius." *Nature*, **178**:1046–1048, 1956.

[IO05] Junichiro Inoue and Hideo Ohno. "Taking the Hall Effect for a Spin." *Science*, **309**(5743):2004–2005, 2005.

[Jai89a] J. K. Jain. "Composite-fermion approach for the fractional quantum Hall effect." *Phys. Rev. Lett.*, **63**:199–202, Jul 1989.

[Jai89b] J. K. Jain. "Incompressible quantum Hall states." *Phys. Rev. B*, **40**:8079–8082, Oct 1989.

[JB95] M. J. M. de Jong and C. W. J. Beenakker. "Andreev Reflection in Ferromagnet-Superconductor Junctions." *Phys. Rev. Lett.*, **74**:1657–1660, Feb 1995.

[Kan07] C. L. Kane. "Graphene and the Quantum Spin Hall Effect." *International Journal of Modern Physics B*, **21**(08n09):1155–1164, 2007.

[Kaw01] Shiro Kawabata. "Test of Bell's Inequality using the Spin Filter Effect in Ferromagnetic Semiconductor Microstructures." *Journal of the Physical Society of Japan*, **70**(5):1210–1213, 2001.

[KBM08] Markus König, Hartmut Buhmann, Laurens W. Molenkamp, Taylor Hughes, Chao-Xing Liu, Xiao-Liang Qi, and Shou-Cheng Zhang. "The Quantum Spin Hall Effect: Theory and Experiment." *Journal of the Physical Society of Japan*, **77**(3):031007, 2008.

[KBT09] A. Kleine, A. Baumgartner, J. Trbovic, and C. Schnenberger. "Contact resistance dependence of crossed Andreev reflection." *EPL (Europhysics Letters)*, **87**(2):27011, 2009.

[KDP80] K. v. Klitzing, G. Dorda, and M. Pepper. "New Method for High-Accuracy Determination of the Fine-Structure Constant Based on Quantized Hall Resistance." *Phys. Rev. Lett.*, **45**:494–497, Aug 1980.

[KM05a] C. L. Kane and E. J. Mele. "Quantum Spin Hall Effect in Graphene." *Phys. Rev. Lett.*, **95**:226801, Nov 2005.

[KM05b] C. L. Kane and E. J. Mele. "Z_2 Topological Order and the Quantum Spin Hall Effect." *Phys. Rev. Lett.*, **95**:146802, Sep 2005.

[KMG04] Y. K. Kato, R. C. Myers, A. C. Gossard, and D. D. Awschalom. "Observation of the Spin Hall Effect in Semiconductors." *Science*, **306**(5703):1910–1913, 2004.

[KMW95] Paul G. Kwiat, Klaus Mattle, Harald Weinfurter, Anton Zeilinger, Alexander V. Sergienko, and Yanhua Shih. "New High-Intensity Source of Polarization-Entangled Photon Pairs." *Phys. Rev. Lett.*, **75**:4337–4341, Dec 1995.

[KNA02] Takaaki Koga, Junsaku Nitta, Tatsushi Akazaki, and Hideaki Takayanagi. "Rashba Spin-Orbit Coupling Probed by the Weak Antilocalization Analysis in InAlAs/InGaAs/InAlAs Quantum Wells as a Function of Quantum Well Asymmetry." *Phys. Rev. Lett.*, **89**:046801, Jul 2002.

[Koh85] Mahito Kohmoto. "Topological invariant and the quantization of the Hall conductance." *Annals of Physics*, **160**(2):343 – 354, 1985.

[KVF04] Eun-Ah Kim, Smitha Vishveshwara, and Eduardo Fradkin. "Cooper-Pair Tunneling in Junctions of Singlet Quantum Hall States and Superconductors." *Phys. Rev. Lett.*, **93**:266803, Dec 2004.

[KWB07] Markus König, Steffen Wiedmann, Christoph Brne, Andreas Roth, Hartmut Buhmann, Laurens W. Molenkamp, Xiao-Liang Qi, and Shou-Cheng Zhang. "Quantum Spin Hall Insulator State in HgTe Quantum Wells." *Science*, **318**(5851):766–770, 2007.

[Lau81] R. B. Laughlin. "Quantized Hall conductivity in two dimensions." *Phys. Rev. B*, **23**:5632–5633, May 1981.

[Lau83] R. B. Laughlin. "Anomalous Quantum Hall Effect: An Incompressible Quantum Fluid with Fractionally Charged Excitations." *Phys. Rev. Lett.*, **50**:1395–1398, May 1983.

[LCM05] Andrei V. Lebedev, Adeline Crépieux, and Thierry Martin. "Electron injection in a nanotube with leads: Finite-frequency noise correlations and anomalous charges." *Phys. Rev. B*, **71**:075416, Feb 2005.

[LD98] Daniel Loss and David P. DiVincenzo. "Quantum computation with quantum dots." *Phys. Rev. A*, **57**:120–126, Jan 1998.

[Le 05] Karyn Le Hur. "Dephasing of Mesoscopic Interferences from Electron Fractionalization." *Phys. Rev. Lett.*, **95**:076801, Aug 2005.

[Le 06] Karyn Le Hur. "Electron lifetime in Luttinger liquids." *Phys. Rev. B*, **74**:165104, Oct 2006.

[LHY08] Karyn Le Hur, Bertrand I. Halperin, and Amir Yacoby. "Charge fractionalization in nonchiral Luttinger systems." *Annals of Physics*, **323**(12):3037 – 3058, 2008.

[LLB05] A. V. Lebedev, G. B. Lesovik, and G. Blatter. "Entanglement in a noninteracting mesoscopic structure." *Phys. Rev. B*, **71**:045306, Jan 2005.

[LMB01] G.B. Lesovik, T. Martin, and G. Blatter. "Electronic entanglement in the vicinity of a superconductor." *Eur. Phys. J. B*, **24**:287, 2001.

[LOY98] R. C. Liu, B. Odom, Y. Yamamoto, and S. Tarucha. "Quantum interference in electron collision." *Nature*, **391**(6664):263–265, January 1998.

[MNZ03] Shuichi Murakami, Naoto Nagaosa, and Shou-Cheng Zhang. "Dissipationless Quantum Spin Current at Room Temperature." *Science*, **301**(5638):1348–1351, 2003.

[MNZ04] Shuichi Murakami, Naoto Nagaosa, and Shou-Cheng Zhang. "Spin-Hall Insulator." *Phys. Rev. Lett.*, **93**:156804, Oct 2004.

[Moo10] Joel E. Moore. "The birth of topological insulators." *Nature*, **464**:194–198, 2010.

[MR91] Gregory Moore and Nicholas Read. "Nonabelions in the fractional quantum hall effect." *Nuclear Physics B*, **360**(2):362 – 396, 1991.

[MS95] Dmitrii L. Maslov and Michael Stone. "Landauer conductance of Luttinger liquids with leads." *Phys. Rev. B*, **52**:R5539–R5542, Aug 1995.

[MSS07] Lorenz Meier, Gian Salis, Ivan Shorubalko, Emilio Gini, Silke Schon, and Klaus Ensslin. "Measurement of Rashba and Dresselhaus spin-orbit magnetic fields." *Nat Phys*, **3**:650–654, 2007.

[NAT97] Junsaku Nitta, Tatsushi Akazaki, Hideaki Takayanagi, and Takatomo Enoki. "Gate Control of Spin-Orbit Interaction in an Inverted $In_{0.53}Ga_{0.47}As/In_{0.52}Al_{0.48}As$ Heterostructure." *Phys. Rev. Lett.*, **78**:1335–1338, Feb 1997.

[NC00] M.A. Nielsen and I.L. Chuang. *Quantum Computation and Quantum Information*. Cambridge Series on Information and the Natural Sciences. Cambridge University Press, 2000.

[NN81a] H.B. Nielsen and M. Ninomiya. "Absence of neutrinos on a lattice: (I). Proof by homotopy theory." *Nuclear Physics B*, **185**(1):20–40, 1981.

[NN81b] H.B. Nielsen and M. Ninomiya. "A no-go theorem for regularizing chiral fermions." *Physics Letters B*, **105**:219–223, 1981.

[NSO10] Naoto Nagaosa, Jairo Sinova, Shigeki Onoda, A. H. MacDonald, and N. P. Ong. "Anomalous Hall effect." *Rev. Mod. Phys.*, **82**:1539–1592, May 2010.

[NSS08] Chetan Nayak, Steven H. Simon, Ady Stern, Michael Freedman, and Sankar Das Sarma. "Non-Abelian anyons and topological quantum computation." *Rev. Mod. Phys.*, **80**:1083–1159, Sep 2008.

[OKL99] William D. Oliver, Jungsang Kim, Robert C. Liu, and Yoshihisa Yamamoto. "Hanbury Brown and Twiss-Type Experiment with Electrons." *Science*, **284**(5412):299–301, 1999.

[Per93] A. Peres. *Quantum Theory: Concepts and Methods*. Fundamental Theories of Physics. Springer, 1993.

[PGL00] K.-V. Pham, M. Gabay, and P. Lederer. "Fractional excitations in the Luttinger liquid." *Phys. Rev. B*, **61**:16397–16422, Jun 2000.

[Pra81] R. E. Prange. "Quantized Hall resistance and the measurement of the fine-structure constant." *Phys. Rev. B*, **23**:4802–4805, May 1981.

[PTG82] M. A. Paalanen, D. C. Tsui, and A. C. Gossard. "Quantized Hall effect at low temperatures." *Phys. Rev. B*, **25**:5566–5569, Apr 1982.

[QWZ06] Xiao-Liang Qi, Yong-Shi Wu, and Shou-Cheng Zhang. "Topological quantization of the spin Hall effect in two-dimensional paramagnetic semiconductors." *Phys. Rev. B*, **74**:085308, Aug 2006.

[QZ10] Xiao-Liang Qi and Shou-Cheng Zhang. "The quantum spin Hall effect and topological insulators." *Physics Today*, **63**(1):33–38, 2010.

[QZ11] Xiao-Liang Qi and Shou-Cheng Zhang. "Topological insulators and superconductors." *Rev. Mod. Phys.*, **83**:1057–1110, Oct 2011.

[RBB09] Andreas Roth, Christoph Brne, Hartmut Buhmann, Laurens W. Molenkamp, Joseph Maciejko, Xiao-Liang Qi, and Shou-Cheng Zhang. "Nonlocal Transport in the Quantum Spin Hall State." *Science*, **325**(5938):294–297, 2009.

[RKK05] S. Russo, M. Kroug, T. M. Klapwijk, and A. F. Morpurgo. "Experimental Observation of Bias-Dependent Nonlocal Andreev Reflection." *Phys. Rev. Lett.*, **95**:027002, Jul 2005.

[RL02] Patrik Recher and Daniel Loss. "Superconductor coupled to two Luttinger liquids as an entangler for electron spins." *Phys. Rev. B*, **65**:165327, Apr 2002.

[RL03] Patrik Recher and Daniel Loss. "Dynamical Coulomb Blockade and Spin-Entangled Electrons." *Phys. Rev. Lett.*, **91**:267003, Dec 2003.

[RSL01] Patrik Recher, Eugene V. Sukhorukov, and Daniel Loss. "Andreev tunneling, Coulomb blockade, and resonant transport of nonlocal spin-entangled electrons." *Phys. Rev. B*, **63**:165314, Apr 2001.

[SBS12] J. Schindele, A. Baumgartner, and C. Schönenberger. "Near-Unity Cooper Pair Splitting Efficiency." *Phys. Rev. Lett.*, **109**:157002, Oct 2012.

[SBY08] Hadar Steinberg, Gilad Barak, Amir Yacoby, Loren N. Pfeiffer, Ken W. West, Bertrand I. Halperin, and Karyn Le Hur. "Charge fractionalization in quantum wires." *Nat Phys*, **4**(2):116–119, February 2008.

[SCN04] Jairo Sinova, Dimitrie Culcer, Q. Niu, N. A. Sinitsyn, T. Jungwirth, and A. H. MacDonald. "Universal Intrinsic Spin Hall Effect." *Phys. Rev. Lett.*, **92**:126603, Mar 2004.

[SEL03] John Schliemann, J. Carlos Egues, and Daniel Loss. "Nonballistic Spin-Field-Effect Transistor." *Phys. Rev. Lett.*, **90**:146801, Apr 2003.

[SFM04] Olivier Sauret, Denis Feinberg, and Thierry Martin. "Quantum master equations for the superconductor͡quantum dot entangler." *Phys. Rev. B*, **70**:245313, Dec 2004.

[SGS07] Jianmin Sun, Suhas Gangadharaiah, and Oleg A. Starykh. "Spin-Orbit-Induced Spin-Density Wave in a Quantum Wire." *Phys. Rev. Lett.*, **98**:126408, Mar 2007.

[SJ09] Anders Ström and Henrik Johannesson. "Tunneling between Edge States in a Quantum Spin Hall System." *Phys. Rev. Lett.*, **102**:096806, Mar 2009.

[SKK08] Matthias Scheid, Makoto Kohda, Yoji Kunihashi, Klaus Richter, and Junsaku Nitta. "All-Electrical Detection of the Relative Strength of Rashba and Dresselhaus Spin-Orbit Interaction in Quantum Wires." *Phys. Rev. Lett.*, **101**:266401, Dec 2008.

[SLT10] Koji Sato, Daniel Loss, and Yaroslav Tserkovnyak. "Cooper-Pair Injection into Quantum Spin Hall Insulators." *Phys. Rev. Lett.*, **105**:226401, Nov 2010.

[SLT12] Koji Sato, Daniel Loss, and Yaroslav Tserkovnyak. "Crossed Andreev reflection in quantum wires with strong spin-orbit interaction." *Phys. Rev. B*, **85**:235433, Jun 2012.

[SS95] I. Safi and H. J. Schulz. "Transport in an inhomogeneous interacting one-dimensional system." *Phys. Rev. B*, **52**:R17040–R17043, Dec 1995.

[SSB03] P. Samuelsson, E. V. Sukhorukov, and M. Büttiker. "Orbital Entanglement and Violation of Bell Inequalities in Mesoscopic Conductors." *Phys. Rev. Lett.*, **91**:157002, Oct 2003.

[SSB04] P. Samuelsson, E. V. Sukhorukov, and M. Büttiker. "Electrical current noise of a beamsplitter as a test of spin entanglement." *Phys. Rev. B*, **70**:115330, Sep 2004.

[SU91] Manfred Sigrist and Kazuo Ueda. "Phenomenological theory of unconventional superconductivity." *Rev. Mod. Phys.*, **63**:239–311, Apr 1991.

[TKN82] D. J. Thouless, M. Kohmoto, M. P. Nightingale, and M. den Nijs. "Quantized Hall Conductance in a Two-Dimensional Periodic Potential." *Phys. Rev. Lett.*, **49**:405–408, Aug 1982.

[TMS70] P. M. Tedrow, R. Meservey, and B. B. Schwartz. "Experimental Evidence for a First-Order Magnetic Transition in Thin Superconducting Aluminum Films." *Phys. Rev. Lett.*, **24**:1004–1007, May 1970.

[Tru83] S. A. Trugman. "Localization, percolation, and the quantum Hall effect." *Phys. Rev. B*, **27**:7539–7546, Jun 1983.

[TSG82] D. C. Tsui, H. L. Stormer, and A. C. Gossard. "Two-Dimensional Magnetotransport in the Extreme Quantum Limit." *Phys. Rev. Lett.*, **48**:1559–1562, May 1982.

[VR12] Pauli Virtanen and Patrik Recher. "Signatures of Rashba spin-orbit interaction in the superconducting proximity effect in helical Luttinger liquids." *Phys. Rev. B*, **85**:035310, Jan 2012.

[WBZ06] Congjun Wu, B. Andrei Bernevig, and Shou-Cheng Zhang. "Helical Liquid and the Edge of Quantum Spin Hall Systems." *Phys. Rev. Lett.*, **96**:106401, Mar 2006.

[WC10] Jian Wei and V. Chandrasekhar. "Positive noise cross-correlationin hybrid superconducting and normal-metal three-terminal devices." *Nat Phys*, **6**:494– 498, July 2010.

[WCW09] Miao Wang, Kai Chang, L G Wang, Ning Dai, and F M Peeters. "Crystallographic plane tuning of charge and spin transport in semiconductor quantum wires." *Nanotechnology*, **20**(36):365202, 2009.

[Wen92] Xiao-Gang Wen. "Theory of the Edge States in Fractional Quqntum Hall Effects." *International Journal of Modern Physics B*, **06**(10):1711–1762, 1992.

[Wer89] Reinhard F. Werner. "Quantum states with Einstein-Podolsky-Rosen correlations admitting a hidden-variable model." *Phys. Rev. A*, **40**:4277–4281, Oct 1989.

[WES87] R. Willett, J. P. Eisenstein, H. L. Störmer, D. C. Tsui, A. C. Gossard, and J. H. English. "Observation of an even-denominator quantum number in the fractional quantum Hall effect." *Phys. Rev. Lett.*, **59**:1776–1779, Oct 1987.

[Wil82] Frank Wilczek. "Magnetic Flux, Angular Momentum, and Statistics." *Phys. Rev. Lett.*, **48**:1144–1146, Apr 1982.

[WKS05] J. Wunderlich, B. Kaestner, J. Sinova, and T. Jungwirth. "Experimental Observation of the Spin-Hall Effect in a Two-Dimensional Spin-Orbit Coupled Semiconductor System." *Phys. Rev. Lett.*, **94**:047204, Feb 2005.

[XM06] Cenke Xu and J. E. Moore. "Stability of the quantum spin Hall effect: Effects of interactions, disorder, and $\mathbb{Z}_2$ topology." *Phys. Rev. B*, **73**:045322, Jan 2006.

[Yos10] D. Yoshioka. *The Quantum Hall Effect*. Springer Series in Solid-State Sciences. Springer, 2010.

[ZHX11] M. Zahid Hasan, D. Hsieh, Y. Xia, L. A. Wray, S.-Y. Xu, and C. L. Kane. "A new experimental approach for the exploration of topological quantum phenomena : Topological Insulators and Superconductors." *ArXiv e-prints*, May 2011.